

Naval Research Laboratory

Stennis Space Center, MS 39529-5004



NRL/FR/7322--97-9680

Review and Verification of Numerical Wave Models for Near Coastal Areas – Part 2: Verification of Near Coastal Numerical Wave Models

W. ERICK ROGERS

*Planning Systems Incorporated
Slidell, LA*

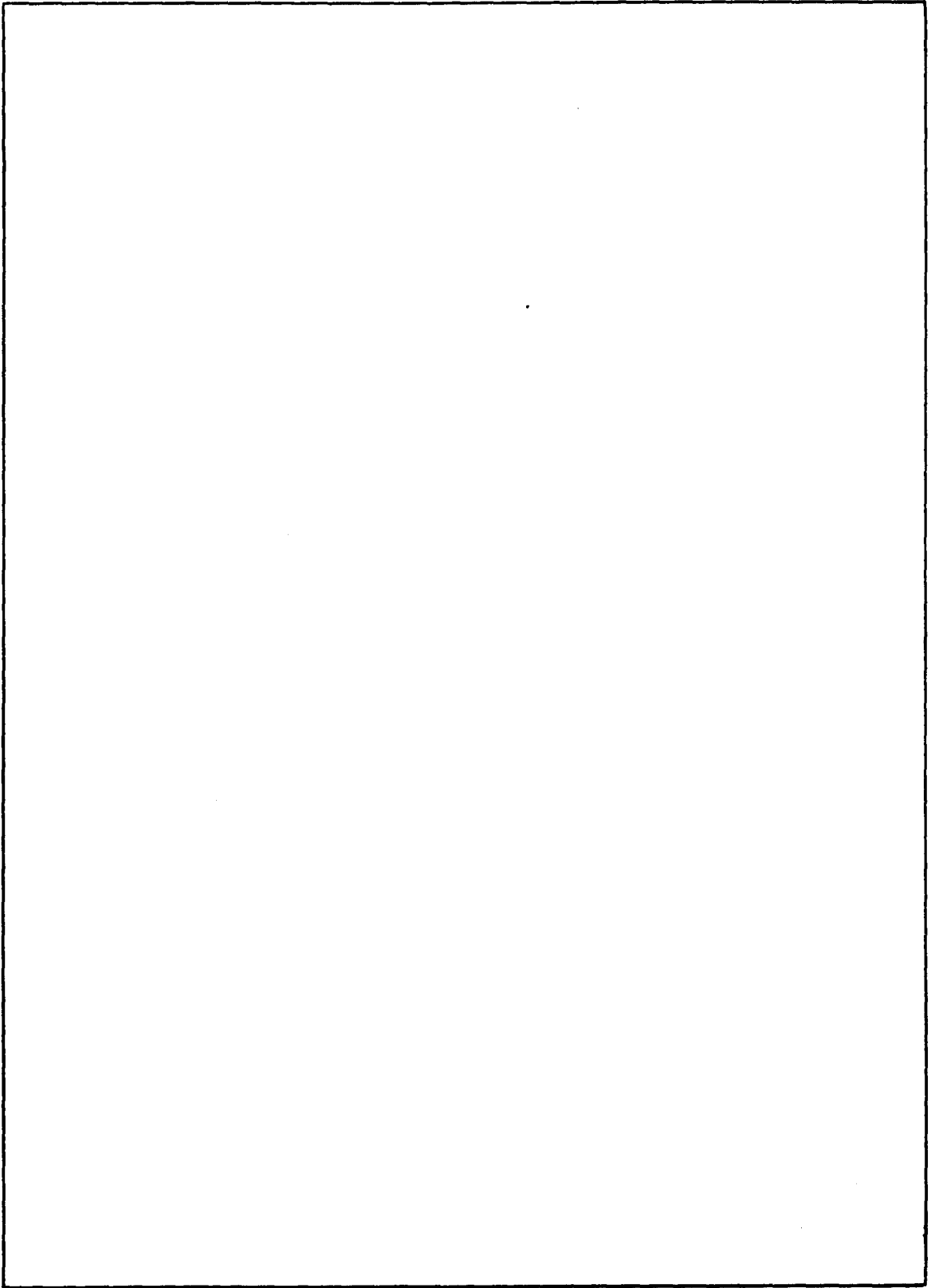
JAMES M. KAIHATU
Y. LARRY HSU

*Ocean Dynamics and Prediction Branch
Oceanography Division*

January 30, 1998

Approved for public release; distribution unlimited.

SECURITY CLASSIFICATION OF THIS PAGE(When Data Entered)



REPORT DOCUMENTATION PAGE

Form Approved
OBM No. 0704-0188

Public reporting burden for this collection of information is estimated to average 1 hour per response, including the time for reviewing instructions, searching existing data sources, gathering and maintaining the data needed, and completing and reviewing the collection of information. Send comments regarding this burden or any other aspect of this collection of information, including suggestions for reducing this burden, to Washington Headquarters Services, Directorate for Information Operations and Reports, 1215 Jefferson Davis Highway, Suite 1204, Arlington, VA 22202-4302, and to the Office of Management and Budget, Paperwork Reduction Project (0704-0188), Washington, DC 20503.

1. AGENCY USE ONLY (<i>Leave blank</i>)		2. REPORT DATE January 30, 1998	3. REPORT TYPE AND DATES COVERED Final	
4. TITLE AND SUBTITLE Review and Verification of Numerical Wave Models For Near Coastal Areas – Part 2: Verification of Near Coastal Numerical Wave Models			5. FUNDING NUMBERS Job Order No. 573672008 Program Element No. 0602435N Project No. Task No. BE-35-2-15 Accession No. DN16-3783	
6. AUTHOR(S) W. Erick Rogers*, James M. Kaihatu, and Y. Larry Hsu				
7. PERFORMING ORGANIZATION NAME(S) AND ADDRESS(ES) Naval Research Laboratory Oceanography Division Stennis Space Center, MS 39529-5004			8. PERFORMING ORGANIZATION REPORT NUMBER NRL/FR/7322--97-9680	
9. SPONSORING/MONITORING AGENCY NAME(S) AND ADDRESS(ES) Office of Naval Research 800 N. Quincy St. Arlington, VA 22217-5000			10. SPONSORING/MONITORING AGENCY REPORT NUMBER	
11. SUPPLEMENTARY NOTES Planning Systems Incorporated, 115 Christian Lane, Slidell, LA				
12a. DISTRIBUTION/AVAILABILITY STATEMENT Approved for public release; distribution unlimited.			12b. DISTRIBUTION CODE	
13. ABSTRACT (<i>Maximum 200 words</i>) This report details the validation of the numerical wave models REF/DEF1 and REF/DIF-S. The monochromatic model REF/DIF1 is used to test most model physics, while the irregular wave model REF/DIF-S is used to investigate model applicability to realistic situations. Comparisons of the models to available analytical solutions, synthetic cases, and laboratory and field scenarios are performed. Where applicable, we also compare the two models to the wave model RCPWAVE, which is based on a different formulation. We find that the REF/DIF models are reasonably accurate in most of the situations tested. The REF/DIF models also outperform RCPWAVE in most of the instances where the models can be compared. In particular, it is found that the RCPWAVE model underpredicts the effect of wave diffraction. Model robustness to bathymetric uncertainty is also tested. It is found that neither REF/DIF1 nor REF/DIF-S is overly sensitive to bathymetric uncertainty. In areas where the diffraction effect is large, the REF/DIF-S model tends to have more robust characteristics than the monochromatic model, due primarily to its irregular nature. Details of the modified spectral input program used in this study appear in the appendix.				
14. SUBJECT TERMS wave modeling, tide modeling, coupled waves, coupled tides			15. NUMBER OF PAGES 107	
			16. PRICE CODE	
17. SECURITY CLASSIFICATION OF REPORT Unclassified	18. SECURITY CLASSIFICATION OF THIS PAGE Unclassified	19. SECURITY CLASSIFICATION OF ABSTRACT Unclassified	20. LIMITATION OF ABSTRACT Same as report	

INTRODUCTION AND OVERVIEW

This Report covers recent NRL research and development related to the AEC laser-pellet fusion program. The work covered in this report was primarily carried out under AEC Contract No. AT(04-3)-878 between July, 1973 and June, 1974. In some cases, for the sake of clarity, work not performed during this period has been included. In addition, the report discusses the large complementary program supported by the Defense Nuclear Agency at NRL on the study of laser produced plasmas in high atomic number materials. A significant part of the soft x-ray experimental studies (Chapter V) and all of the numerical modelling studies (Chapter VIII and Chapter IX) were supported by the DNA program. This work has been included in the present report for the sake of completeness and since many of the results obtained are of direct benefit to the AEC laser-fusion effort.

There is some overlap in time, with the period covered by the last NRL report, which was presented to the Laser-Fusion Coordinating Committee in November, 1973. However, it was felt useful to establish the precedent of fiscal year reporting starting with this Annual Report. In the future, a report on the AEC supported laser-fusion studies at NRL will appear on a semi-annual basis.

Studies of laser produced plasmas began at NRL in 1968. Development of a large Q-switched glass laser facility was carried out under ARPA sponsorship. Additional support for laser development was received as part of a DNA-supported program to study the interactions between an expanding laser-produced plasma and an ambient magnetized plasma background. The DNA program also provided NRL with the genesis of its expertise in the study of laser plasma generation and interactions. The glass laser system was developed under joint ARPA and DNA sponsorship to the point where, by FY 72, it represented the state-of-the-art in high power short pulse lasers. The system included an NRL designed mode-locked YAG oscillator system and a disc amplifier which became a prototype for those now in use and under development in the laser-fusion program.

When a large AEC supported laser-fusion effort began in FY 72, NRL was a logical place to turn to for support in building up the programs of the AEC laboratories. Shortly after the start of AEC-supported work at NRL, a DNA program at NRL was initiated to study laser produced high atomic number plasmas. The aim of this program was to develop a new source of soft x-rays for weapons effect simulation. The combined AEC and DNA supported programs have been known within NRL as the Laser-Matter Interaction (LMI) Program and Dr. John Stamper has served as Program Manager since its inception. The LMI Program has included contributions from a number of divisions at NRL and has involved both experimental and theoretical studies. The funding of the program during FY 74 consisted of \$500,000 from the AEC for laser-fusion studies as well as additional funding from DNA for x-ray source investigations.

One of the unique features of the NRL laser-fusion program has been the availability of a reliable Nd:glass laser system which produces exceptionally clean pulses (i.e., spatially, temporally and spectrally pure) at sufficient power levels ($\lesssim 0.5$ TW) for many studies of interest to laser fusion. Over 1500 laser shots were put on target in FY 74 for our AEC

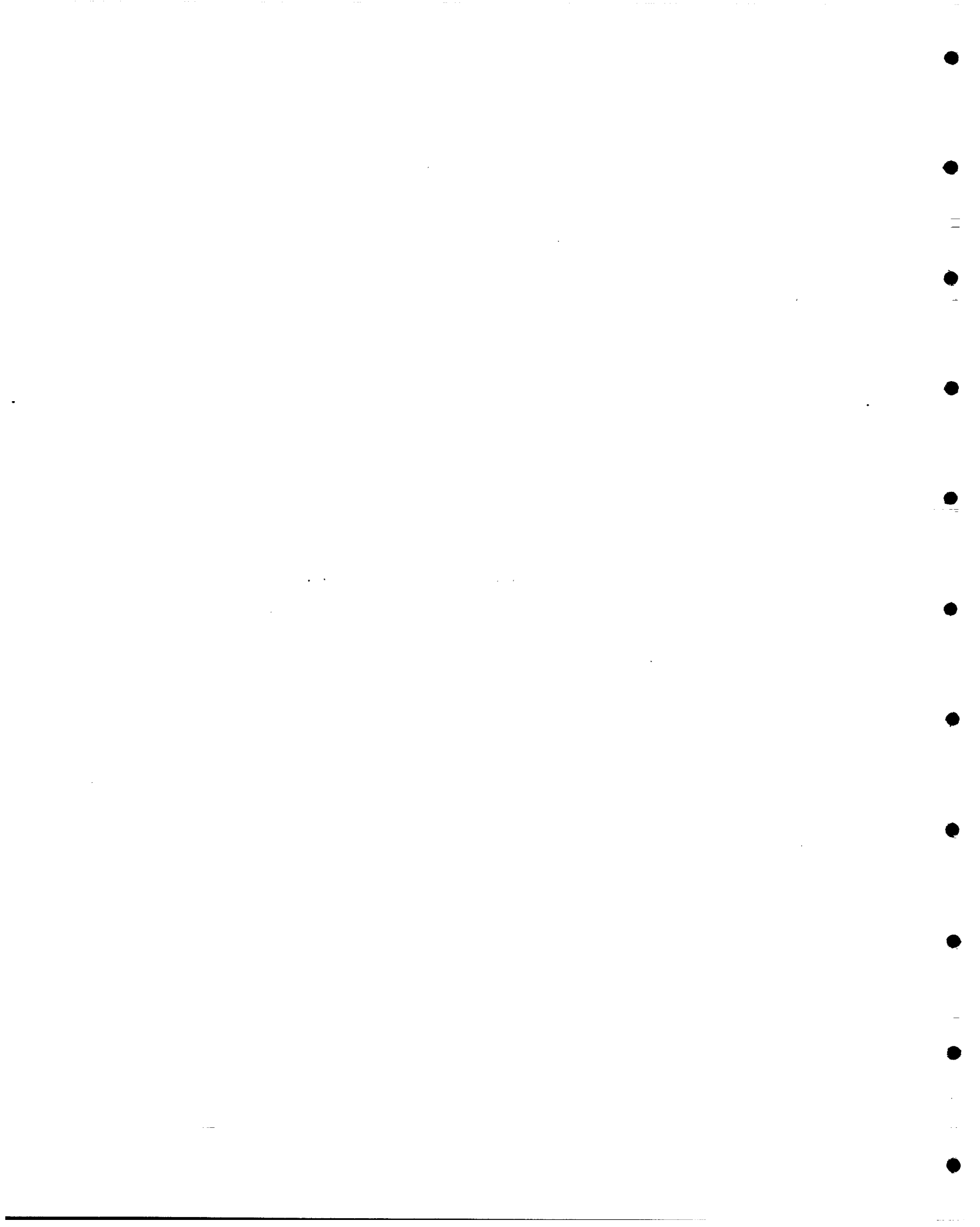
CONTENTS

EXECUTIVE SUMMARY	E-1
1.0 INTRODUCTION	1
2.0 COMPARISONS OF MODEL TO ANALYTICAL SOLUTIONS	1
2.1 Tests of Refraction and Shoaling	1
3.0 MODEL TESTS WITH IDEALIZED BATHYMETRIES	22
4.0 COMPARISON OF MODELS TO LABORATORY EXPERIMENTS	23
4.1 Berkhoff-Booij-Radder Shoal Experiment	27
4.2 Hales Shore-Normal Breakwater Experiment	29
5.0 COMPARISON TO FIELD DATA	34
5.1 The DELILAH Field Experiment—General Information	37
5.2 Comparisons of REF/DIF-S Output to Data	40
5.3 Comparisons To Field Data—Conclusions	55
6.0 SENSITIVITY TO BATHYMETRIC UNCERTAINTY	67
6.1 Perturbed Planar Slope	67
6.2 Bathymetric Shoal	75
6.3 Other Issues Regarding Bathymetric Uncertainty	84
7.0 WAVE SHOALING AND BREAKING WITH REF/DIF-S	85
8.0 CORRECTIONS TO REF/DIF-S	87
8.1 Wave Number Dimensioning Correction	87
8.2 Central Differencing for Wave Angle Calculation	94
8.3 Nonphysical Numerical Damping	94
9.0 DIRECTIONAL SPECTRA	94

10.0 CONCLUSIONS	96
11.0 ACKNOWLEDGMENTS	98
12.0 REFERENCES	98
APPENDIX A — Details of the Spectral Input Program SPECGEN	101

EXECUTIVE SUMMARY

This report details the validation of the numerical wave models REF/DEF1 and REF/DIF-S. The monochromatic model REF/DIF1 is used to test most model physics, while the irregular wave model REF/DIF-S is used to investigate model applicability to realistic situations. Comparisons of the models to available analytical solutions, synthetic cases, and laboratory and field scenarios are performed. Where applicable, we also compare the two models to the wave model RCPWAVE, which is based on a different formulation. We find that the REF/DIF models are reasonably accurate in most of the situations tested. The REF/DIF models also outperform RCPWAVE in most of the instances where the models can be compared. In particular, it is found that the RCPWAVE model underpredicts the effect of wave diffraction. Model robustness to bathymetric uncertainty is also tested. It is found that neither REF/DIF1 nor REF/DIF-S is overly sensitive to bathymetric uncertainty. In areas where the diffraction effect is large, the REF/DIF-S model tends to have more robust characteristics than the monochromatic model, due primarily to its irregular nature. Details of the modified spectral input program used in this study appear in the appendix.



REVIEW AND VERIFICATION OF NUMERICAL WAVE MODELS FOR NEAR COASTAL AREAS - PART 2: VERIFICATION OF NEAR COASTAL NUMERICAL WAVE MODELS

1.0 INTRODUCTION

In Part 1 of this report, some of the theoretical aspects of wave modeling were outlined, as well as a few of the numerical techniques used. Some of the technical details embedded within the models REF/DIF1 (Kirby and Dalrymple 1994), REF/DIF-S (Kirby and Ozkan 1994), and RCPWAVE (Ebersole et al. 1986) were also discussed. In Part 2, verification of the models with analytical solutions (where available), laboratory data, and field data will be discussed. Some issues of model robustness and simulation of directional spectra will also be investigated, and some general conclusions will be offered.

2.0 COMPARISONS OF MODEL TO ANALYTICAL SOLUTIONS

Since the models are essentially extensions of theoretical developments for simplified cases, it is logical to expect the models to resemble the analytical expressions for cases where the analytical theory is valid. In this section of the report, the models REF/DIF1 and RCPWAVE are compared to analytical expressions.

2.1 Tests of Refraction and Shoaling

As noted in Part 1, Sec. 2.2, the mild-slope equation reverts to the eikonal transport equations for wave refraction for the case of negligible diffraction. In this section, the refractive properties of the wave models to the analytical expressions from linear theory are related.

The wave height in water of finite depth is related to the deep-water wave height H_o by:

$$H = K_s K_r H_o, \quad (2.1)$$

where the shoaling coefficient K_s is given by

$$K_s = \sqrt{\frac{1}{\left(1 + \frac{2kh}{\sinh 2kh}\right) \tanh kh}} \quad (2.2)$$

and the refraction coefficient K_r is

$$K_r = \sqrt{\frac{\cos \theta_o}{\cos \theta}}, \quad (2.3)$$

where the subscript "o" denotes deep-water conditions.

The model performance was checked against linear refraction and shoaling by setting up the following model scenario:

Domain: 720 × 720 m

Grid resolution: $\Delta x = \Delta y = 3$ m

Wave periods: $T = 3$ s, 10 s, 17 s

Wave angles at boundary $x = 0$ m: $\theta = 15, 30, 45,$ and 60°

Bathymetry: Planar slope with offshore depth of 7 m and a slope of 0.009

Wave height at boundary: $H = 1$ m

The range of wave periods were chosen to represent deep-, intermediate-, and shallow-water conditions. The wave angles go beyond the validity of the wide-angle Pade approximation employed by REF/DIF1. Representation of some of these conditions in RCPWAVE proved to be problematic because the corresponding deep-water conditions could not be determined by backward transformation using Snell's Law (e.g., $\theta = 60^\circ$, $T = 17$ s).

Results are shown in Figs. 2.1–2.7. The ability for REF/DIF1 to reproduce the wave heights from theory is lessened for the cases of larger angles of incidence. This is particularly true for the $\theta = 60^\circ$ cases. It appears that REF/DIF1 at this high angle of incidence is underpredicting the effect of refraction. The wave angle predictions from REF/DIF1 also suffer in comparison to linear theory at the high angles. It should be noted here that wave angle is a supplemental calculation in the model and does not enter as a critical part of the numerical procedure. It is also noted that the problem would likely be alleviated if the grid were rotated to be coincident to the wave direction.

For the cases where RCPWAVE could be run, the model compares quite well to the analytical solution; there is no noticeable decrease in accuracy for the larger angles. Breaking occurs at different locations in the surf zone for the two models because the incipient breaking conditions in the models are different.

2.1.2 Diffraction Tests

The mild-slope equation reduces to the Helmholtz equation for the case of time-periodic waves propagating over constant water depth; this was noted in an earlier section. Specific cases of wave propagation modeled by the Helmholtz equation depend on the initial and boundary conditions. The numerical wave models will be compared to analytical solutions for wave diffraction in two cases: waves propagating around a semi-infinite breakwater and waves propagating past a breakwater gap.

2.1.2.1 Wave Diffraction by a Semi-Infinite Breakwater

RCPWAVE and REF/DIF1 model results for the case of a semi-infinite breakwater were compared to an analytical solution for the wave field due to combined reflection and diffraction by a vertical wedge of arbitrary angle on a flat bottom (Chen 1987; Kaihatu and Chen 1988). For these semi-infinite breakwater runs a wedge angle of 0° was used. Because the numerical models do not

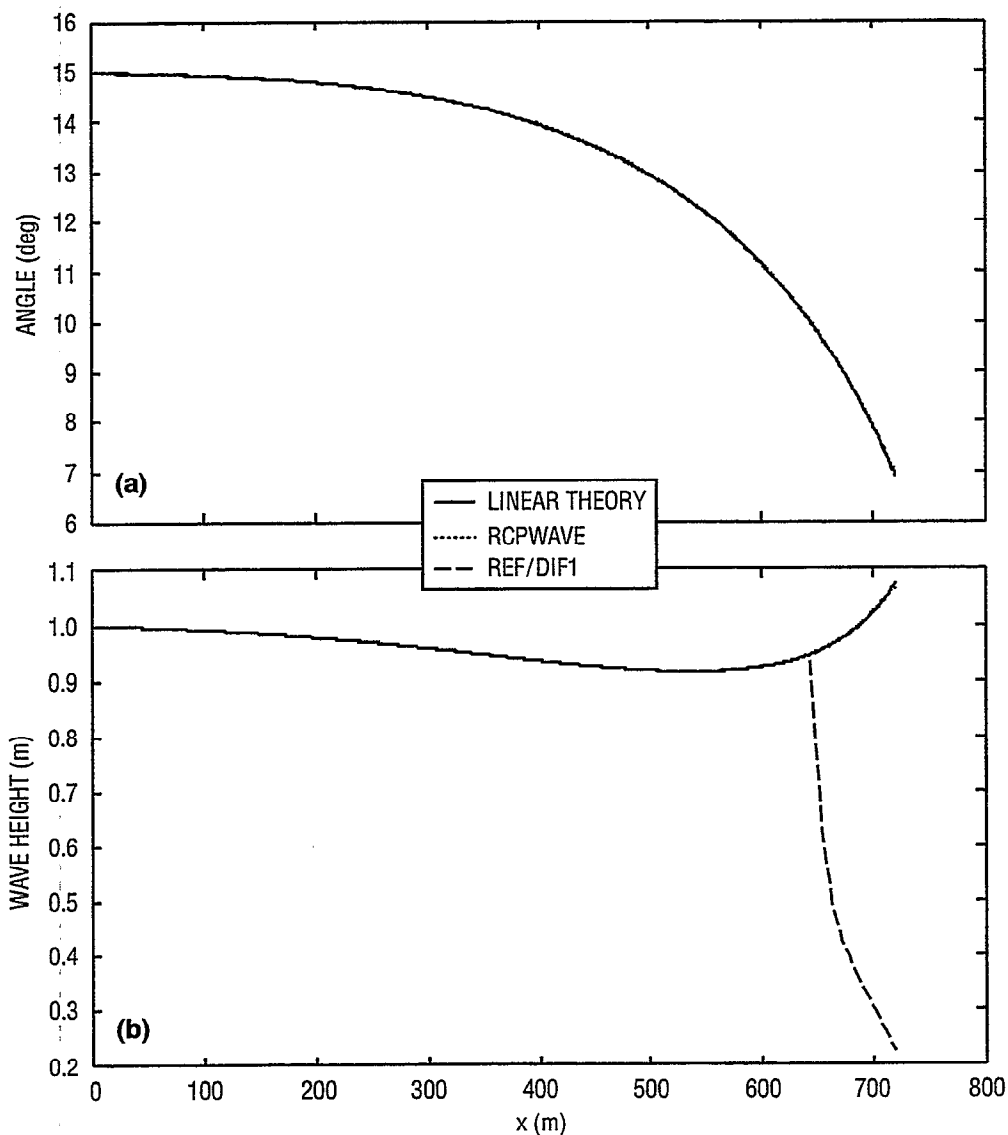


Fig. 2.1 — Comparison of RCPWAVE and REF/DIF1 to linear shoaling and refraction theory, $T=3$ s, $\theta=15^\circ$, (a) angle comparison and (b) wave height comparison

include backward-scattered wave reflection, only the portion of the analytical solution past the breakwater was used for comparison; thus, diffraction is the only true transformation characteristic.

The analytical solution for waves propagating into a vertical wedge of arbitrary angle was derived by Chen (1987) and developed into a computer code by Kaihatu and Chen (1988). The solution was derived from the boundary value problem for water waves with the vertical wedge of arbitrary angle used as a boundary condition. This problem was first treated by Stoker (1957); Chen (1987) extended it by refraining from taking the final cosine transform employed by Stoker (1957), who used it to avoid having to sum up the terms in the Bessel functions in the solution. The cosine transform, while not requiring the summation of possibly many terms in the Bessel function, is a far-field approximation to the Bessel function, and thus, is only strictly valid several wavelengths away from the scattering obstacle. Chen (1987) used International Mathematics and Statistics

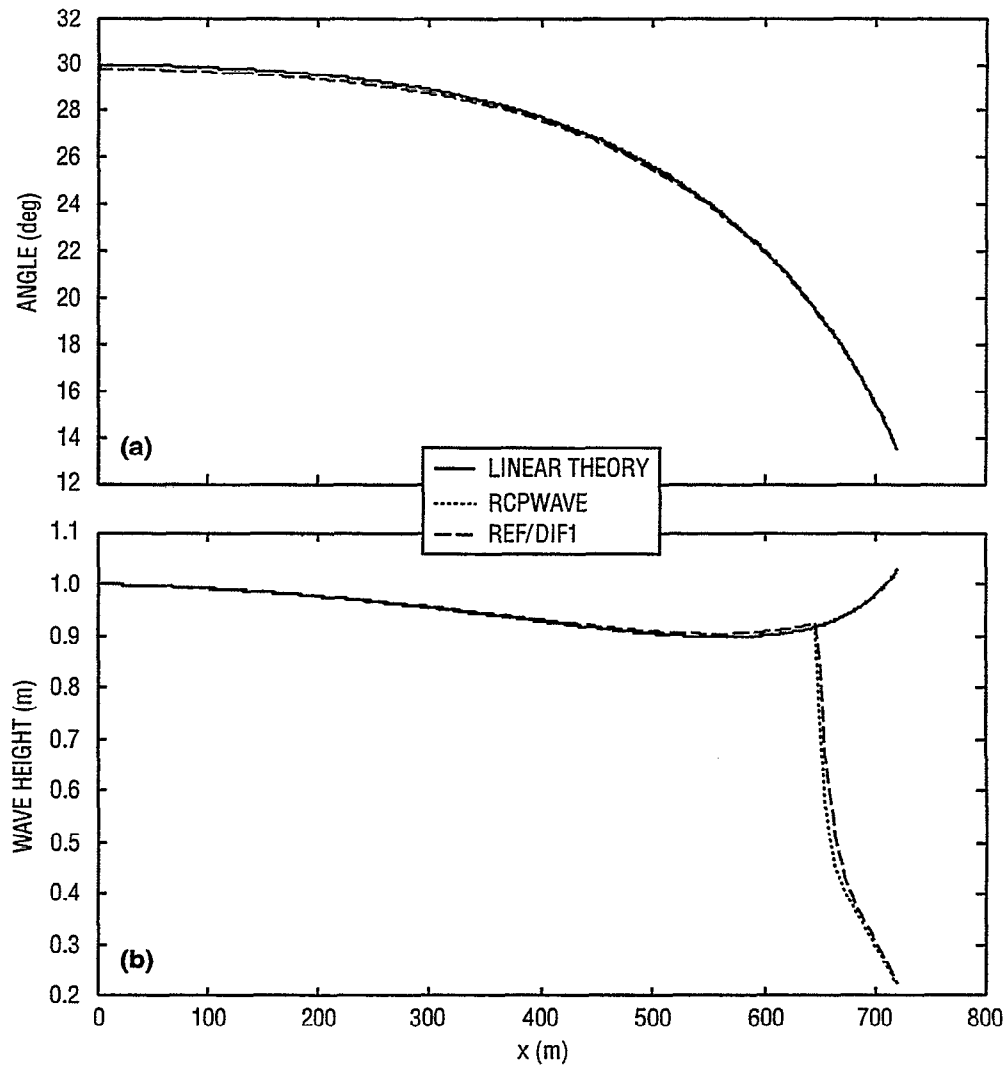


Fig. 2.2 — Comparison of RCPWAVE and REF/DIF1 to linear shoaling and refraction theory, $T = 3$ s, $\theta = 30^\circ$, (a) angle comparison and (b) wave height comparison

Library (IMSL) routines for Bessel function calculation to sum the terms and, thus, obtained a universally valid solution.

The model setup is shown in Fig. 2.8. The following modeling parameters were used:

Wave period: $T = 8$ s

Water depth: $h = 6.1$ m

Wave height at offshore boundary: $H = 1$ m

Domain size: 576×1152 m or $10 \times 20 L$ in x and y , respectively (where L is wavelength)

Grid resolution: $\Delta x = \Delta y = 19$ m

Open lateral boundaries were used.

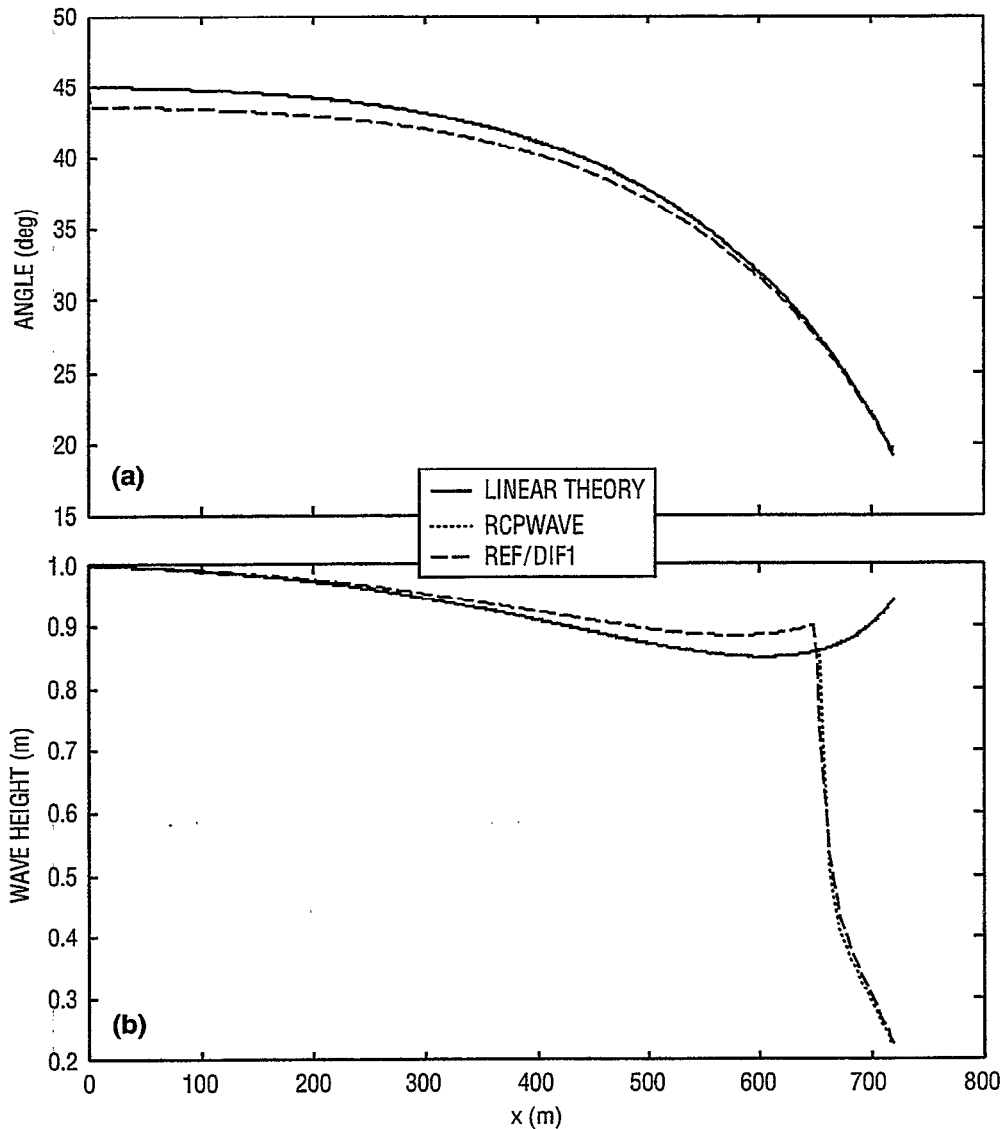


Fig. 2.3 — Comparison of RCPWAVE and REF/DIF1 to linear shoaling and refraction theory, $T = 3$ s, $\theta = 45^\circ$, (a) angle comparison and (b) wave height comparison

REF/DIF1 has a parameter value that allows the y -wise resolution to be increased to a multiple of the stated Δy at which bathymetry is specified. In anticipation of the high wave angles in the lee of the breakwater (due to the spreading of wave rays), this parameter was set to 6; thus, the actual resolution at which the model operated was $\Delta y = 3.2$ m. No such resolution adjustment was made to RCPWAVE since the model is not formally limited to small wave angles. For both models, the breakwater was simulated at the offshore boundary by setting the amplitudes along that part of the boundary equal to 0. The impact the wide-angle correction has on REF/DIF1 by reverting the coefficients back to the small-angle model of Radder (1979) was also tested.

Model results comparing wide-angle REF/DIF1 to RCPWAVE are shown in Figs. 2.9–2.13. REF/DIF1 compares better with the analytic solution for the wave conditions where the waves are propagated into the lee of the breakwater ($\theta < 0$). In these cases, the diffracted wave height

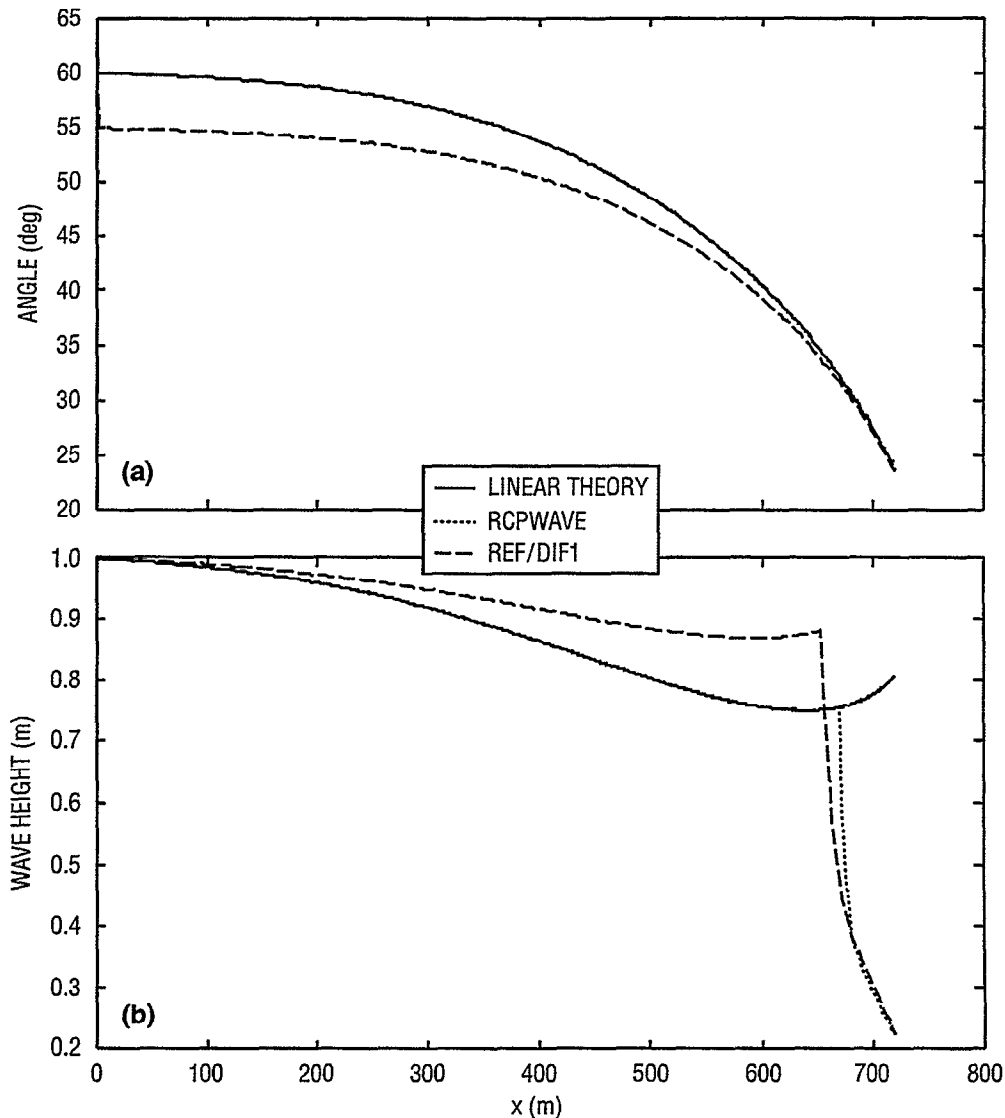


Fig. 2.4 — Comparison of RCPWAVE and REF/DIF1 to linear shoaling and refraction theory, $T = 3$ s, $\theta = 60^\circ$, (a) angle comparison and (b) wave height comparison

oscillations do not spread laterally with increasing x to the extent observed in the analytical solution. The effect of the open lateral boundary can be seen in Fig. 2.9; the wave amplification factor for $x/L = 9.615$ predicted by the model evidences some very local oscillation near the left boundary. This is because in the cases where the wave is propagated into the sheltered area behind the breakwater, the waves in the illuminated region (negative x/L) are not plane waves and, thus, deviate from the assumptions used in the development of the open lateral boundary conditions in the model. In general, REF/DIF1 is more accurate in the illuminated region than in the sheltered area.

For most of the wave angles simulated, RCPWAVE does not reproduce the wave height oscillations observed in the analytical solution and REF/DIF1 results, though it reasonably predicts the magnitude of the wave heights in the absence of these wave forms. For large negative values of θ ,

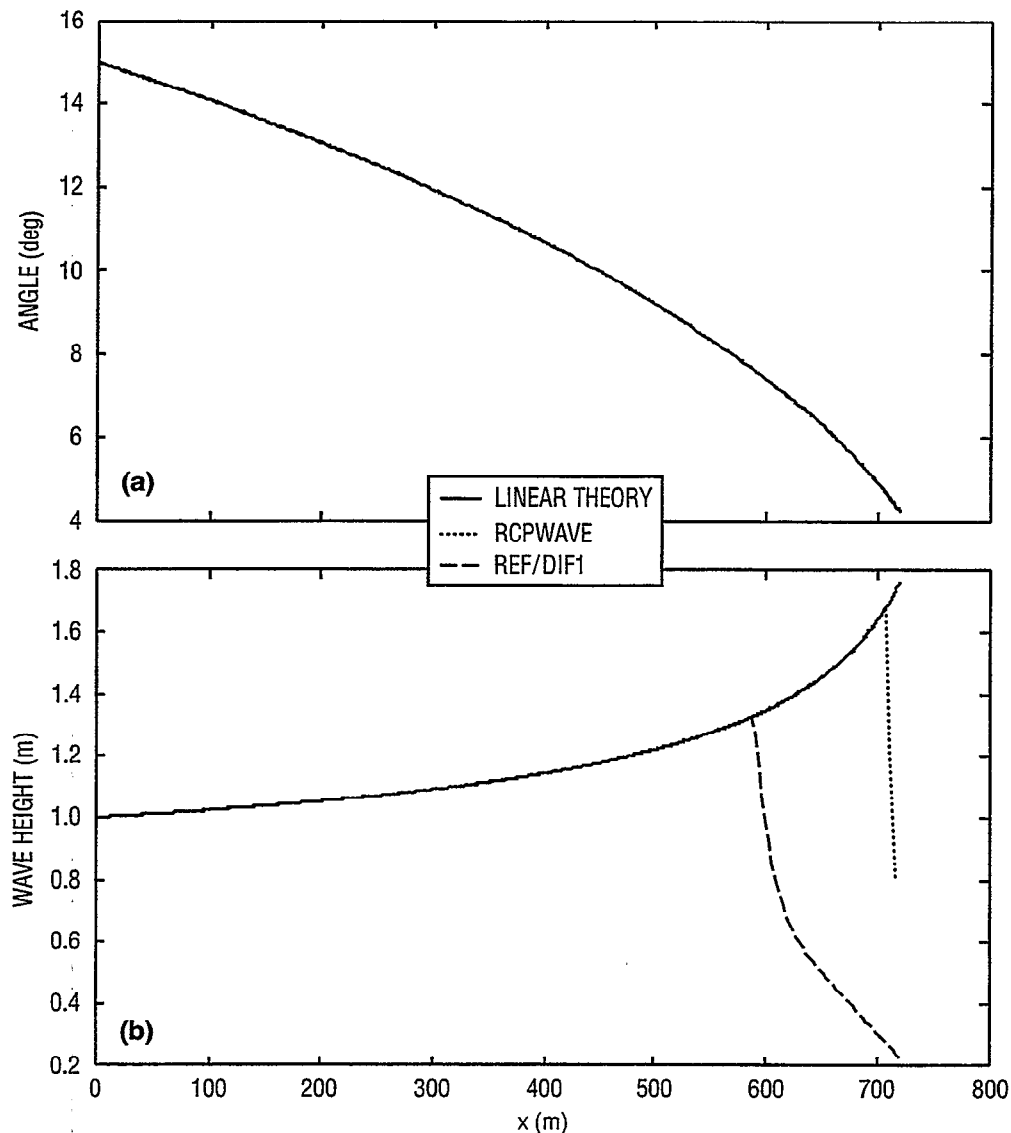


Fig. 2.5 — Comparison of RCPWAVE and REF/DIF1 to linear shoaling and refraction theory, $T = 10$ s, $\theta = 15^\circ$, (a) angle comparison and (b) wave height comparison

a single wave form is observed from RCPWAVE; in some cases the amplitude of this wave near $x/L = 0$ is unrealistically large (see Fig. 2.9).

Figures 2.14–2.20 show the comparisons of the wide-angle REF/DIF1 to the narrow-angle model (REF/DIF1 reduced to the small angle approximation of Radder 1979). Neither model does particularly well for the $\theta = \pm 45^\circ$ cases, most likely because this approach angle is the stated limit for the wide-angle correction employed by REF/DIF1 (the Pade approximation of Booij 1981) and the wave angle is expected to increase beyond this in the domain. In general, however, the wide-angle version of the model compares somewhat better to the analytical solution than the small-angle model. This is evident in the illuminated region as the wave form from the small-angle model is slightly out of phase with respect to that from both the analytical solution and the wide-angle model (see Fig. 2.18).

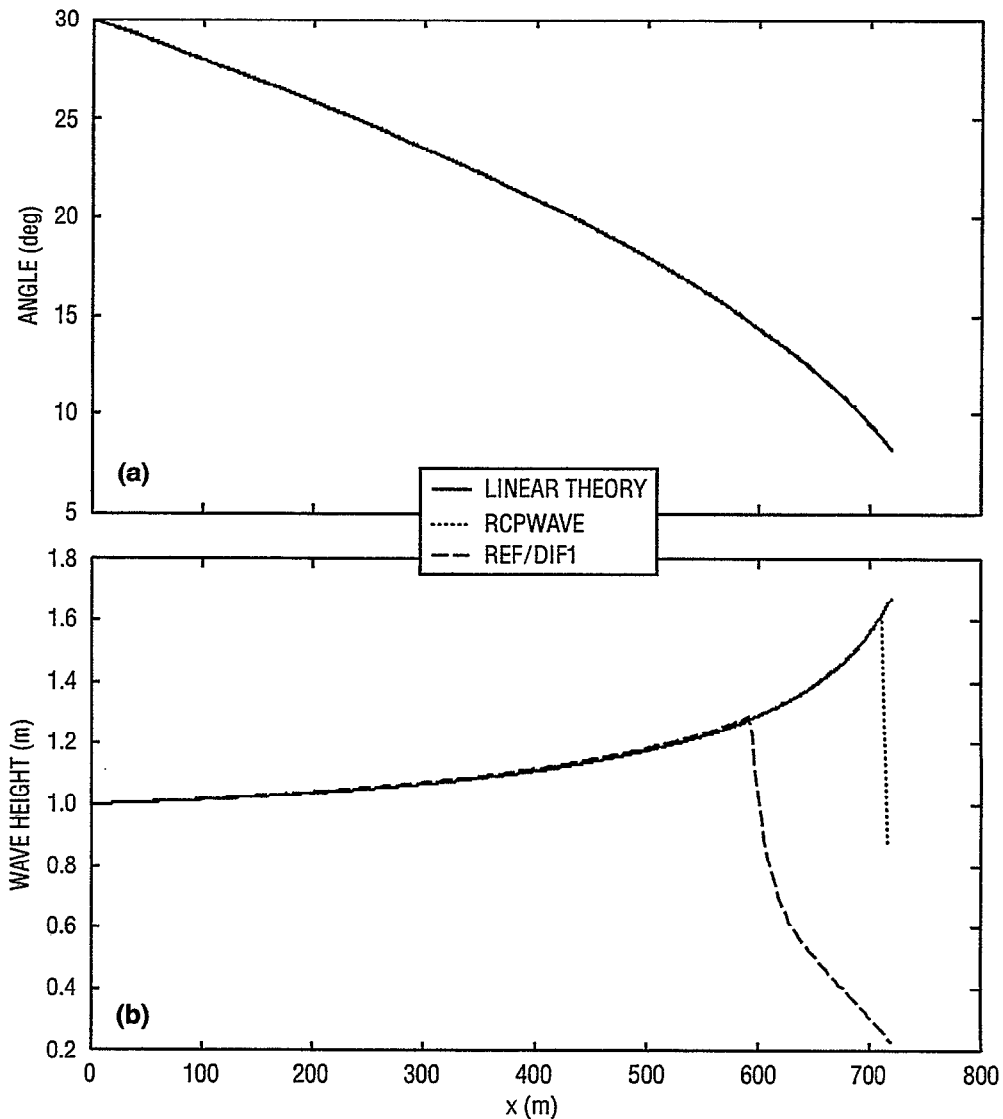


Fig. 2.6— Comparison of RCPWAVE and REF/DIF1 to linear shoaling and refraction theory, $T = 10$ s, $\theta = 30^\circ$, (a) angle comparison and (b) wave height comparison

Neither REF/DIF1 nor RCPWAVE diffracts waves into the sheltered region immediately behind the breakwater. Figure 2.21 shows instantaneous free surface pictures from both the analytical solution and REF/DIF1. The analytical solution shows how the wave is propagated right behind the breakwater near $x/L = 0$. This is not evident in the REF/DIF1 (wide-angle model) result; the area behind the breakwater in general is relatively quiet compared to that shown in the analytical solution. The effect of the partial reflection from the open boundary is evident as well in the model result, appearing as a traverse wave.

It is interesting that RCPWAVE does not propagate the wave behind the breakwater either, since it does not have any restriction on the angle of propagation. Figure 2.22 depicts the wave height field for RCPWAVE, REF/DIF1, and the analytic solution. Both REF/DIF1 and the analytic

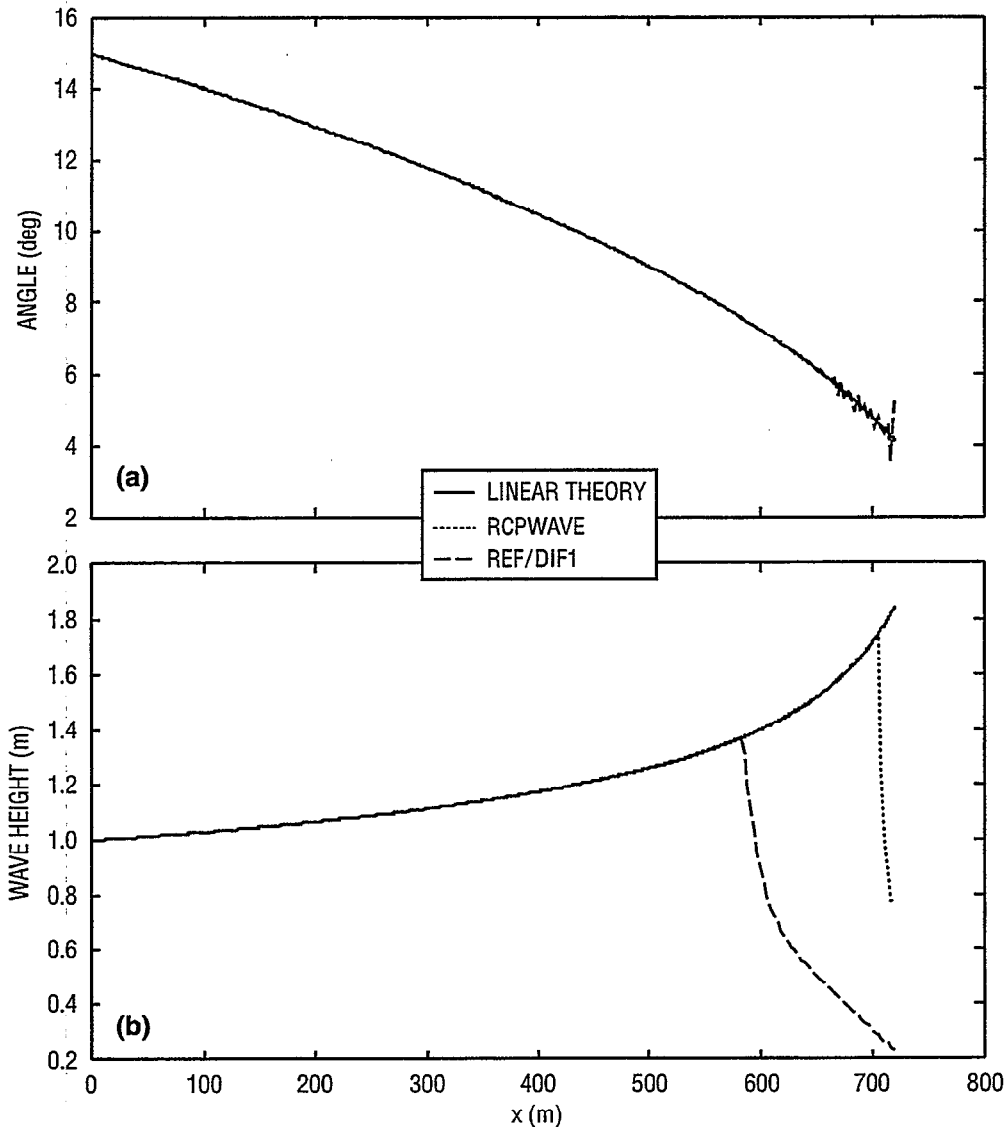


Fig. 2.7 — Comparison of RCPWAVE and REF/DIF1 to linear shoaling and refraction theory, $T = 17$ s, $\theta = 15^\circ$, (a) angle comparison and (b) wave height comparison

solution show about the same amount of spreading of energy into the lee of the breakwater. RCPWAVE, on the other hand, shows a strong gradient between the illuminated and sheltered regions; there almost seems to be an amplification of wave height near the boundary between these two regions that seems to grow downwave of the breakwater. This may be indicative of insufficient diffraction in RCPWAVE. As mentioned in Part 1, Sec. 2.5, Kirby (1988) demonstrated that the formulation of RCPWAVE caused oversmoothing of the wave amplitude comparisons of the model to the data of Berkhoff et al. (1982), particularly with respect to the lateral diffraction fringes. The explicit comparisons to this experiment will be discussed in a later section; this is pointed out here because it appears that the discussion by Kirby (1988) of RCPWAVE is relevant here. The oversmoothing of the lateral diffraction fringes pointed out by Kirby implies that diffraction is underpredicted; this explains the strong wave height gradient in the lee of the breakwater in the RCPWAVE results. Because these diffraction effects were smaller than expected, RCPWAVE results were compared to

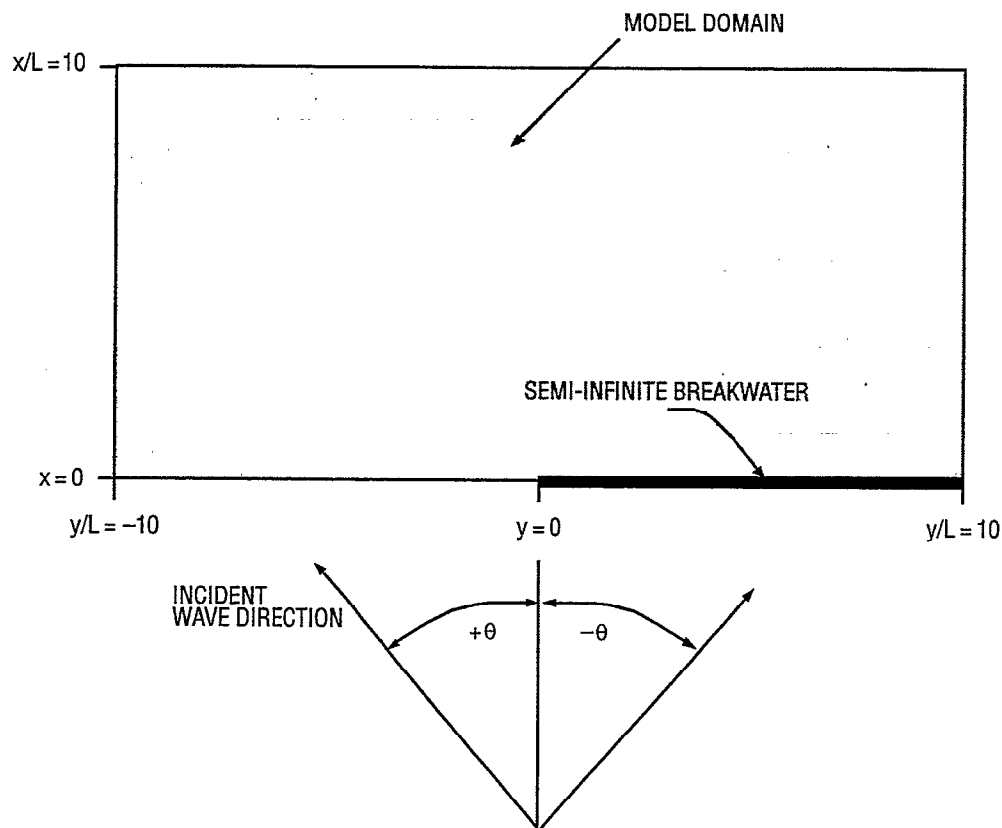


Fig. 2.8 — Layout of semi-infinite breakwater tests

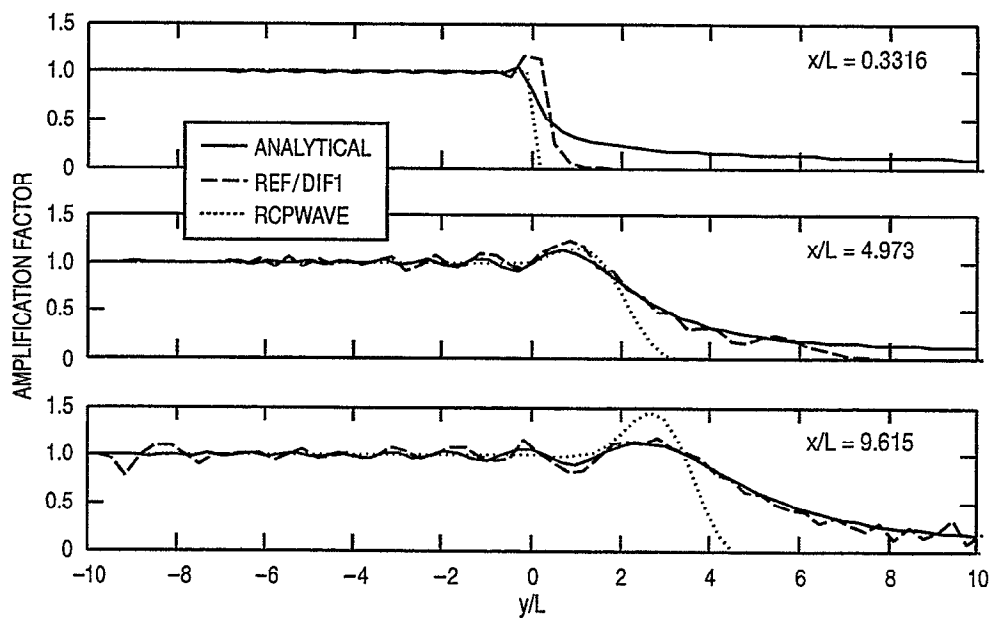


Fig. 2.9 — Comparison of wave amplification factors from REF/DIF1 and RCPWAVE to analytical solution, semi-infinite breakwater test, $\theta = -30^\circ$, x/L from 0.3316 to 9.615

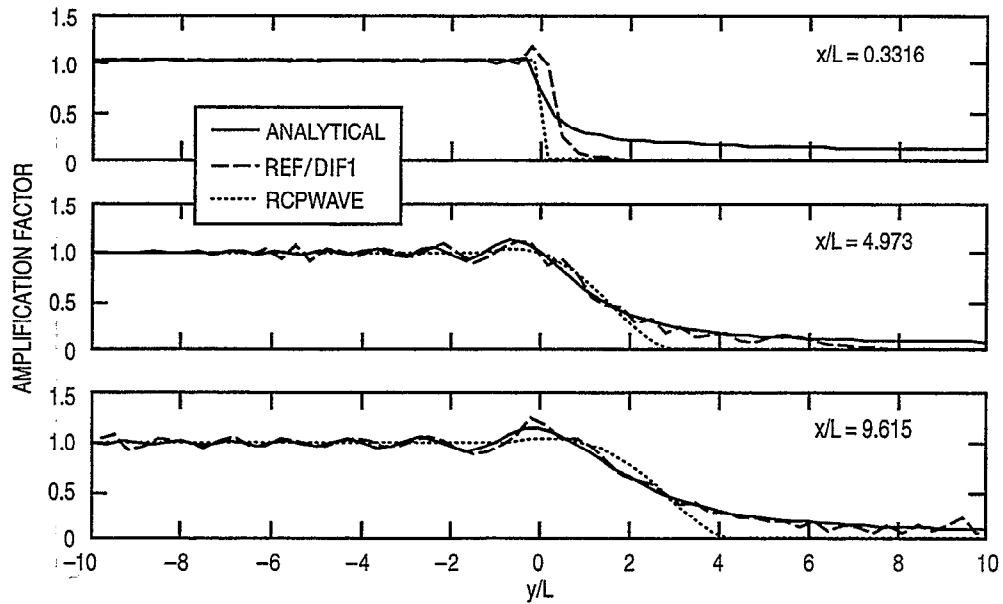


Fig. 2.10 — Comparison of wave amplification factors from REF/DIF1 and RCPWAVE to analytical solution, semi-infinite breakwater test, $\theta = -15^\circ$, x/L from 0.3316 to 9.615

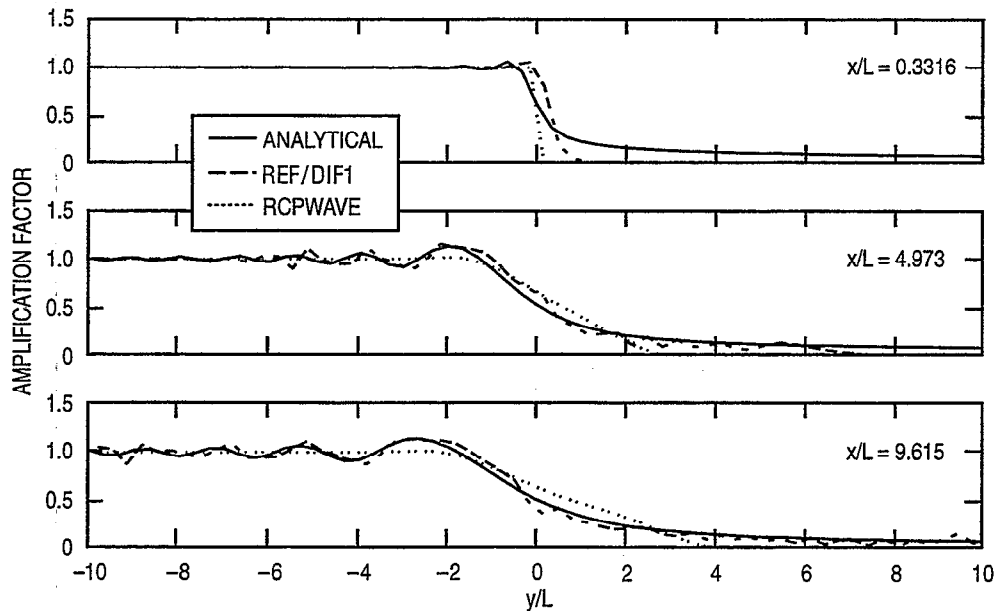


Fig. 2.11 — Comparison of wave amplification factors from REF/DIF1 and RCPWAVE to analytical solution, semi-infinite breakwater test, $\theta = 0^\circ$, x/L from 0.3316 to 9.615

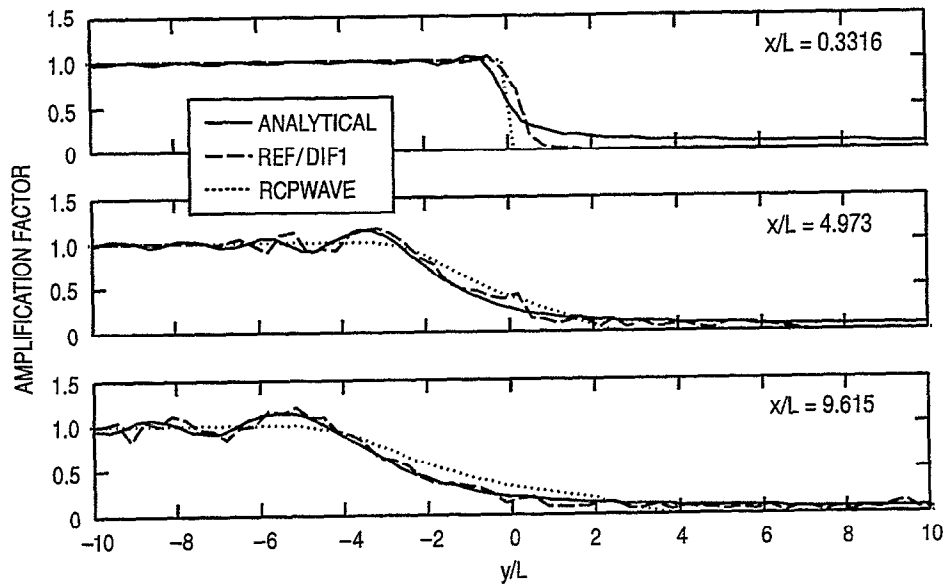


Fig. 2.12 — Comparison of wave amplification factors from REF/DIF1 and RCPWAVE to analytical solution, semi-infinite breakwater test, $\theta = 15^\circ$, x/L from 0.3316 to 9.615

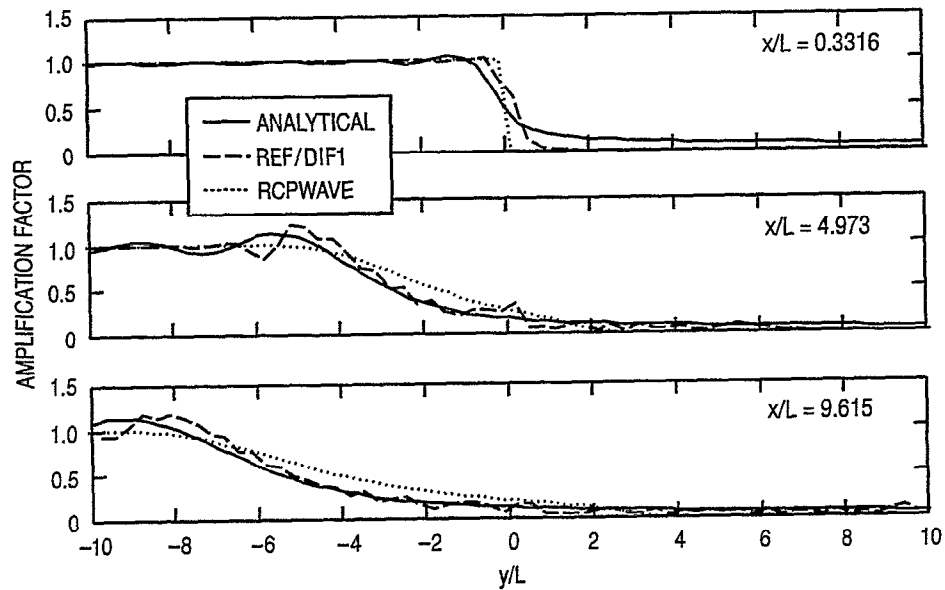


Fig. 2.13 — Comparison of wave amplification factors from REF/DIF1 and RCPWAVE to analytical solution, semi-infinite breakwater test, $\theta = 30^\circ$, x/L from 0.3316 to 9.615

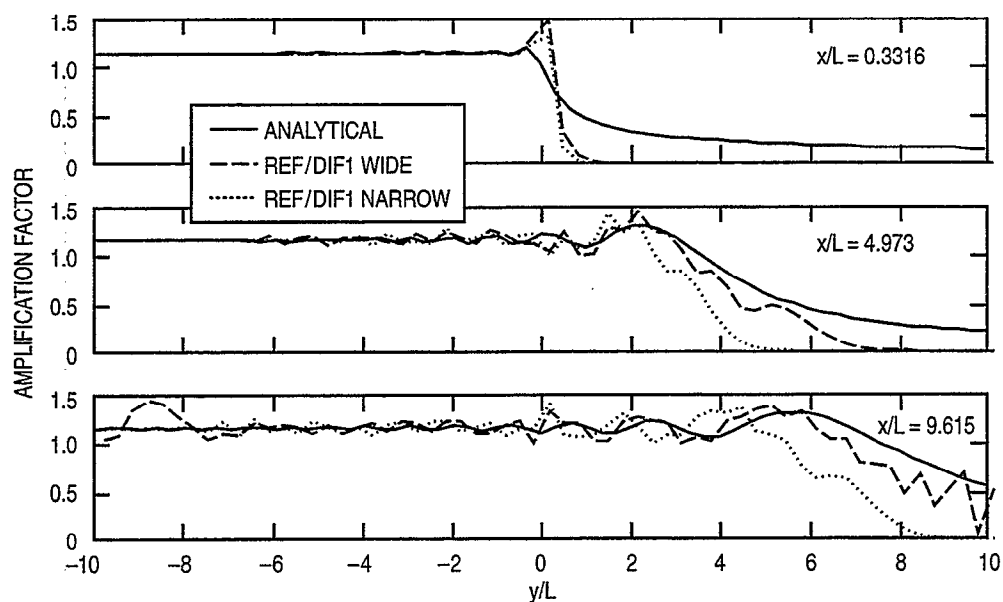


Fig. 2.14 — Comparison of wave amplification factors from wide-angle and narrow-angle REF/DIF1 to analytical solution, semi-infinite breakwater test, $\theta = -45^\circ$, x/L from 0.3316 to 9.615

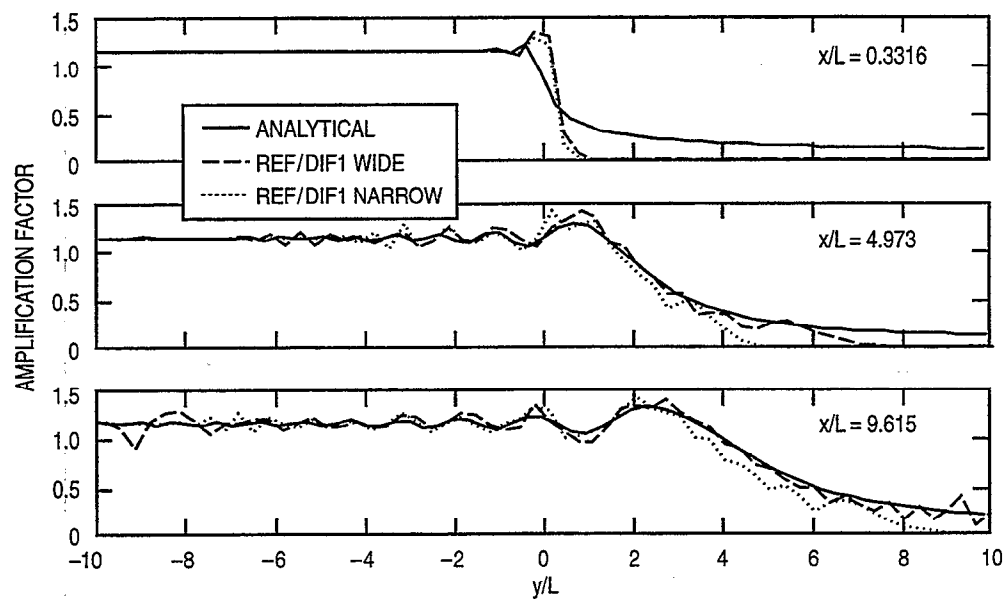


Fig. 2.15 — Comparison of wave amplification factors from wide-angle and narrow-angle REF/DIF1 to analytical solution, semi-infinite breakwater test, $\theta = -30^\circ$, x/L from 0.3316 to 9.615

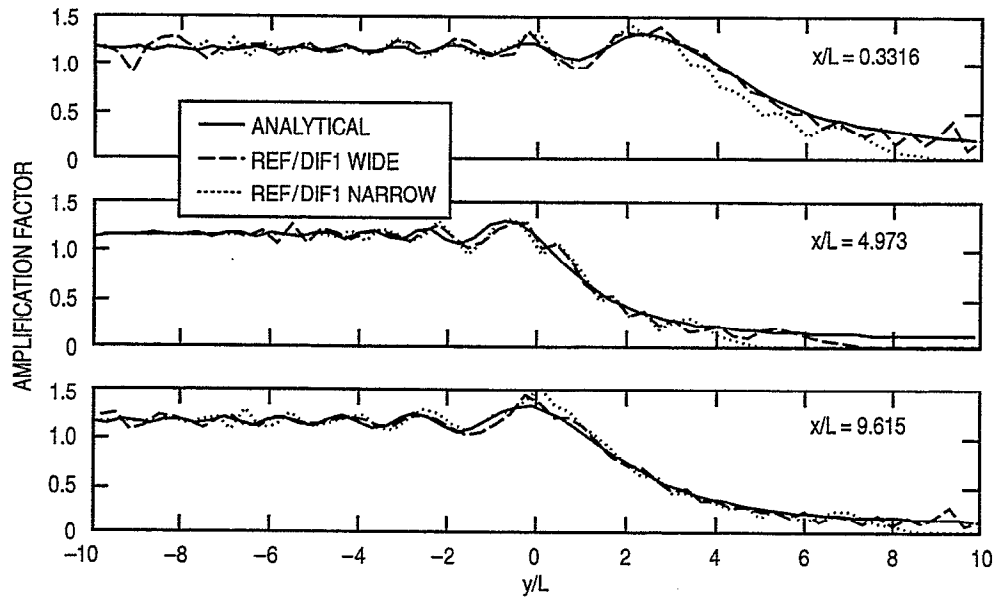


Fig. 2.16 — Comparison of wave amplification factors from wide-angle and narrow-angle REF/DIF1 to analytical solution, semi-infinite breakwater test, $\theta = -15^\circ$, x/L from 0.3316 to 9.615

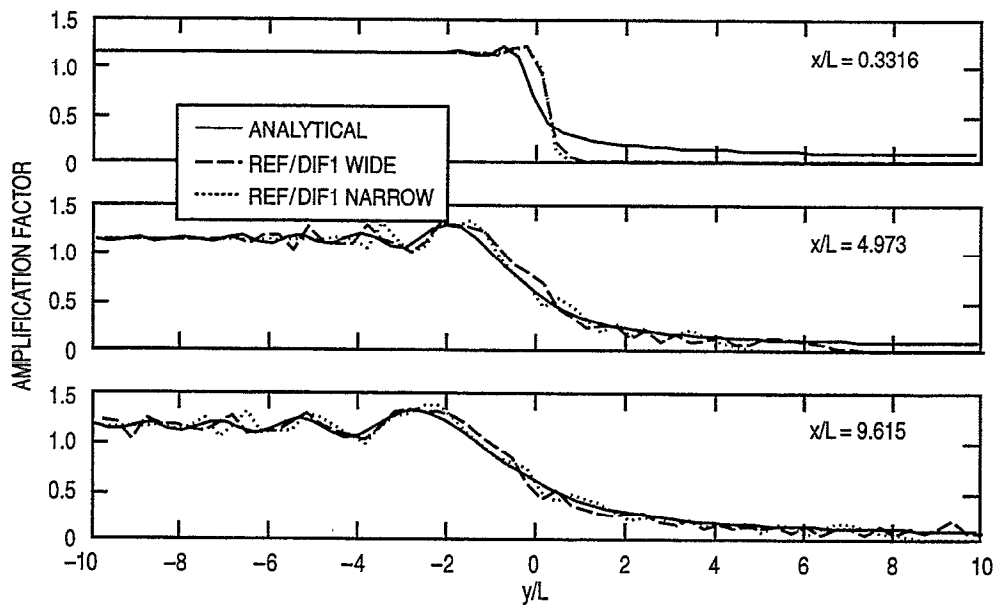


Fig. 2.17 — Comparison of wave amplification factors from wide-angle and narrow-angle REF/DIF1 to analytical solution, semi-infinite breakwater test, $\theta = 0^\circ$, x/L from 0.3316 to 9.615

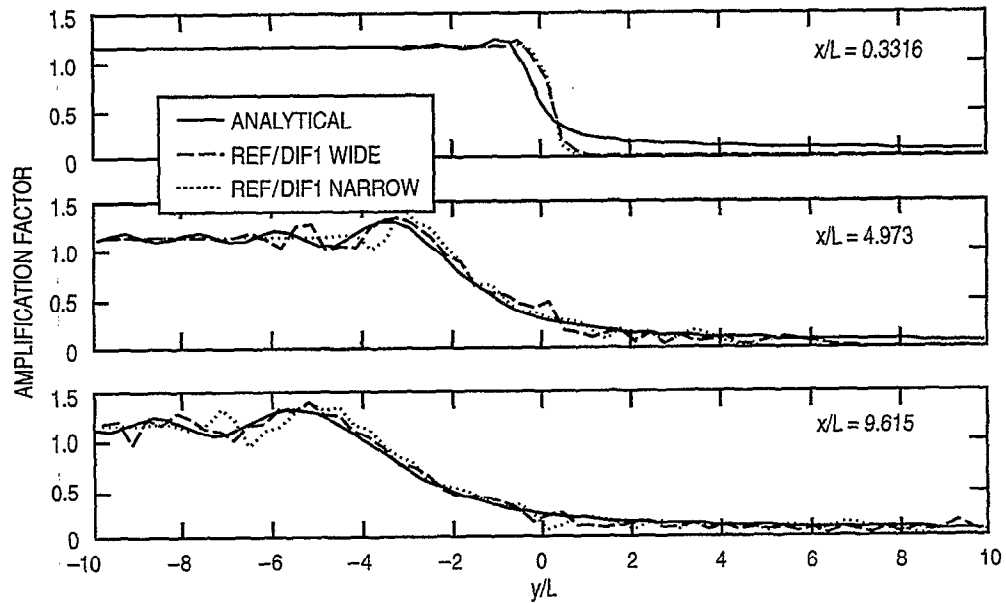


Fig. 2.18 — Comparison of wave amplification factors from wide-angle and narrow-angle REF/DIF1 to analytical solution, semi-infinite breakwater test, $\theta = 15^\circ$, x/L from 0.3316 to 9.615

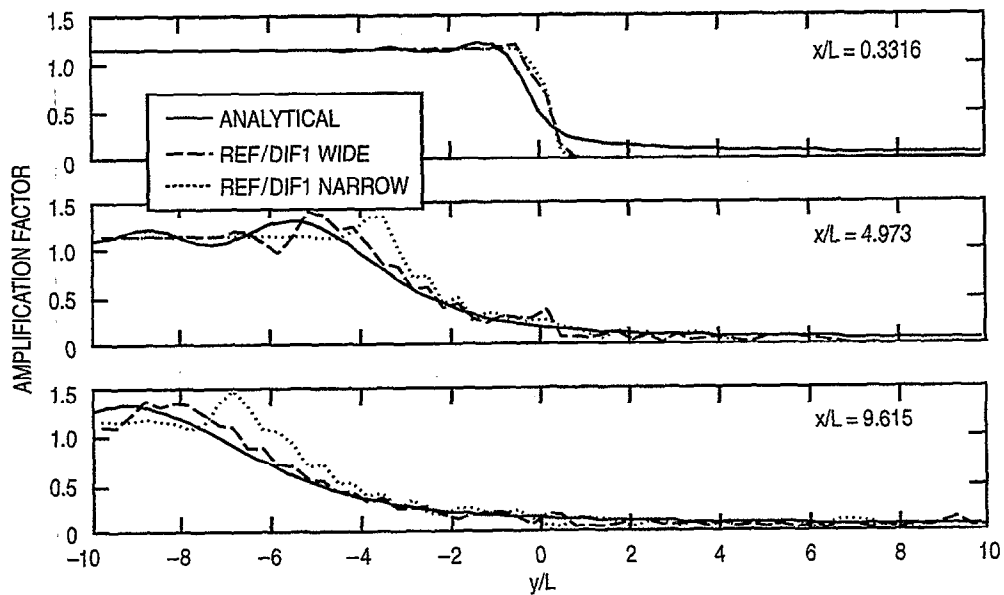


Fig. 2.19 — Comparison of wave amplification factors from wide-angle and narrow-angle REF/DIF1 to analytical solution, semi-infinite breakwater test, $\theta = 30^\circ$, x/L from 0.3316 to 9.615

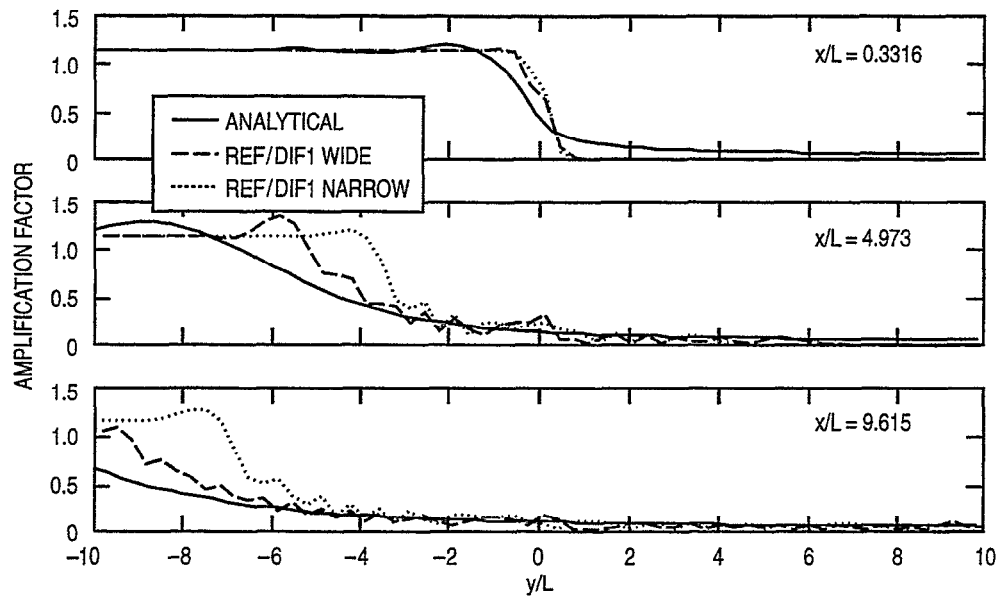


Fig. 2.20 — Comparison of wave amplification factors from wide-angle and narrow-angle REF/DIF1 to analytical solution, semi-infinite breakwater test, $\theta = 45^\circ$, x/L from 0.3316 to 9.615

those generated with diffraction effects disabled (Fig. 2.23). It is apparent that, save for some attenuation of the wave height with diffraction enabled, there is very little difference between the spatial patterns of the two results. The demonstrated lateral spread of energy in the “no diffraction” case is likely a purely numerical artifact; there is no physical process other than diffraction that will spread energy behind the breakwater otherwise.

2.1.2.2 Diffraction by a Breakwater Gap

Another scenario was tested in which the effects of diffraction can be isolated: that of a breakwater with a small gap. The model scenario is shown in Fig. 2.24. Analytical solutions have been derived by Penney and Price (1952) for the case of a breakwater gap greater than 1 wavelength; these solutions were generated by superimposing the two solutions for the individual breakwaters. Sobey and Johnson (1986) revisited the problem and developed a solution valid for any arbitrary gap width.

In this case, the equation of Penney and Price (1952) was used for comparison to the models. If it is assumed that the solution to the Laplace equation (the governing equation for water waves) has a solution of the following form:

$$\phi(x, y, z, t) = AF(x, y) \cosh k(h+z)e^{-i\omega t}, \quad (2.4)$$

where A is an amplitude and F is a complex function. Then an equation can be written in terms of the function F by substituting Eq. (2.4) into the Helmholtz equation, leading to:

$$\frac{\partial^2 F}{\partial x^2} + \frac{\partial^2 F}{\partial y^2} + k^2 F = 0. \quad (2.5)$$

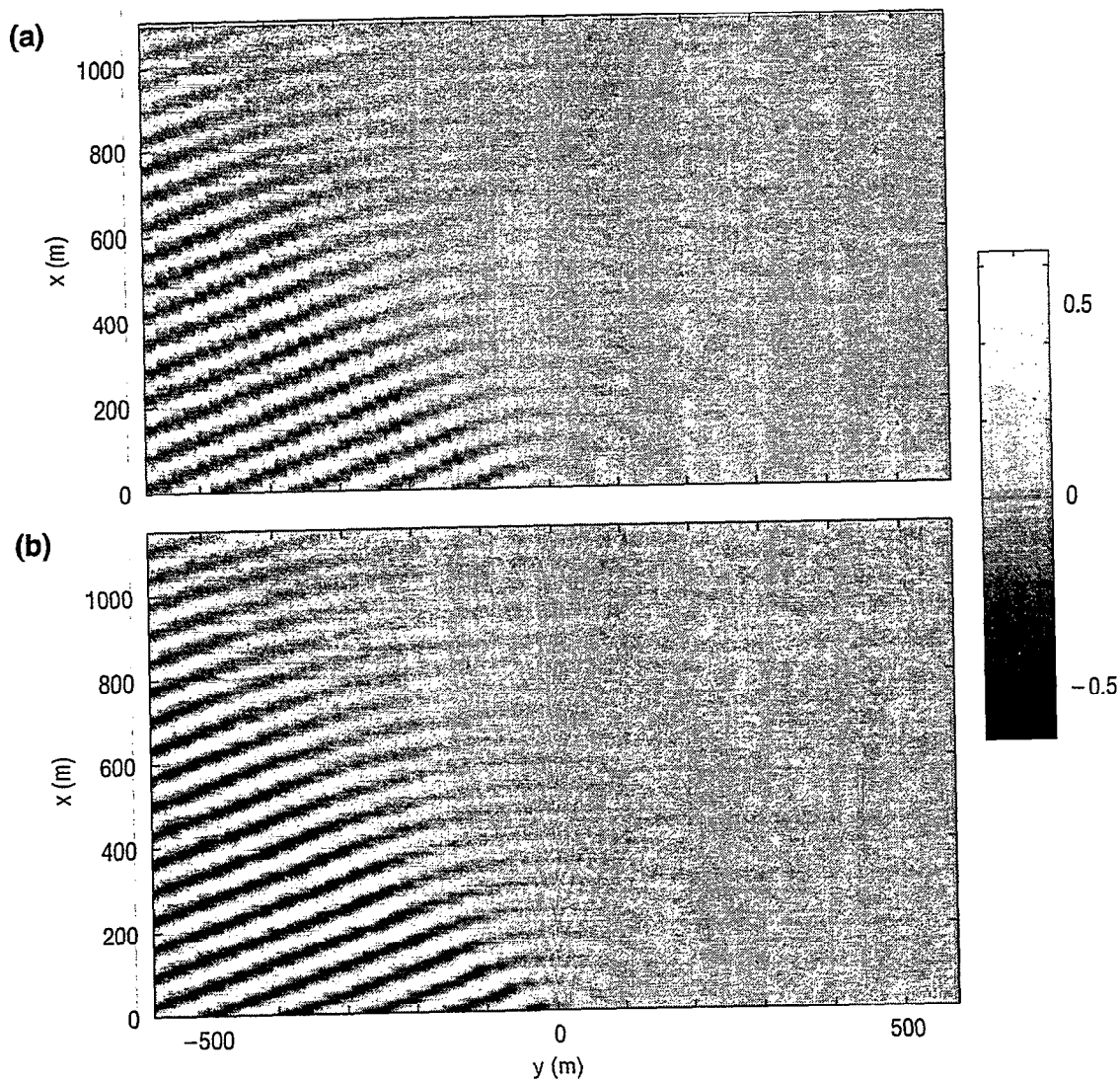


Fig. 2.21 — Free surface from analytical solution and wide-angle REF/DIF1, semi-infinite breakwater test, $\theta = 30^\circ$, (a) analytical solution and (b) REF/DIF1

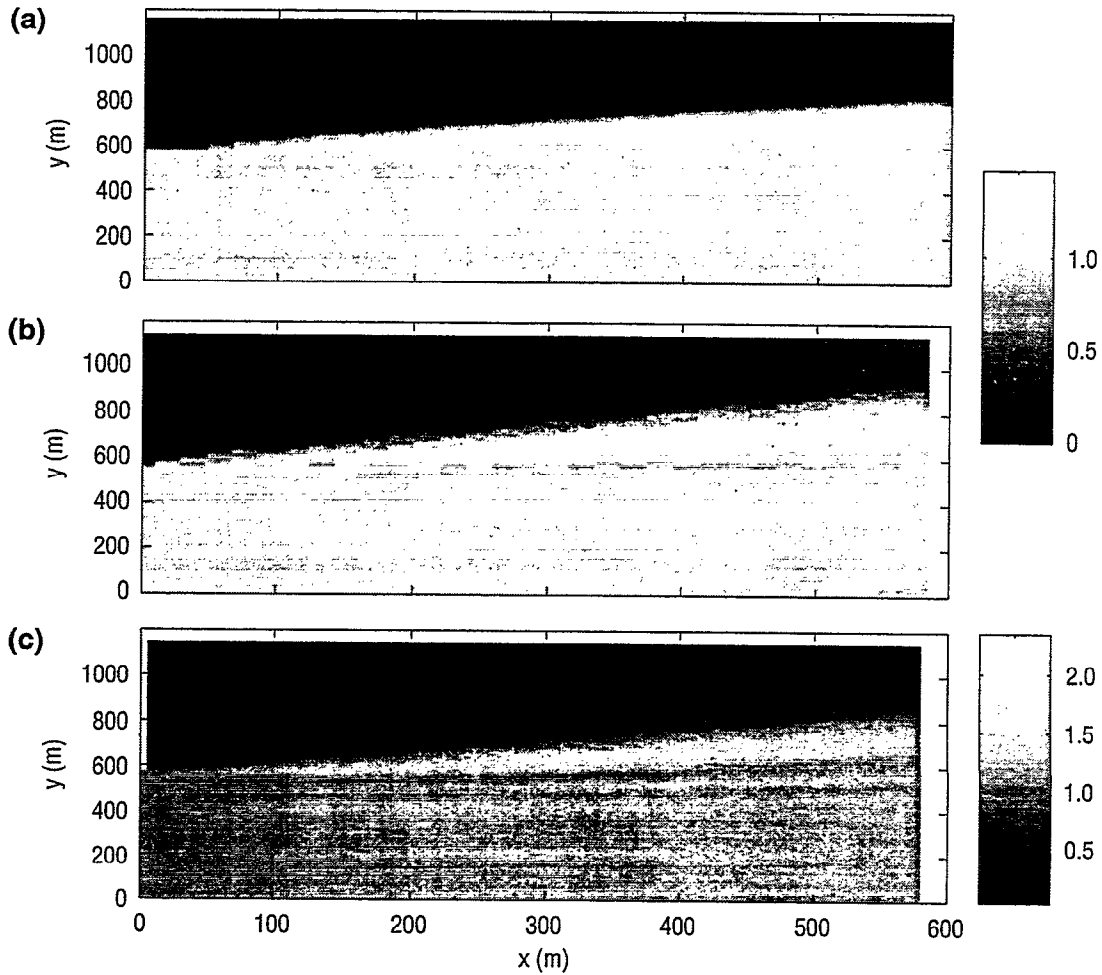


Fig. 2.22 — Comparison of wave height fields from RCPWAVE, REF/DIF1, and analytic solution, semi-infinite breakwater test, (a) RCPWAVE, (b) REF/DIF1, and (c) analytic solution

Penney and Price (1952) applied the boundary conditions appropriate for a semi-infinite breakwater and obtained the following solution:

$$F(x,y) = \frac{(1+i)}{2} \left(e^{-ikx} \int_{\infty}^{\sigma} e^{-\frac{1}{2}i\pi u^2} du \pm e^{-ikx} \int_{-\infty}^{\sigma} e^{-\frac{1}{2}i\pi u^2} du \right), \quad (2.6)$$

where

$$\sigma = \sqrt{\frac{4}{L}(r-x)} \quad (2.7)$$

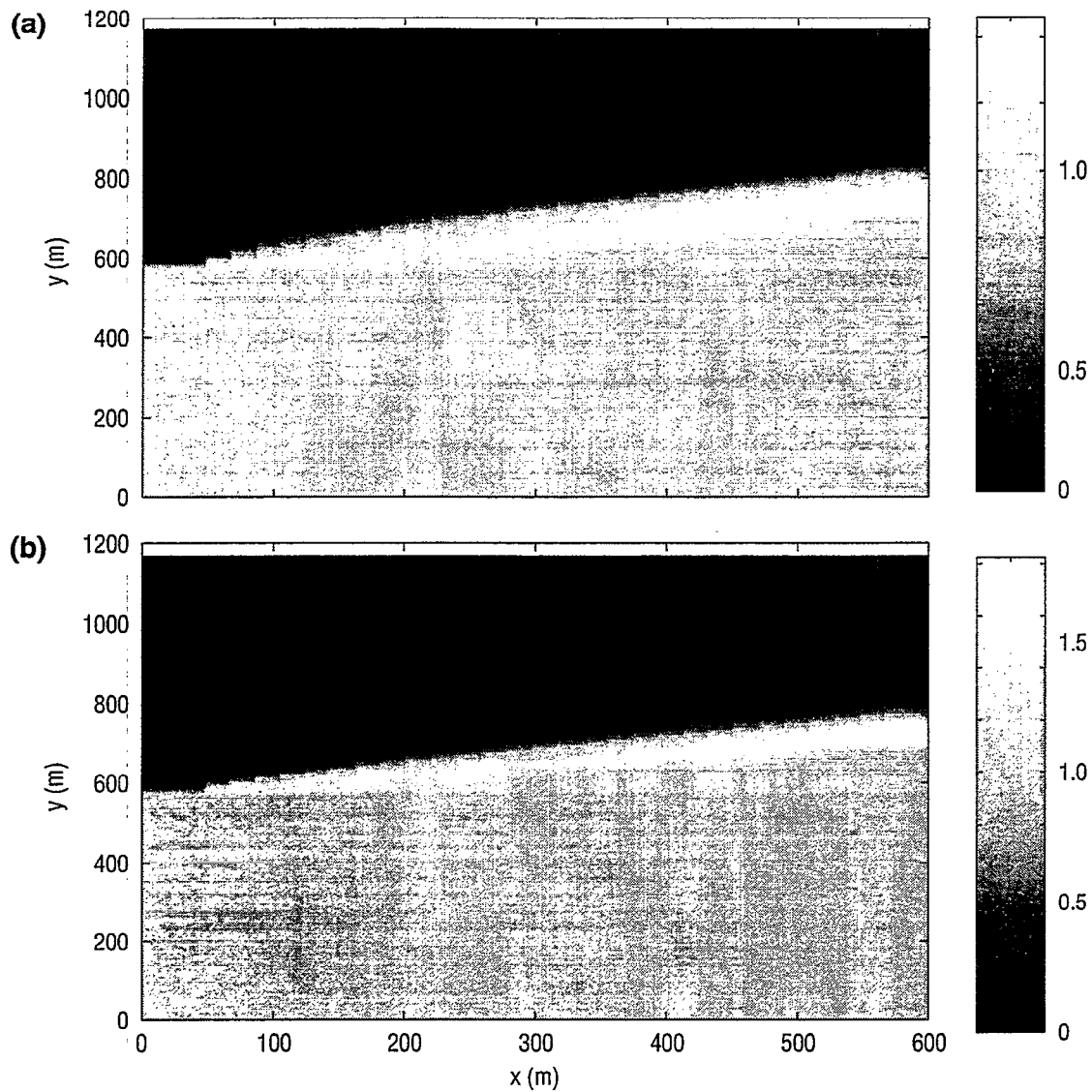


Fig. 2.23 — Comparison of wave height fields from RCPWAVE with diffraction and without diffraction, semi-infinite breakwater test, (a) RCPWAVE with diffraction and (b) RCPWAVE without diffraction

and

$$\sigma = \sqrt{\frac{4}{L}(r+x)} \quad (2.8)$$

where r is the radial distance from the tip of the breakwater and L is the wavelength. The approximate solution for a breakwater gap can be obtained by superposition. The Penney and Price solution (Eq. (2.6)) is adapted from the Sommerfeld solution for light diffraction (Sommerfeld 1896).

For this simulation, the following modeling parameters were used:

Wave period: 9.3 s

Water depth: 6.1 m

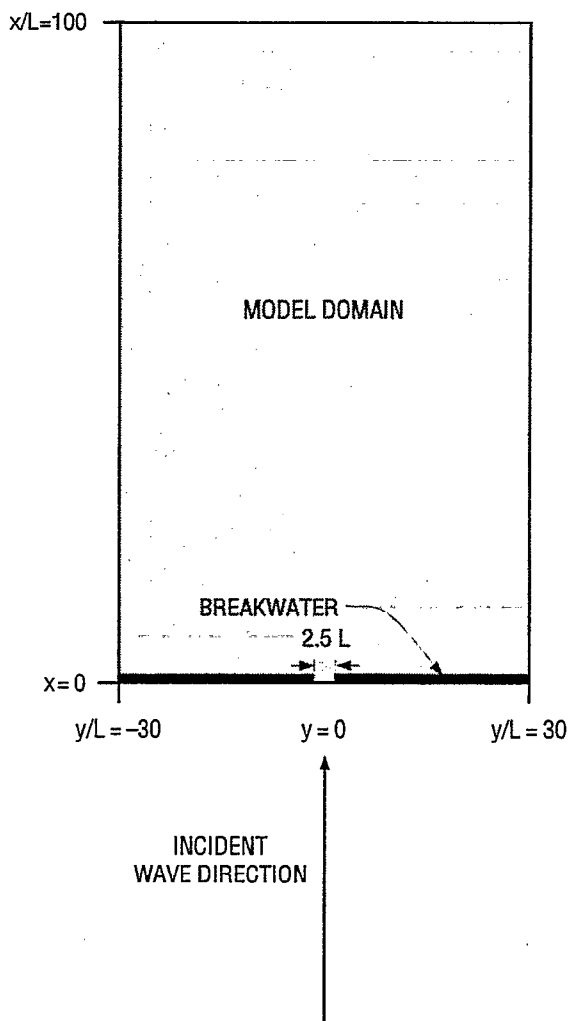


Fig. 2.24 — Layout of breakwater gap tests

Domain size: 7000×4200 m or approximately $100 \times 60 L$ in x and y , respectively

Grid resolution: $\Delta x = 20$ m, $\Delta y = 19$ m

Incident angle: 0°

It was determined that model performance with breakwater gaps of around 1 wavelength was quite poor. For a breakwater gap width equal to 2.5 times the incident wavelength, output from the models was improved. Model comparisons to the analytical solution are shown in Figs. 2.25–2.27.

In general, REF/DIF1 results compare much better with the analytical solution than output from RCPWAVE. The REF/DIF1 results show some high-frequency oscillations in the wave heights that are not seen in the analytical solution, though the mean of these oscillations seems to match the analytical solutions quite closely. These oscillations could be due to the lack of sufficient resolution in y , or (more likely) to forward scattering caused by the open lateral boundaries. This suggests that care is required in applying these open boundary conditions in general situations. RCPWAVE results, on the other hand, show very little diffusion of wave energy from areas of high energy to areas of low energy. Wave heights farther into the domain take on an odd, double-peaked form.

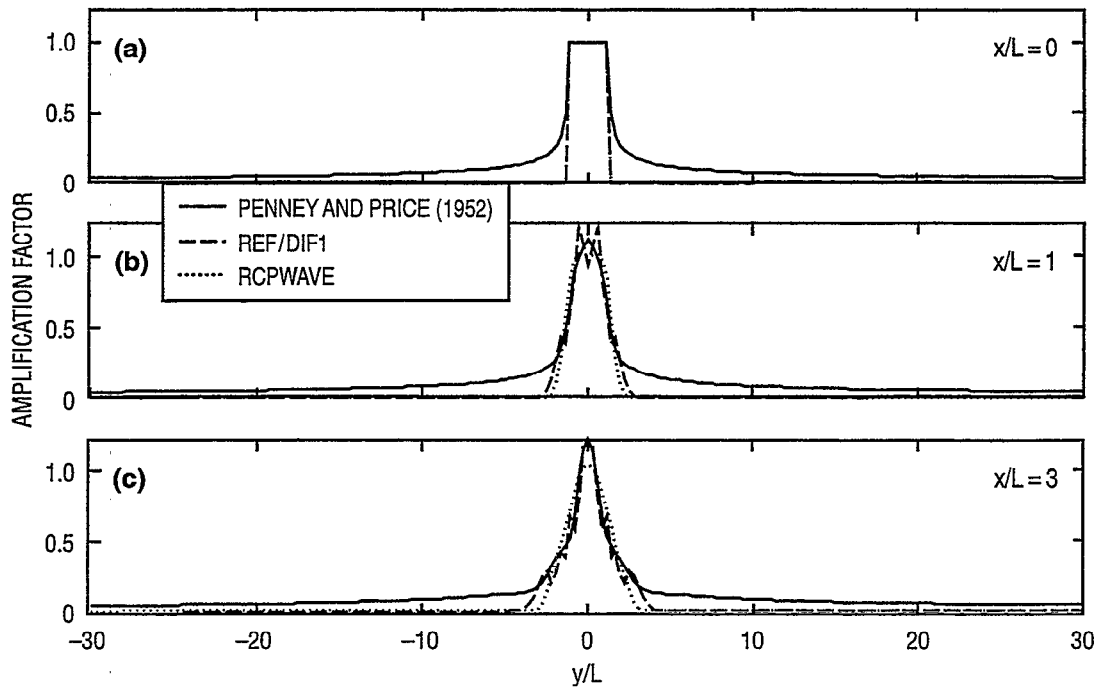


Fig. 2.25 — Comparison of wave amplification factors from REF/DIF1 and RCPWAVE to analytic solution, breakwater gap test, (a) $x/L = 0$, (b) $x/L = 1$, and (c) $x/L = 3$

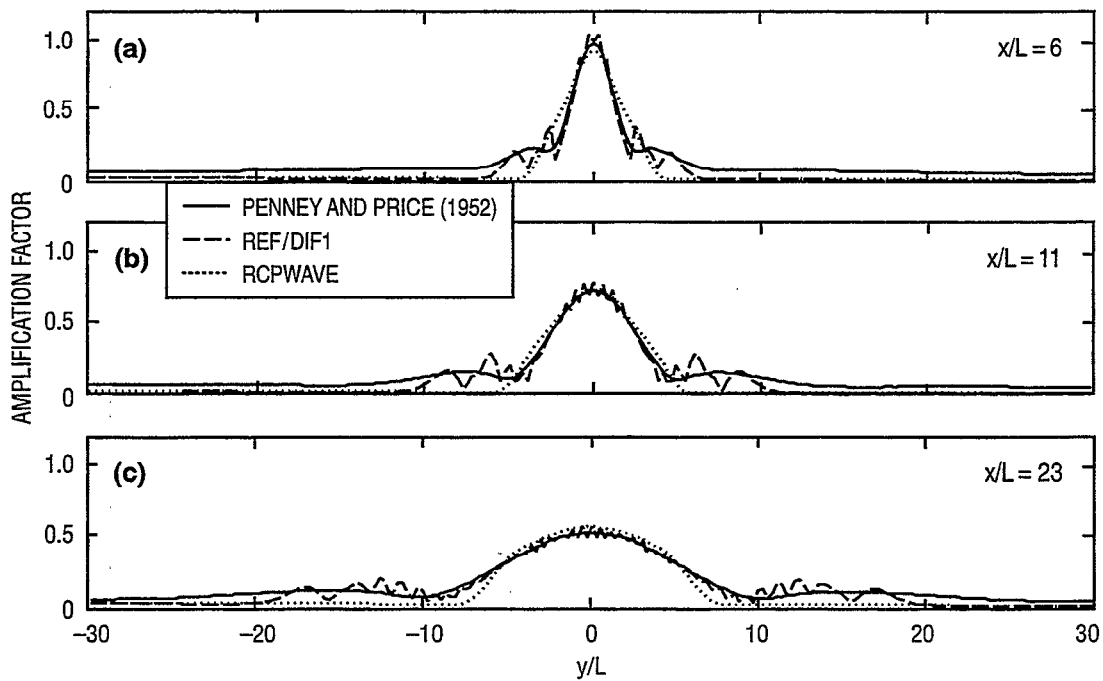


Fig. 2.26 — Comparison of wave amplification factors from REF/DIF1 and RCPWAVE to analytic solution, breakwater gap test, (a) $x/L = 6$, (b) $x/L = 11$, and (c) $x/L = 23$

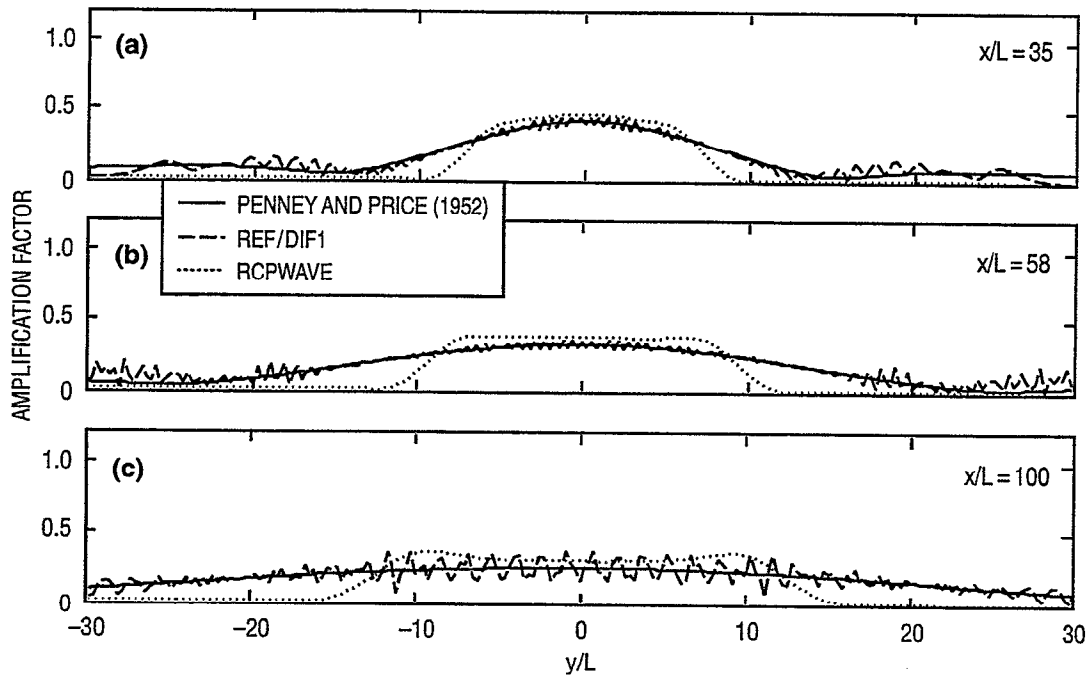


Fig. 2.27 — Comparison of wave amplification factors from REF/DIF1 and RCPWAVE to analytic solution, breakwater gap test, (a) $x/L = 35$, (b) $x/L = 58$, and (c) $x/L = 100$

3.0 MODEL TESTS WITH IDEALIZED BATHYMETRIES

In this section, testing the wave models with more complex bathymetry begins. No analytical solutions or experimental results exist for the cases in this section; these bathymetries are used as a means for testing model stability. This aspect of wave modeling will be addressed more quantitatively in a later section.

For this series of tests, idealized bathymetries are used that are somewhat representative of natural conditions. The first case involves two offset bars superimposed on a planar beach used for the linear wave theory test of Sec. 2.1 (Fig. 3.1). The second case involves two colinear bars and a shoal placed just seaward of the channel between the bars (Fig. 3.4).

Bedform amplitudes (the bedform heights above the plane) used were varied to test the stability limits of RCPWAVE on complex bathymetries.

Offshore depth: 7 m
 Slope of planar beach: 0.009
 Bedform amplitudes: 1, 2, and 3.4 m
 Wave period: $T = 3, 7, \text{ and } 17$ s
 Wave angle of approach: $\theta = -30^\circ, 0^\circ, 30^\circ, \text{ and } 60^\circ$
 Domain size: 720×720 m
 Grid resolution: $\Delta x = \Delta y = 3$ m
 Wave height at offshore boundary: $H = 1$ m

With either type of bathymetry, RCPWAVE failed to converge to a solution with longer waves unless very small bedforms were used. For example, with $T = 17$ s, a bedform amplitude of 0.06 m

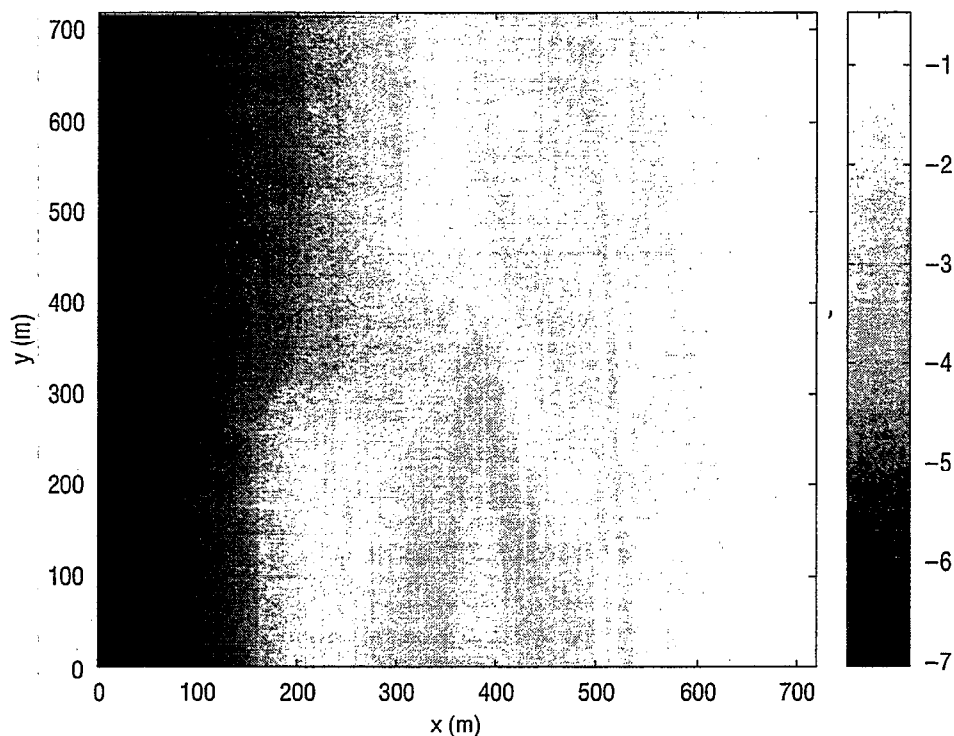


Fig. 3.1 — Layout of bathymetry with offset bars

was the largest feature height for a converged solution to be possible. This difficulty with convergence is more a consequence of the convergence scheme used rather than the governing equations themselves; the iteration of the scheme on the diffraction-affected wave number uses the refraction-only wave number as the initial guess for the entire domain rather than using the diffraction-influenced wave number of the prior row for initialization.

In the case of the offset bars, wave height amplification results exhibited the expected, focusing on wave energy behind the ends of the bars caused by refraction. Figure 3.2 shows a comparison of results from RCPWAVE and REF/DIF1. It is apparent that RCPWAVE yielded more focusing behind the shoals than REF/DIF1, a result of a weaker diffraction effect in RCPWAVE. Longer waves resulted in more refraction and, thus, more focusing of wave energy; this is seen in Fig. 3.3, in which the $T = 3$ s wave has a smaller focus region than the $T = 17$ s wave.

Figure 3.4 shows the bathymetry depicting the colinear bars and offshore shoal. A comparison between RCPWAVE and REF/DIF1 results for this case is shown in Fig. 3.5. Again, as before, it is apparent that there is overall less focusing in the REF/DIF1 results than in the RCPWAVE output; this is again due to the underprediction of wave diffraction in RCPWAVE.

4.0 COMPARISON OF MODELS TO LABORATORY EXPERIMENTS

Comparisons of the models to analytical solutions are instructive in that they can reveal shortcomings in modeling the basic physics. In this section, the models are compared to laboratory

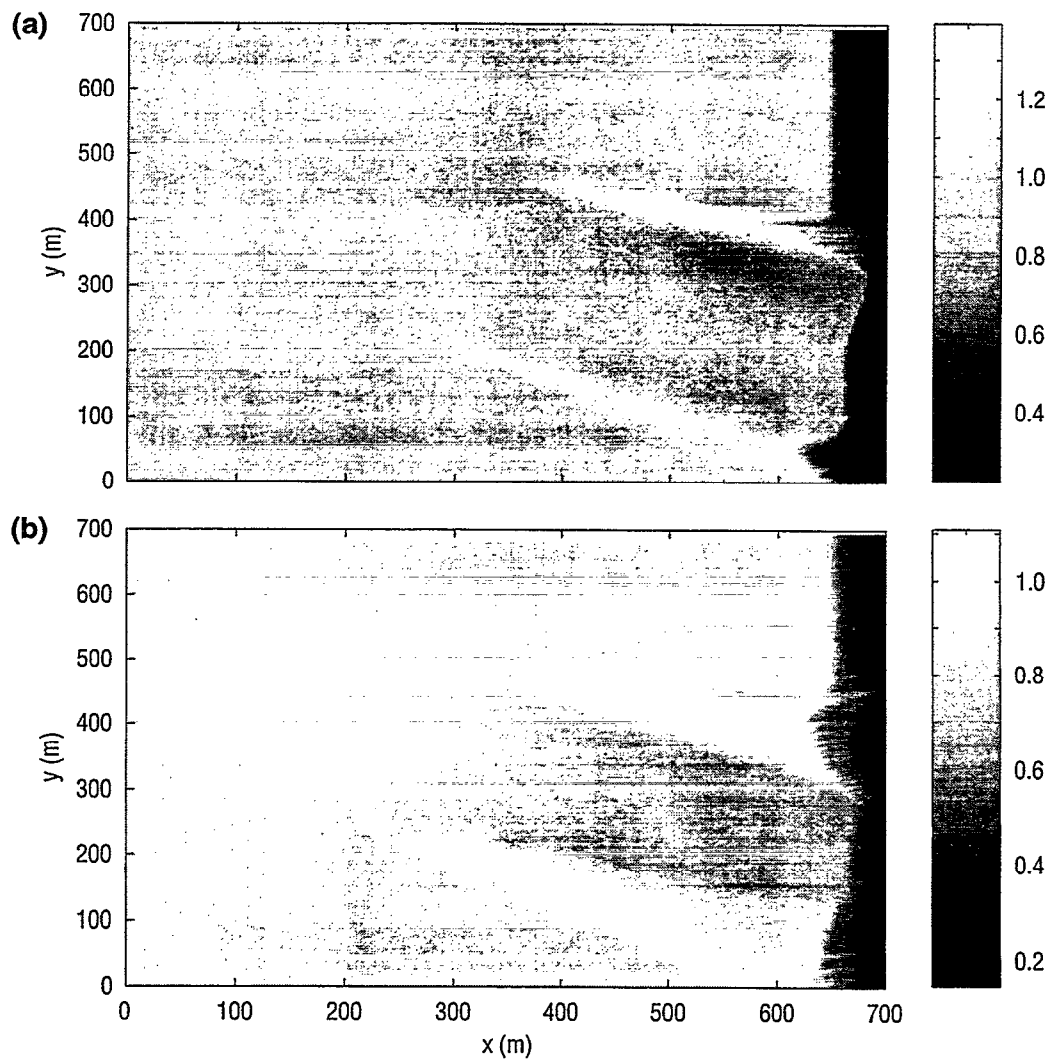


Fig. 3.2 — Wave height amplification factors from RCPWAVE and REF/DIF1, offset bars case, (a) RCPWAVE and (b) REF/DIF1

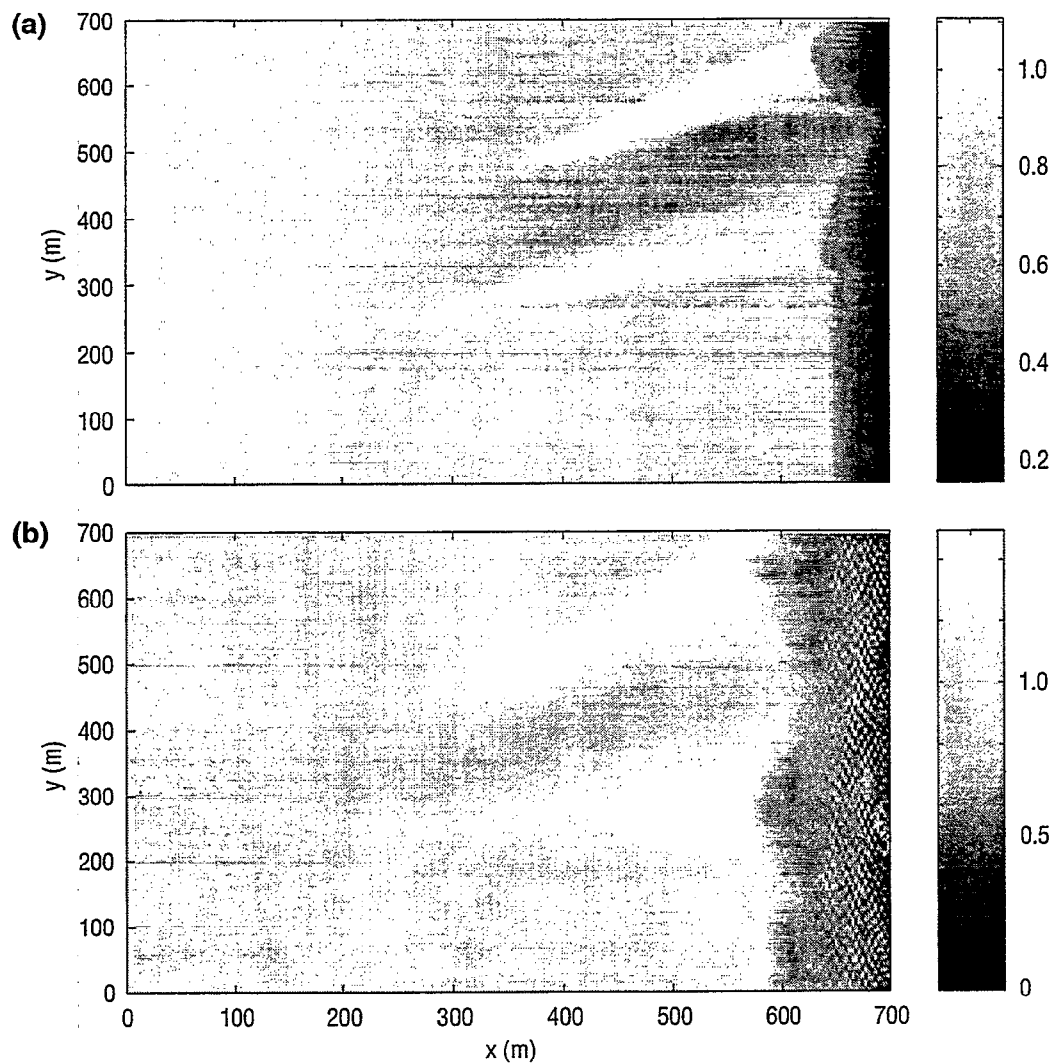


Fig. 3.3 — Wave height amplification factors from REF/DIF1, offset bars case, (a) $T = 3$ s and (b) $T = 17$ s

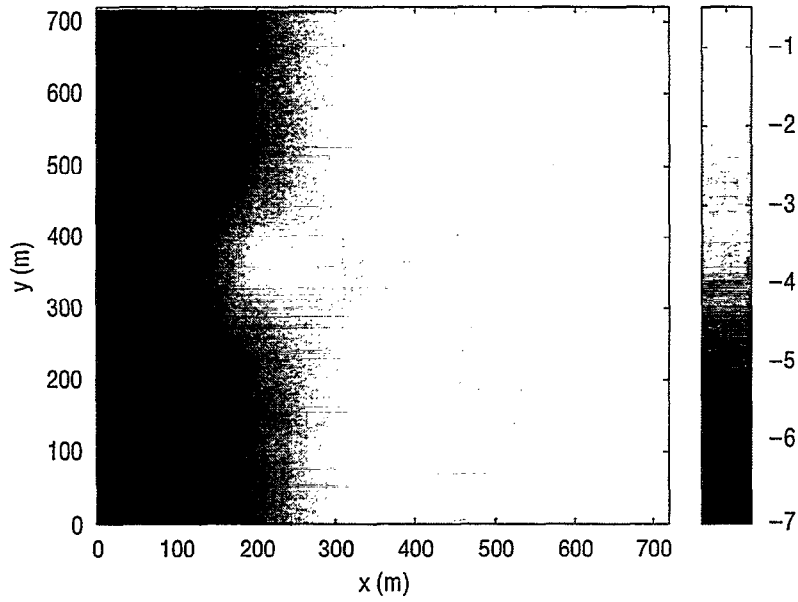


Fig. 3.4 — Layout of bathymetry with two bars and shoal

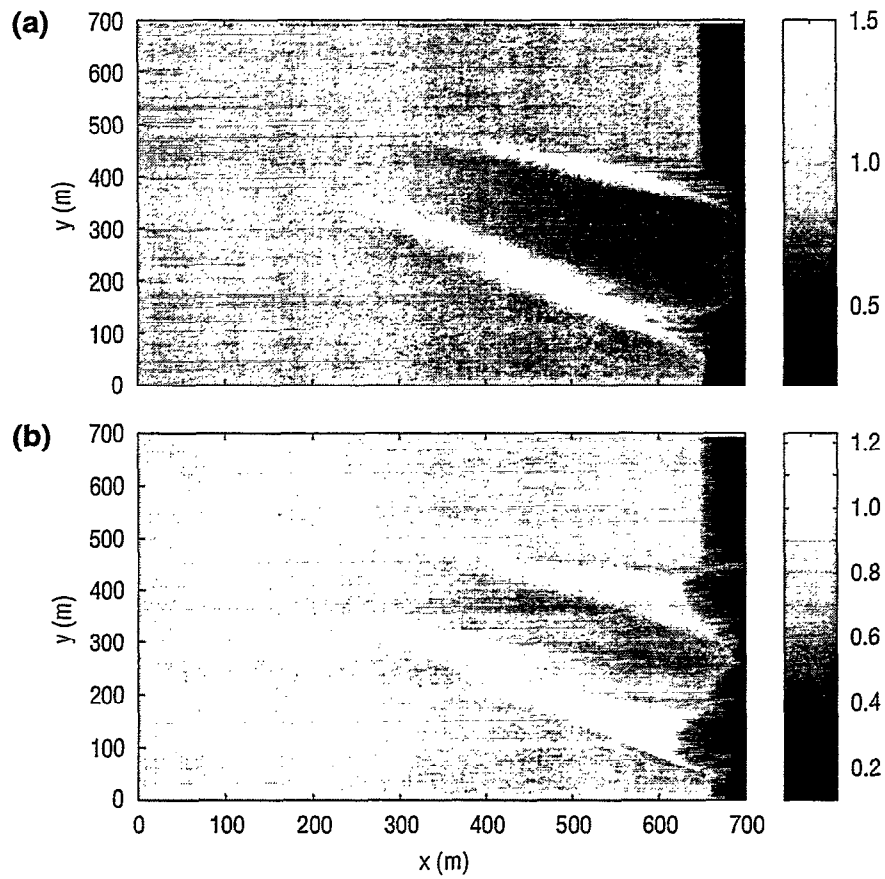


Fig. 3.5 — Wave height amplification factors from RCPWAVE and REF/DIF1, offset bars case, (a) RCPWAVE and (b) REF/DIF1

cases. These are scenarios where analytic solutions may not exist, yet still remain a controlled environment for checking model physics.

4.1 Berkhoff-Booij-Radder Shoal Experiment

Berkhoff et al. (1982) conducted a series of experiments of wave propagation over a submerged elliptical shoal resting on a plane beach. This experimental setup provides a scenario where both refraction and diffraction are significant. The experimental bathymetry and gauge locations are shown in Fig. 4.1.

Domain size: 25×25 m

Grid resolution: $\Delta x = \Delta y = 0.25$ m

Wave height at boundary: $H = 0.0464$ m

Wave period: $T = 1$ s

Wave angle at boundary: $\theta = 0^\circ$

The REF/DIF1 model was run with both the linear and nonlinear dispersion relationships. The nonlinear relationship used was the Stokes-Hedges composite dispersion relation described in Part 1.

Contours of wave height output from the models are shown in Figs. 4.2–4.4. The normalized wave height output from RCPWAVE (Fig. 4.2) shows a much narrower distribution than those from either the linear REF/DIF1 (Fig. 4.3) or the weakly nonlinear REF/DIF1 (Fig. 4.4). It can also be seen that the diffraction fringes on either side of the shoal, present in the REF/DIF1 results, are missing in the RCPWAVE output. This is consistent with the underprediction of diffraction present in the semi-infinite breakwater scenario.

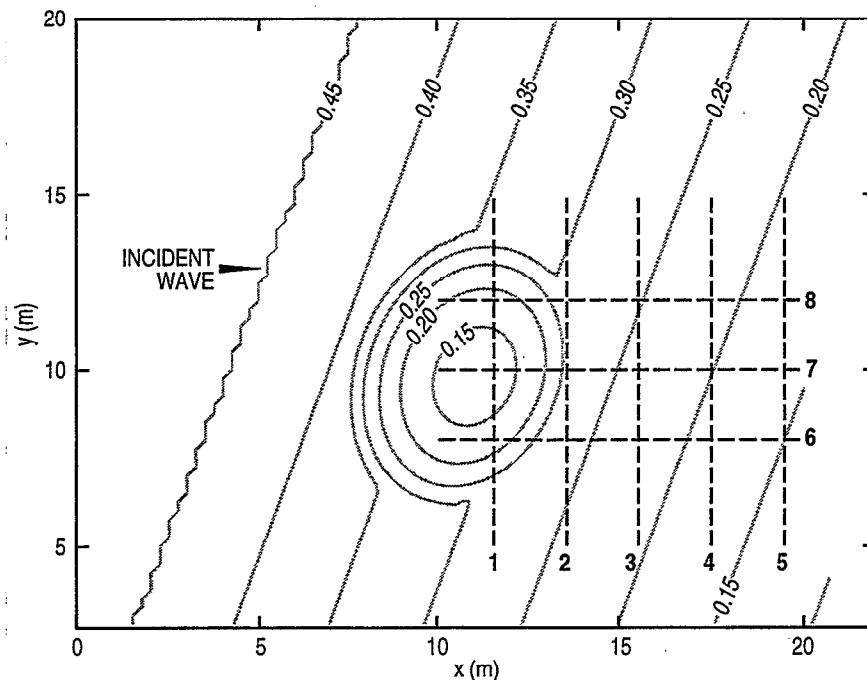


Fig. 4.1 — Layout of Berkhoff-Booij-Radder elliptical shoal experiment; dashed lines indicate wave gauge transects

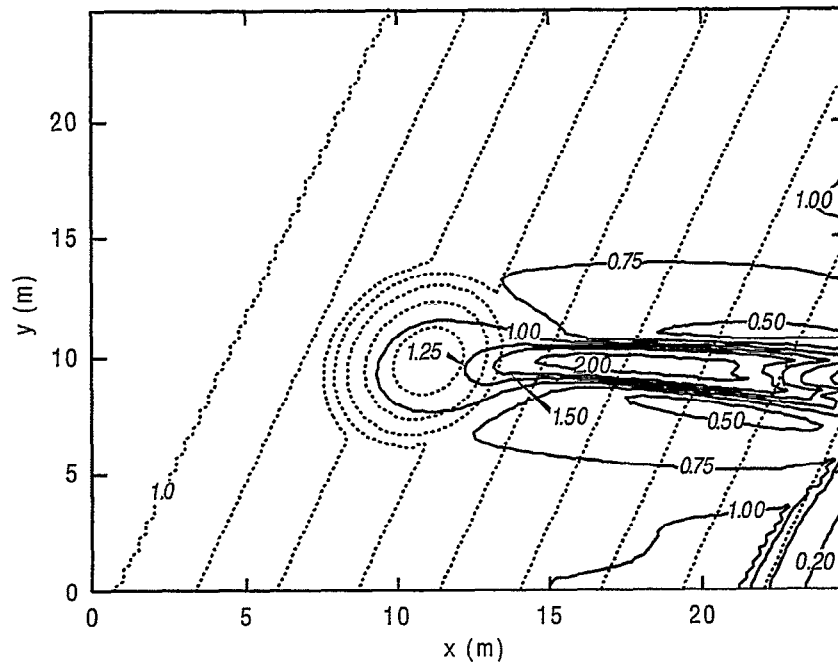


Fig. 4.2 — Normalized wave height contours from RCPWAVE, elliptical shoal experiment

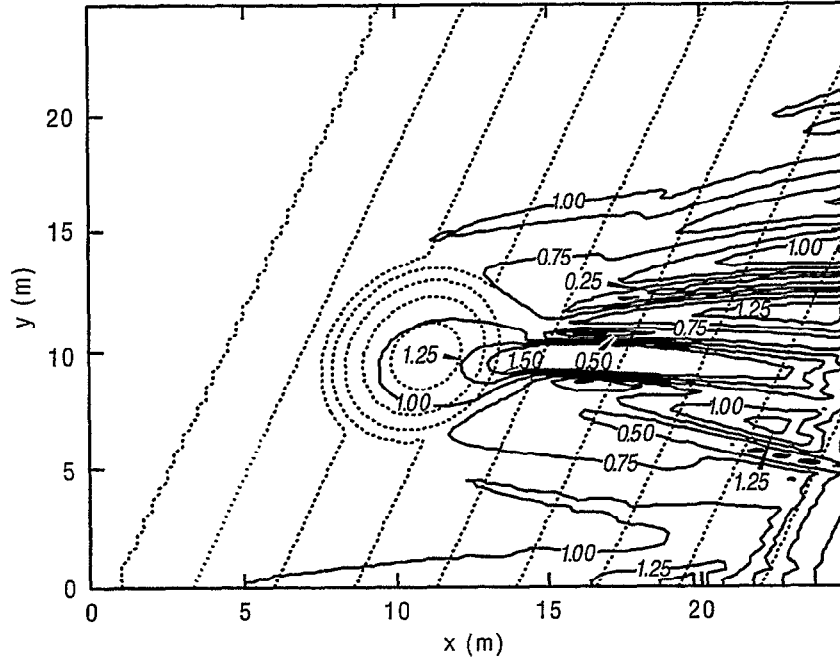


Fig. 4.3 — Normalized wave height contours from REF/DIF1 with linear dispersion, elliptical shoal experiment

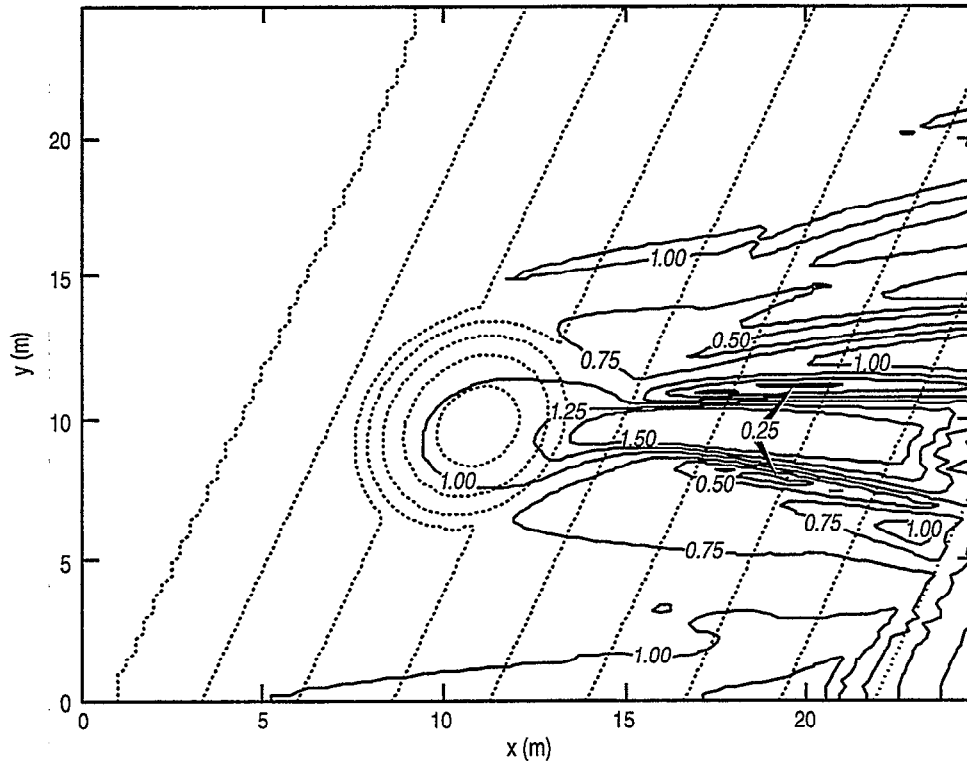


Fig. 4.4 — Normalized wave height contours from REF/DIF1 with composite nonlinear dispersion, elliptical shoal experiment

The actual model-data comparisons are shown in Figs. 4.5–4.12. REF/DIF1, in its weakly nonlinear form, most accurately predicts the magnitude of the focusing behind the shoal; the other two models are inconsistent in this respect. The nonlinear REF/DIF1 better predicts the diffraction-produced oscillations in wave height observed in the data to either side of the focus region. The nonlinear model takes the effect of nonlinear dispersion into account; as nonlinearity increases, the wave travels faster than its linear counterpart causing a defocusing of the wave over the top of the shoal. Thus, the diffraction pattern is wider in the y direction and the amplitudes lower than those from the linear model. Linear REF/DIF1 results show the oscillations, but location and magnitude are generally inaccurate.

4.2 Hales Shore-Normal Breakwater Experiment

Hales (1980) performed a laboratory experiment of wave transformation on a plane slope and diffraction by a shore-normal breakwater. This experiment was performed to model sediment transport in the area of coastal structures. The experimental setup, shown in Fig. 4.13, consists of a planar beach with a shore-normal breakwater. Because only negative angles of incidence were used, reflection from the breakwater does not need to be considered.

In this simulation, only REF/DIF1 was used since RCPWAVE does not allow for closed boundary conditions so the breakwater could not be represented. At first, making use of the “thin-film” capabilities of REF/DIF1 to represent the breakwater was tried; however, a significant portion of wave energy is transmitted through the thin film; a poor representation of an impermeable breakwater.

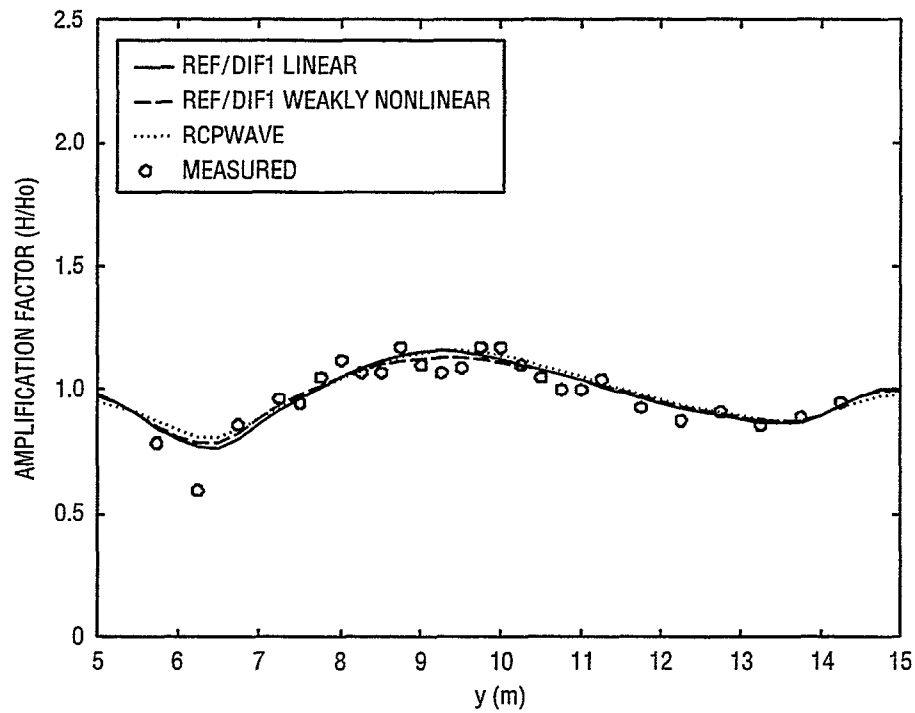


Fig. 4.5 — Comparison of normalized wave heights from RCPWAVE, REF/DIF1 with linear dispersion, and REF/DIF1 with composite nonlinear dispersion, with experimental data, elliptical shoal experiment, transect 1

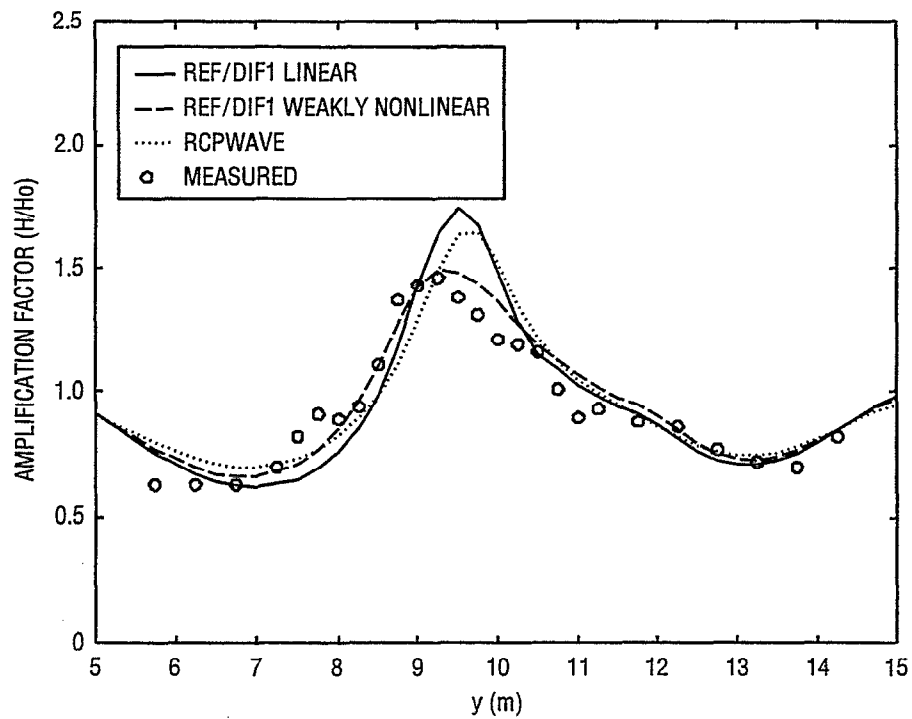


Fig. 4.6 — Comparison of normalized wave heights from RCPWAVE, REF/DIF1 with linear dispersion, and REF/DIF1 with composite nonlinear dispersion, with experimental data, elliptical shoal experiment, transect 2

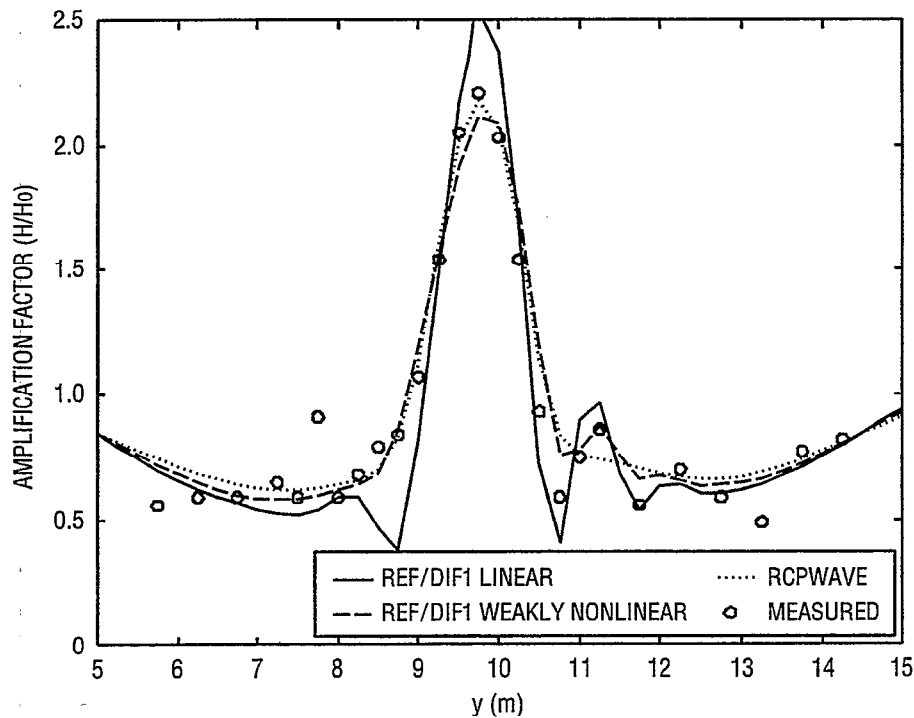


Fig. 4.7 — Comparison of normalized wave heights from RCPWAVE, REF/DIF1 with linear dispersion, and REF/DIF1 with composite nonlinear dispersion, with experimental data, elliptical shoal experiment, transect 3

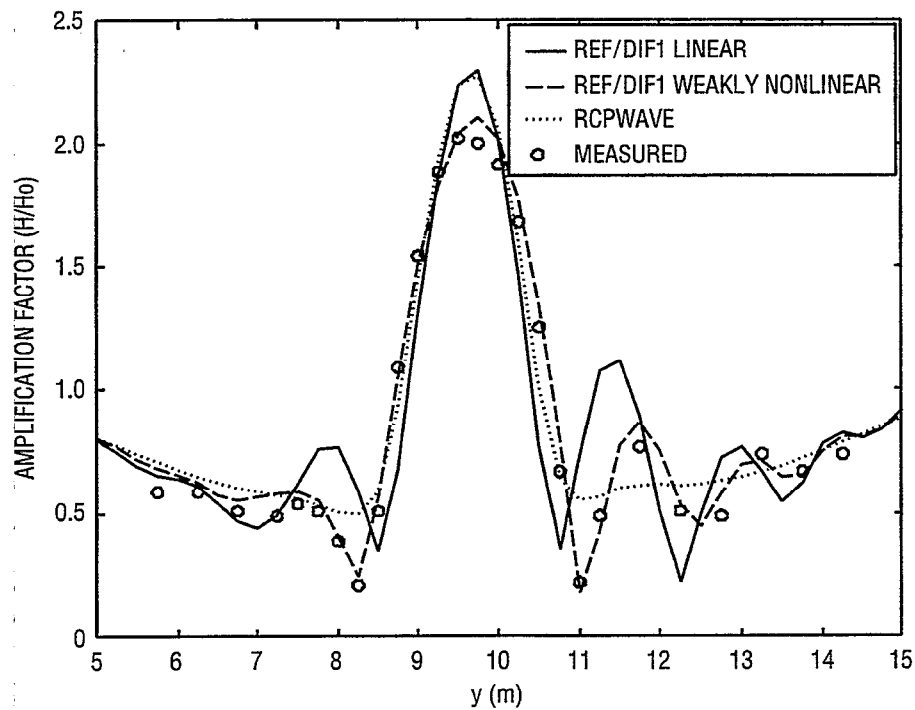


Fig. 4.8 — Comparison of normalized wave heights from RCPWAVE, REF/DIF1 with linear dispersion, and REF/DIF1 with composite nonlinear dispersion, with experimental data, elliptical shoal experiment, transect 4

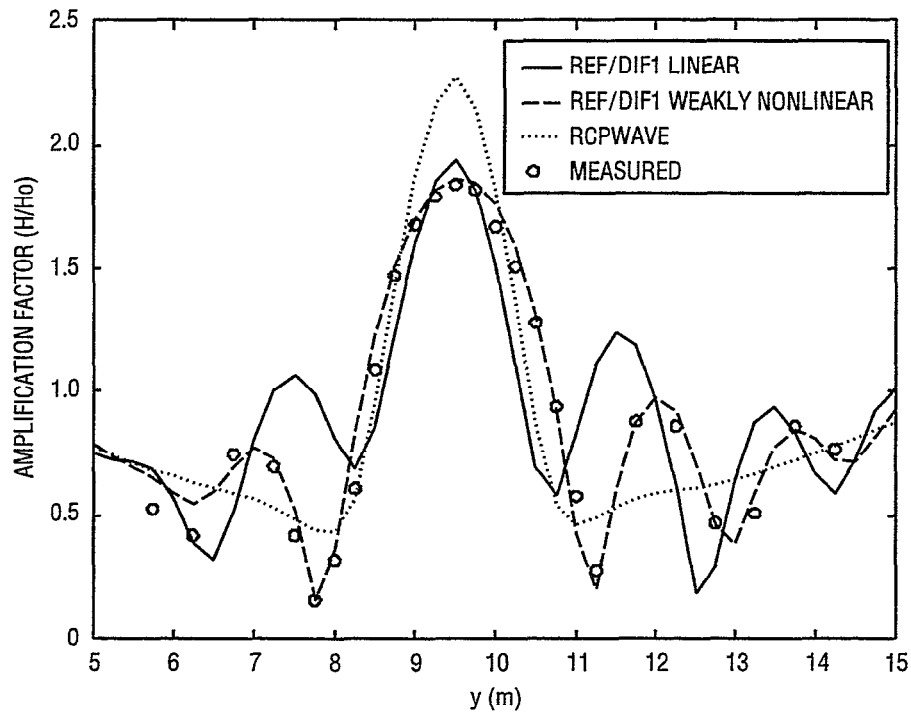


Fig. 4.9 — Comparison of normalized wave heights from RCPWAVE, REF/DIF1 with linear dispersion, and REF/DIF1 with composite nonlinear dispersion, with experimental data, elliptical shoal experiment, transect 5

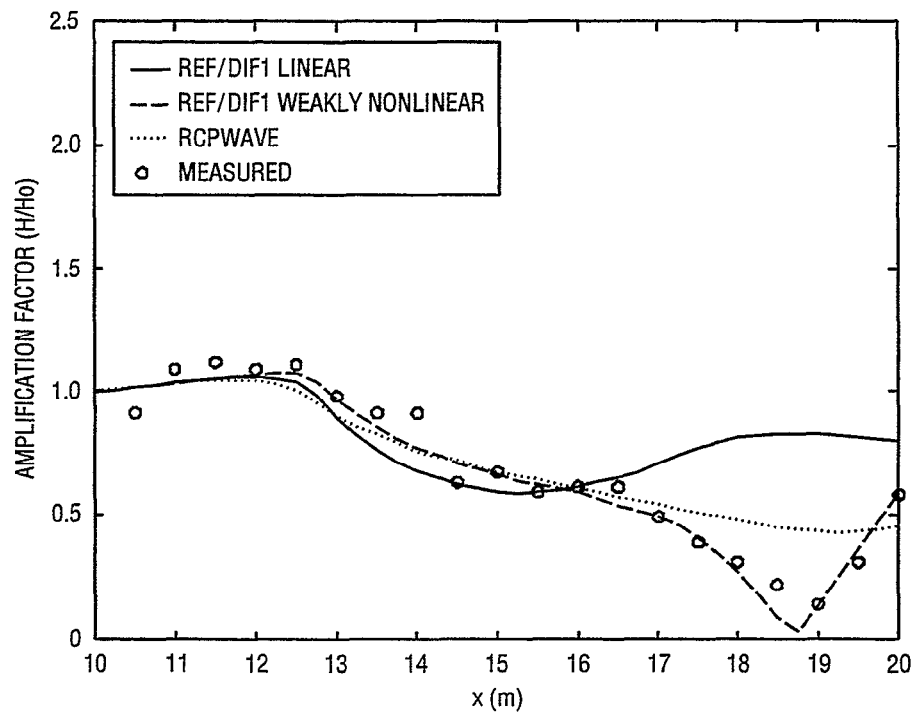


Fig. 4.10 — Comparison of normalized wave heights from RCPWAVE, REF/DIF1 with linear dispersion, and REF/DIF1 with composite nonlinear dispersion, with experimental data, elliptical shoal experiment, transect 6

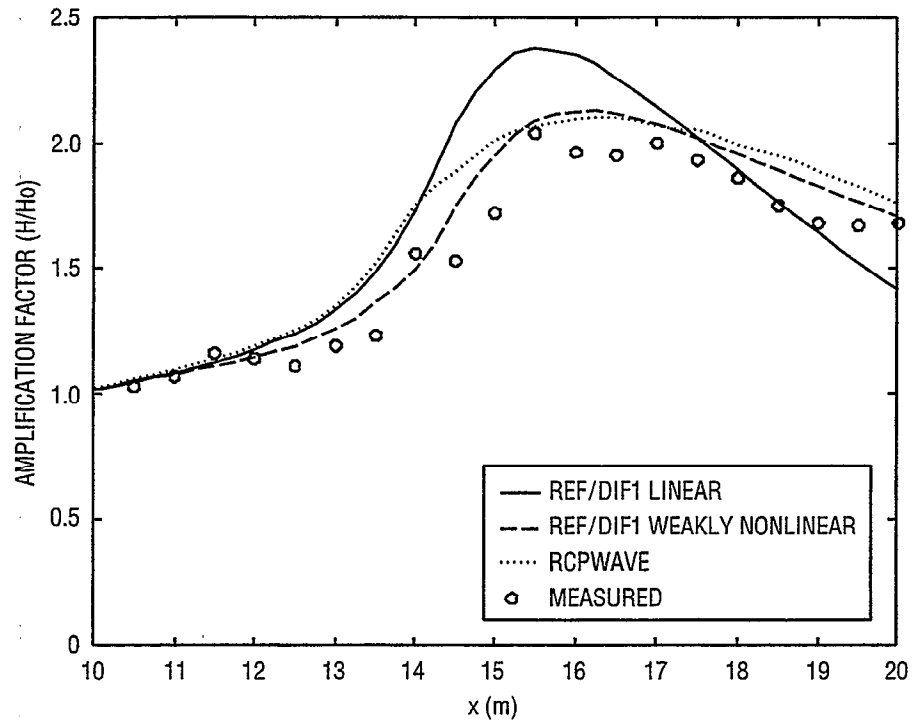


Fig. 4.11 — Comparison of normalized wave heights from RCPWAVE, REF/DIF1 with linear dispersion, and REF/DIF1 with composite nonlinear dispersion, with experimental data, elliptical shoal experiment, transect 7

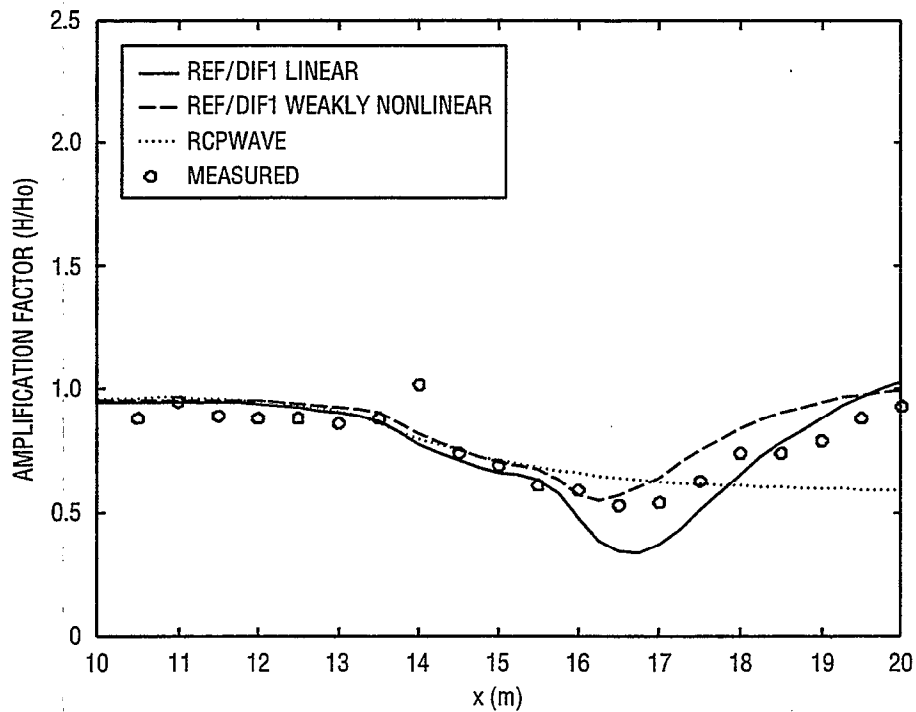


Fig. 4.12 — Comparison of normalized wave heights from RCPWAVE, REF/DIF1 with linear dispersion, and REF/DIF1 with composite nonlinear dispersion, with experimental data, elliptical shoal experiment, transect 8

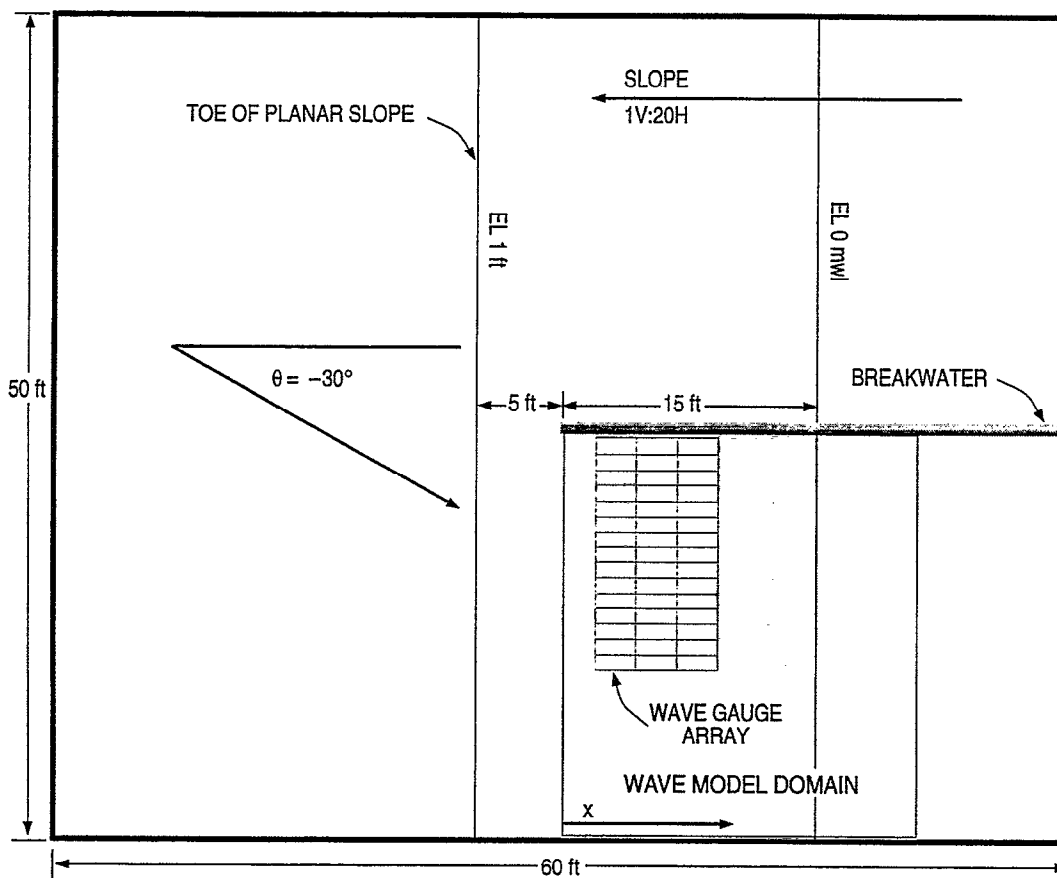


Fig. 4.13 — Layout of Hales' experiment

Therefore, the breakwater was represented by a closed lateral boundary condition, an option with REF/DIF1. Because the breakwater did not extend to the toe of the slope, the x -location of the breakwater tip was used as the offshore boundary with Snell's Law being used to transform the wave from the constant-depth region to the boundary. The y -dimension of the domain was made much larger than the actual size of the wave basin to avoid reflection from the right-side lateral boundary.

Both the linear and composite nonlinear REF/DIF1 were used. The model-data comparisons are shown in Figs. 4.14–4.17. In general, data-model agreement is fair. The oscillations in wave height are out of phase with respect to the experiment, and the modeled wave heights seem slightly smaller than the experimental values. The agreement to data seems to improve farther away from the breakwater tip; the high rate of wave turning associated with the diffraction process is not as severe in this region, which likely suits the parabolic approximation better. There is not much difference between the linear and composite nonlinear models in this case.

5.0 COMPARISON TO FIELD DATA

This section will address preliminary comparisons to field data. At the time of this writing, access to only one set of field data (the data from the DELILAH experiment of 1990) was available.

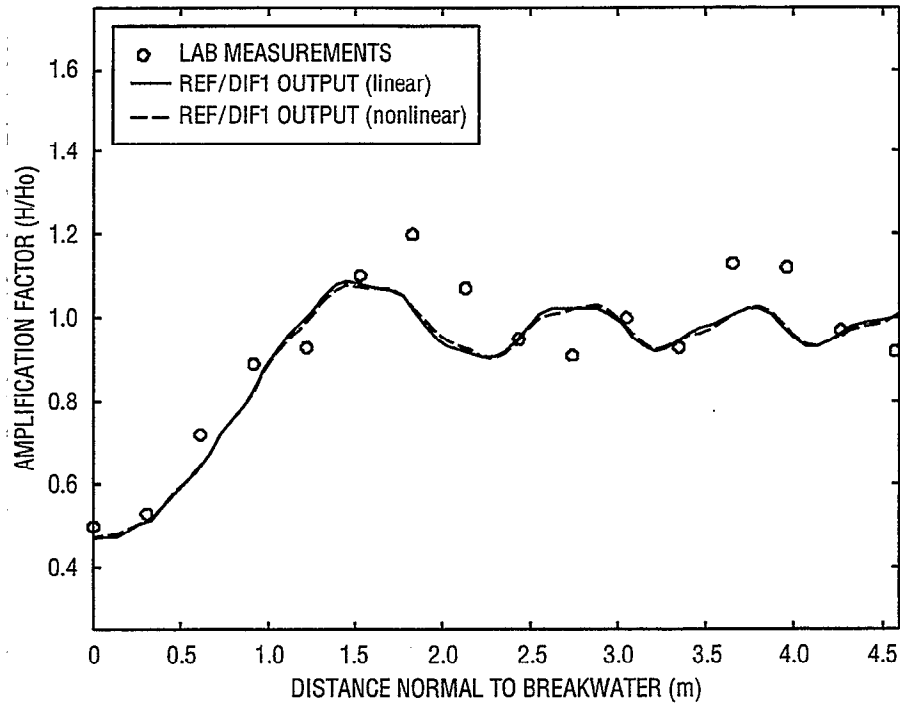


Fig. 4.14 — Comparison of wave height amplification factors from linear and composite nonlinear REF/DIF1, Hales' experiment, $x = 0.91$ m

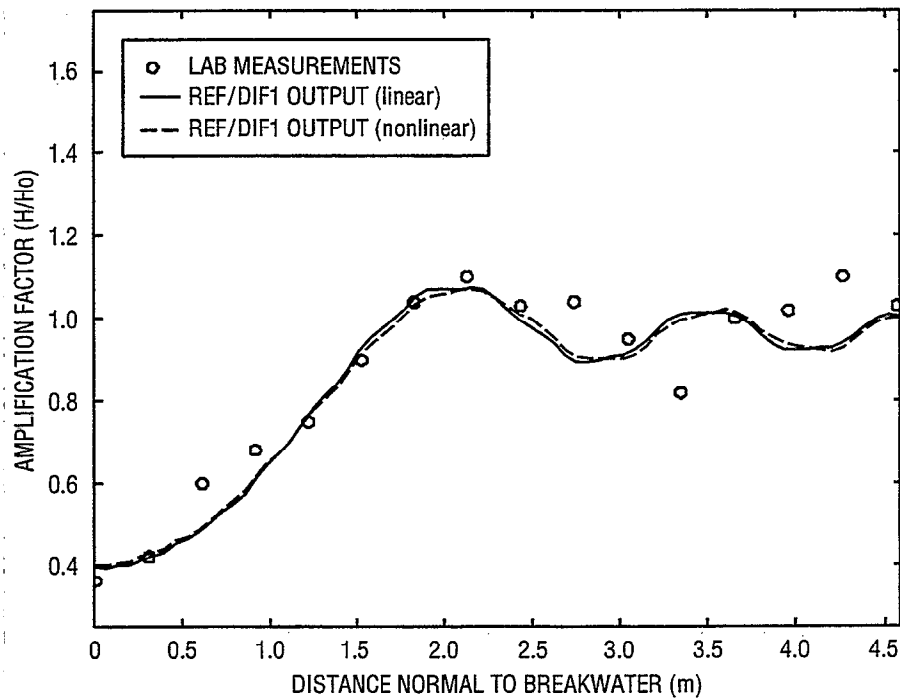


Fig. 4.15 — Comparison of wave height amplification factors from linear and composite nonlinear REF/DIF1, Hales' experiment, $x = 1.52$ m

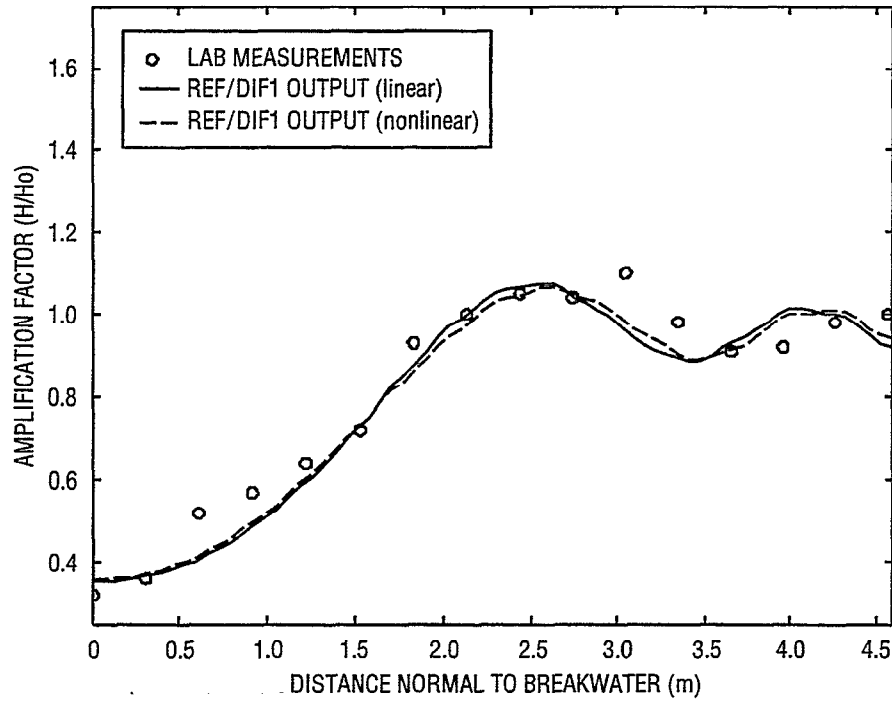


Fig. 4.16 — Comparison of wave height amplification factors from linear and composite nonlinear REF/DIF1, Hales' experiment, $x = 2.13$ m

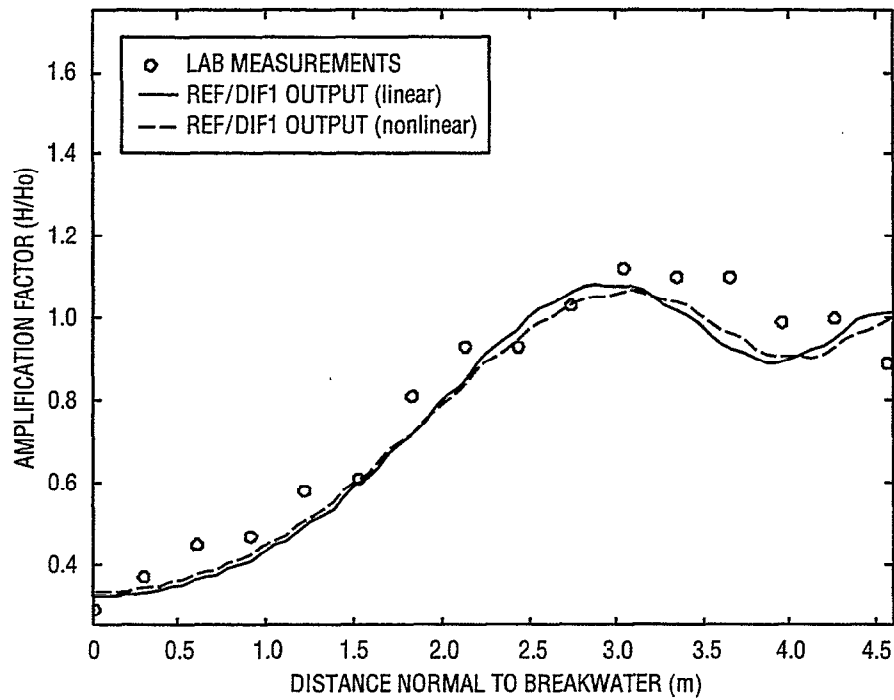


Fig. 4.17 — Comparison of wave height amplification factors from linear and composite nonlinear REF/DIF1, Hales' experiment, $x = 2.74$ m

More field data for model verification is expected to be obtained; however, this data set has been valuable in both validating the model physics and as an aid in diagnosing and correcting potential problems with the model.

5.1 The DELILAH Field Experiment—General Information

The DELILAH (Duck Experiment on Low-frequency and Incident-band Longshore and Across-shore Hydrodynamics) nearshore experiment was held at the Coastal Engineering Research Center Field Research Facility in Duck, NC, during October 1990 (Birkemeier 1991). The DELILAH experiment was designed to investigate the surf zone physics using a variety of techniques and instruments. Bathymetry and wave data were available for use in this study. The bathymetry of the site is nearly homogeneous in the longshore direction except near the instrumentation pier (a large scour hole appears near the offshore piling) and very close to shore where a migrating sandbar was evident during the experiment. Bathymetric data included daily “mini-grid” surveys in the vicinity of the nearshore gauges and one survey of the domain of the DELILAH experiment. The mini-grid surveys were merged with the larger, domain-sized bathymetry to yield wave model bathymetry for each day of the experiment. The wave gauge arrangements and general map of the Duck bathymetry is shown in Fig. 5.1. Figure 5.2 depicts the model domain for 6 Oct 1990. Tidal stages were also measured at the pier.

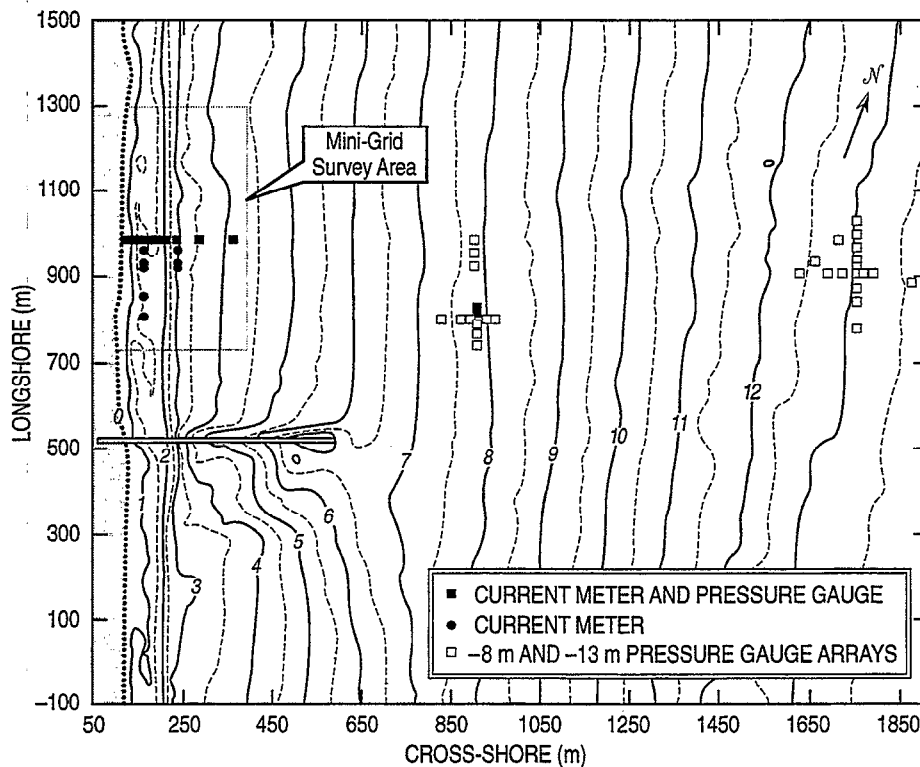


Fig. 5.1 — Layout of instrumentation from DELILAH experiment, Duck, NC, October 1990

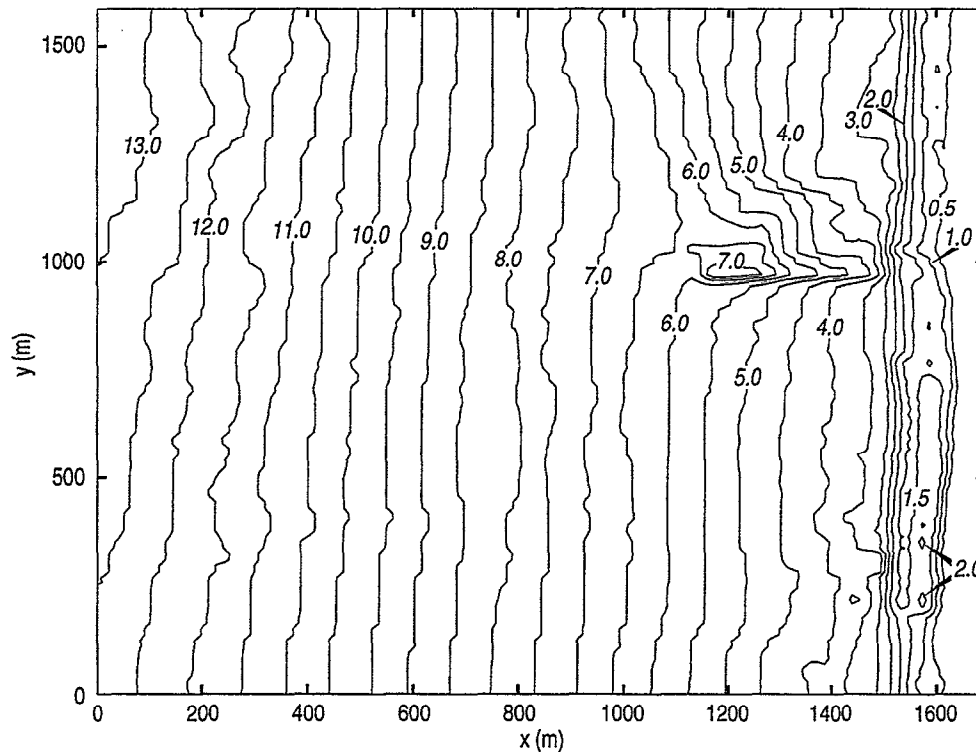


Fig. 5.2 — Bathymetry from DELILAH experiment, Duck, NC, 6 Oct 1990, depth in meters

The available data consisted of daily bathymetry, offshore spectra for model initialization, and nearshore wave gauge data for model verification. The offshore data were provided by the SAMSON (Sources of Ambient Micro-Seismic Oceanic Noise) array, an 11-gauge array arranged in a cross-like pattern located at 13-m water depth. Data were taken at 2 Hz and samples were taken for 2 h, 16 min. This sample represented a 3-h span, with the remaining 44 min taken for data analysis and processing. This gauge array was operated and maintained by the Field Research Facility staff. A sample spectra from the SAMSON array is shown in Fig. 5.3. A linear array of pressure sensors is also located at 8-m water depth; this array is a permanent installation at the Field Research Facility. The nearshore data consisted of H_{rms} values sampled at 8 Hz (nine gauges sampled every 5 min). This nearshore array was augmented by two longshore gauge arrays (one at the crest of the sandbar and one in the trough of the bar) that formed two directional arrays. The nearshore array was maintained and operated by faculty and staff of the Naval Postgraduate School. The data taken at these directional arrays were subsampled to 2 Hz by the Field Research Facility staff and analyzed in the same manner as the SAMSON array data. The resulting spectra are the only measurements of wave angle from this experiment, and as such, do not lend meaningful comparisons for the model.

Fifty-three REF/DIF-S model runs were conducted for comparison to experimental data. These consisted of 5–8 runs per day of the experiment for the days of 6–7 and 12–16 Oct 1990. These days were chosen because of the relative lack of data dropout and the low wind speeds.

As mentioned, REF/DIF-S was initialized with the SAMSON array data. A wave input pre-processor, SPECGEN (spectral wave generator) (Kirby and Ozkan 1994), was used to discretize the measured offshore wave spectrum and divide it into components. Each component of the spectrum

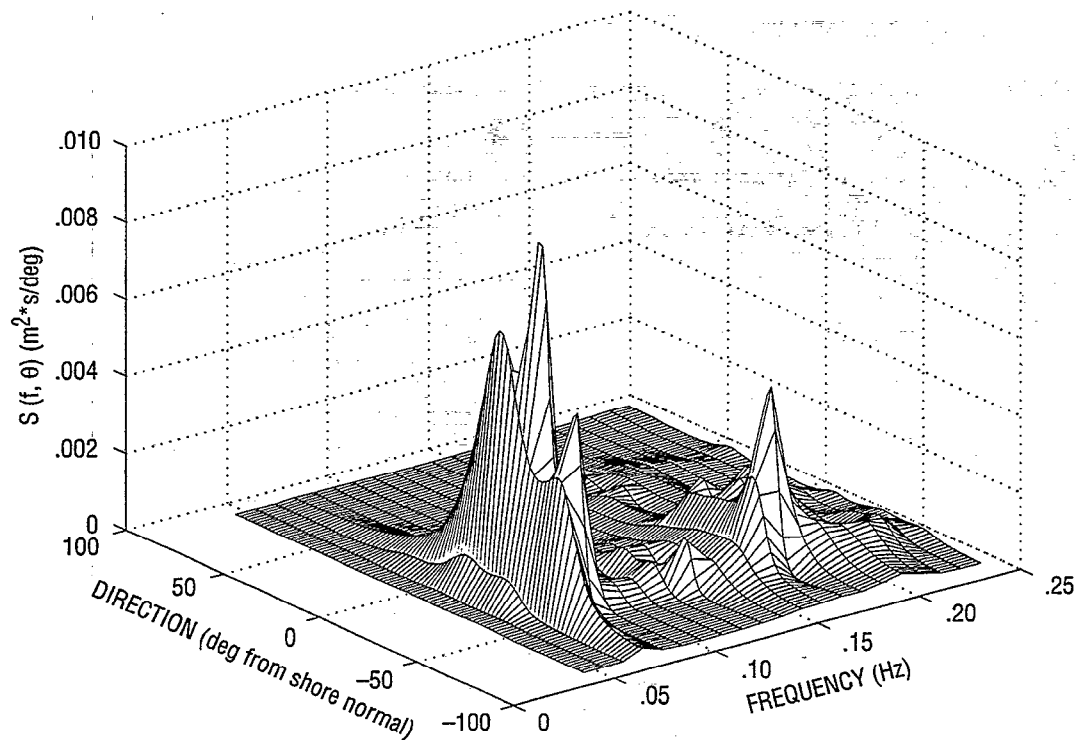


Fig. 5.3 — Sample directional spectra from SAMSON array, DELILAH experiment

represents a particular partition of wave energy for a particular wave angle and frequency. The wave energy in this partition can be related to the wave height; thus, SPECGEN decomposes a spectrum into a series of initial wave conditions that are read by REF/DIF-S.

The actual discretization of the spectrum can be done two ways: using equal Δf , $\Delta\theta$ (equal bandwidth) bins, or by using bins of equal energy. Equal bandwidth bins are simplest, but can be problematic when the spectrum has a symmetric directional distribution; in this case, one can have two waves equal in frequency but opposite in the sign of the direction, giving rise to a short-crested wave pattern. This short-crested pattern invalidates the assumption of spatial homogeneity inherent in directional spectra. This is not a major concern when one has a non-symmetric directional distribution, as is the case with most field data. For the DELILAH data set, 10 frequency bins and 20 directional bins were generally used. (More information on SPECGEN is detailed in App. A.)

During the course of this REF/DIF-S verification, some anomalous model behavior was encountered that necessitated some further investigation. This resulted in the uncovering of several coding errors in REF/DIF-S. Much improved behavior was noted when the errors were corrected; additionally, the corrections allowed the calculation of directional spectra from the model, a feature not included in the delivered version. These corrections and their consequences will be discussed in a later section of this report; for the remainder of the discussion in this section, the "uncorrected" version of the model is referred to. (Note here that the errors are endemic only to REF/DIF-S and not REF/DIF1.)

5.2 Comparisons of REF/DIF-S Output to Data

5.2.1 Anomalous Behavior from the Uncorrected Model

For all cases, wave angles in REF/DIF-S output are very small, even in offshore regions. This is clearly erroneous, as the angles at the spectral peak of the input spectra were moderately large for some cases. Additionally, a large negative gradient in the wave height near the offshore boundary is observed in the model output for most of the cases. Figure 5.4 shows a section cut through a wave height field output from the model; the sudden drop in wave height near the offshore boundary of the grid is evident. This drop is nonphysical since there are no bathymetric features in the offshore region that would cause this.

5.2.2 Comparison of Results of Uncorrected Model to Data

Figures 5.5–5.17 show representative comparisons of model output to data from the nearshore, cross-shore array. For each gauge, the maximum, mean, and minimum wave height for the time period is shown. (Recall that the nearshore data are provided every 5 min, while the offshore data used for initialization represents a span of 2 h, 16 min.) In this region of the domain, the model is fairly accurate. Wave reformation shoreward of the bar is evident in some cases in both model results and data. In general, the model tends to slightly overpredict wave heights in the surf zone and underpredict them seaward of the surf zone.

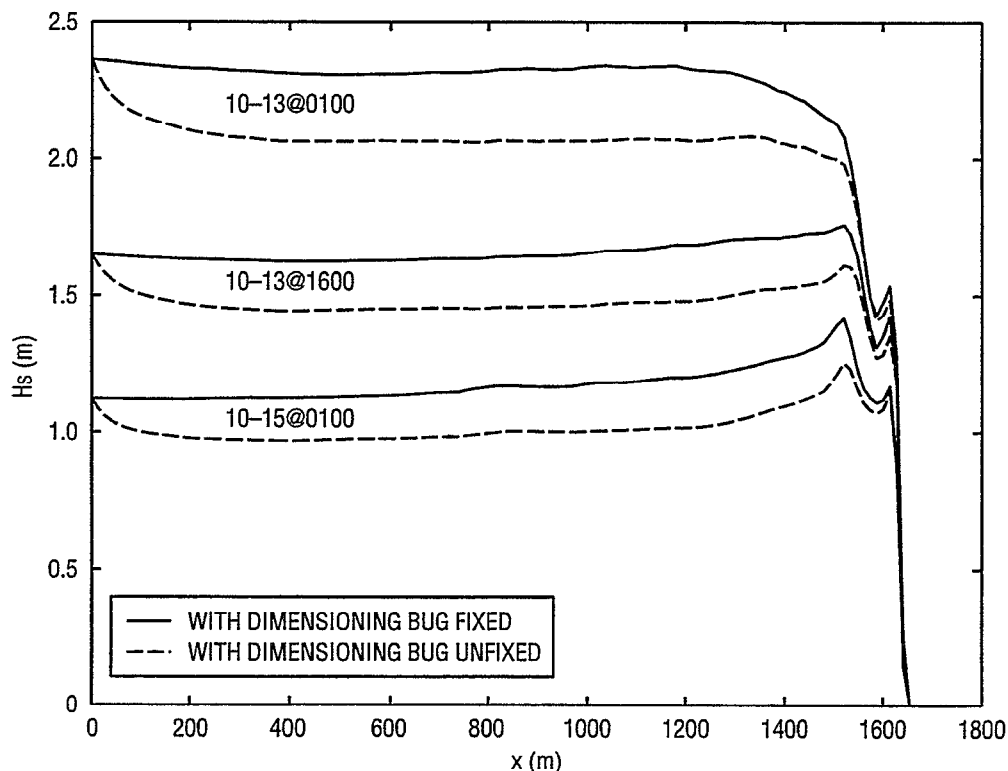


Fig. 5.4 — Comparisons of wave heights from corrected and uncorrected versions of REF/DIF-S

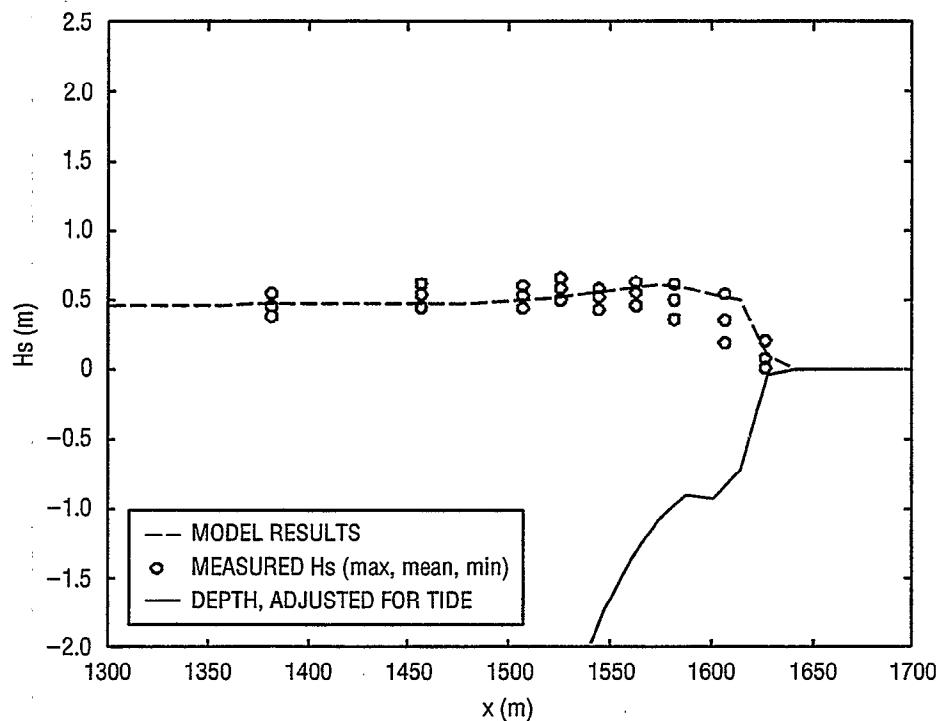


Fig. 5.5 — Comparison of significant wave heights from REF/DIF-S to the DELILAH experiment data for the time period beginning at 0400 EST, 10-6-90

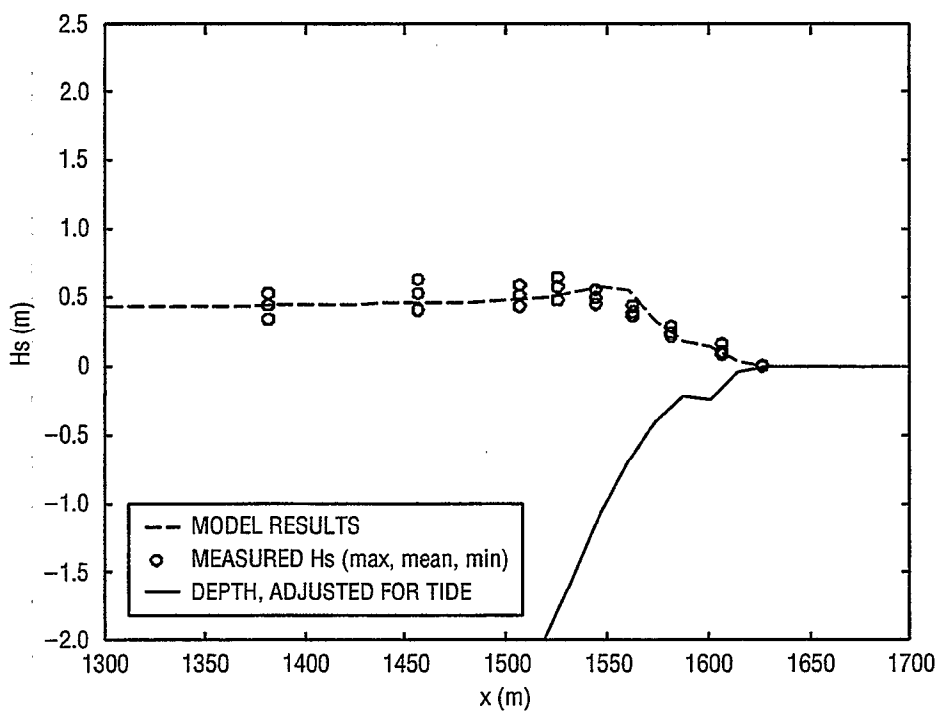


Fig. 5.6 — Comparison of significant wave heights from REF/DIF-S to the DELILAH experiment data for the time period beginning at 1300 EST, 10-6-90

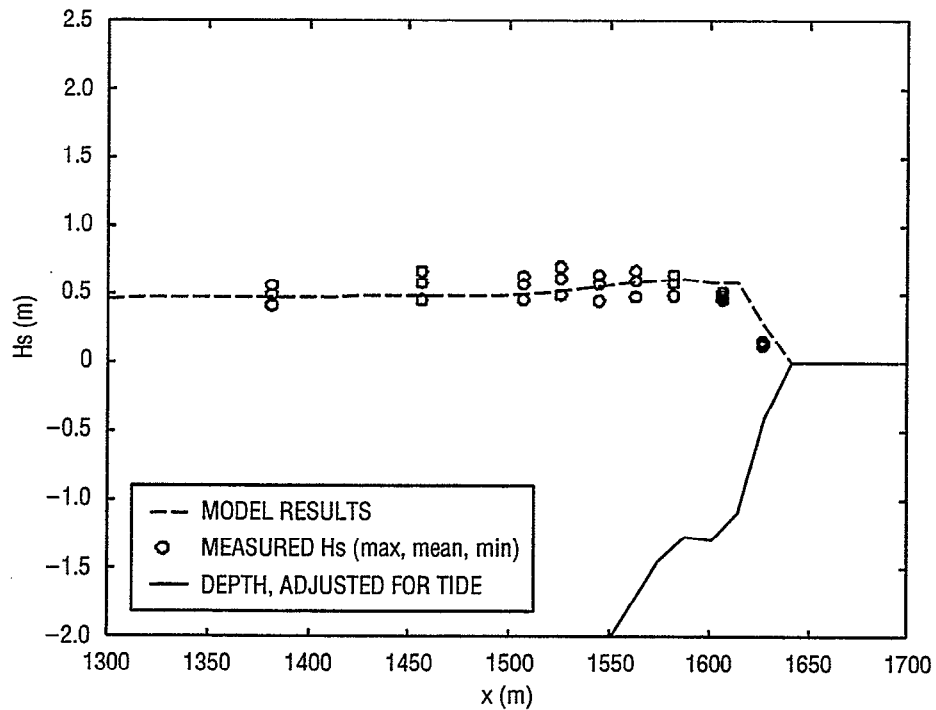


Fig. 5.7 — Comparison of significant wave heights from REF/DIF-S to the DELILAH experiment data for the time period beginning at 1900 EST, 10-6-90

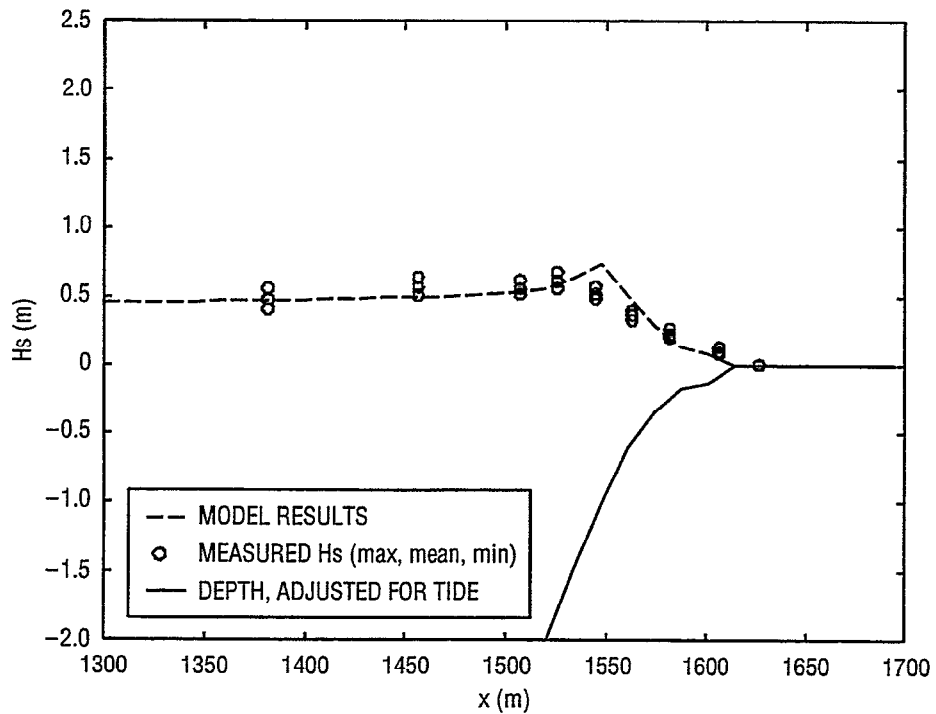


Fig. 5.8 — Comparison of significant wave heights from REF/DIF-S to the DELILAH experiment data for the time period beginning at 0100 EST, 10-7-90

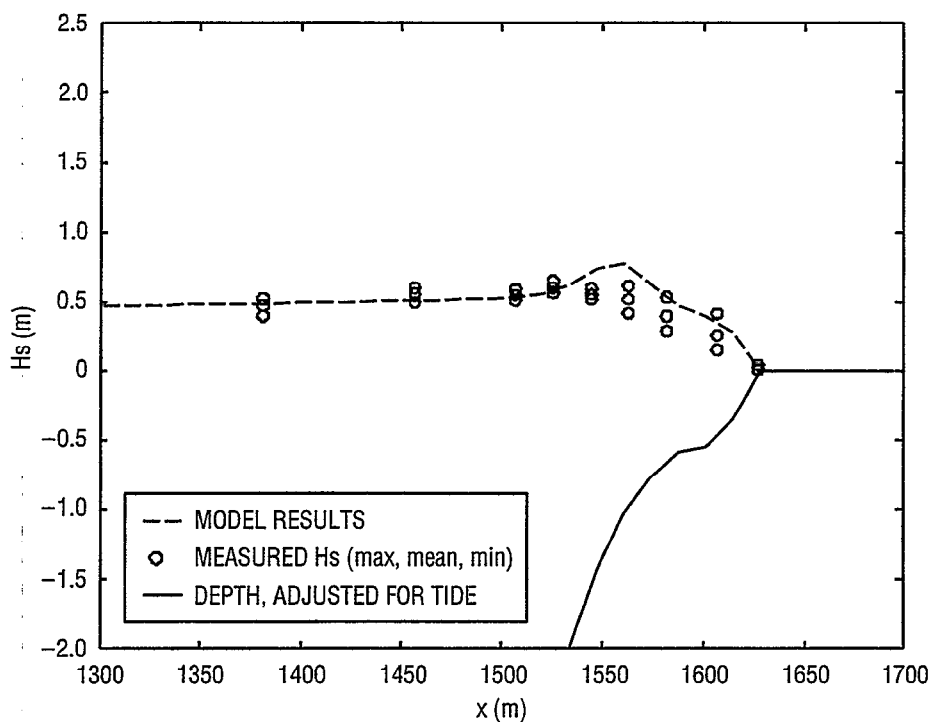


Fig. 5.9 — Comparison of significant wave heights from REF/DIF-S to the DELILAH experiment data for the time period beginning at 0400 EST, 10-7-90

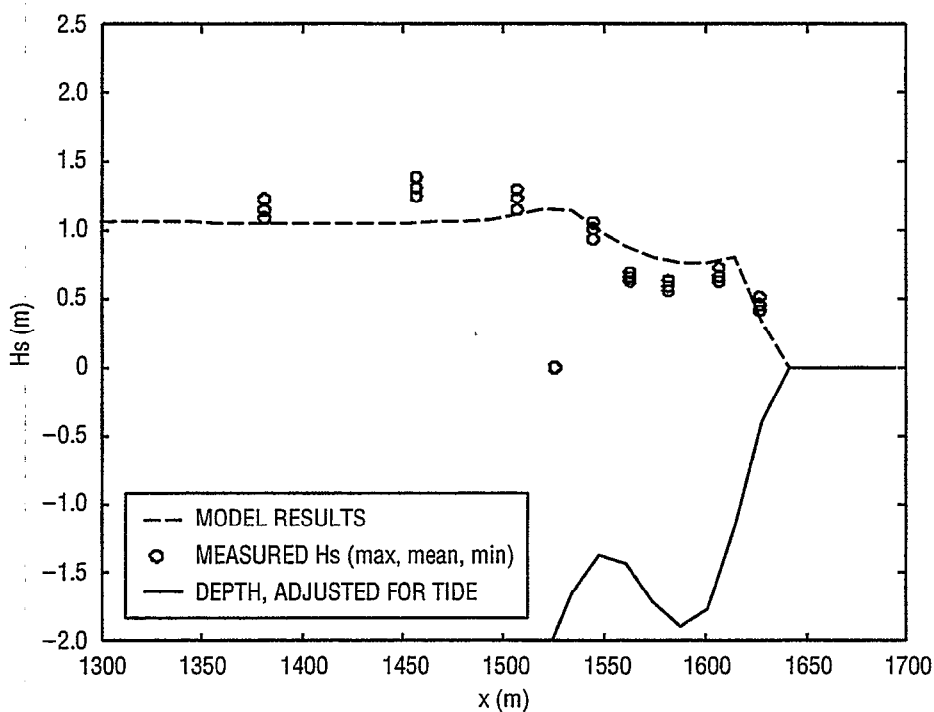


Fig. 5.10 — Comparison of significant wave heights from REF/DIF-S to the DELILAH experiment data for the time period beginning at 0700 EST, 10-12-90

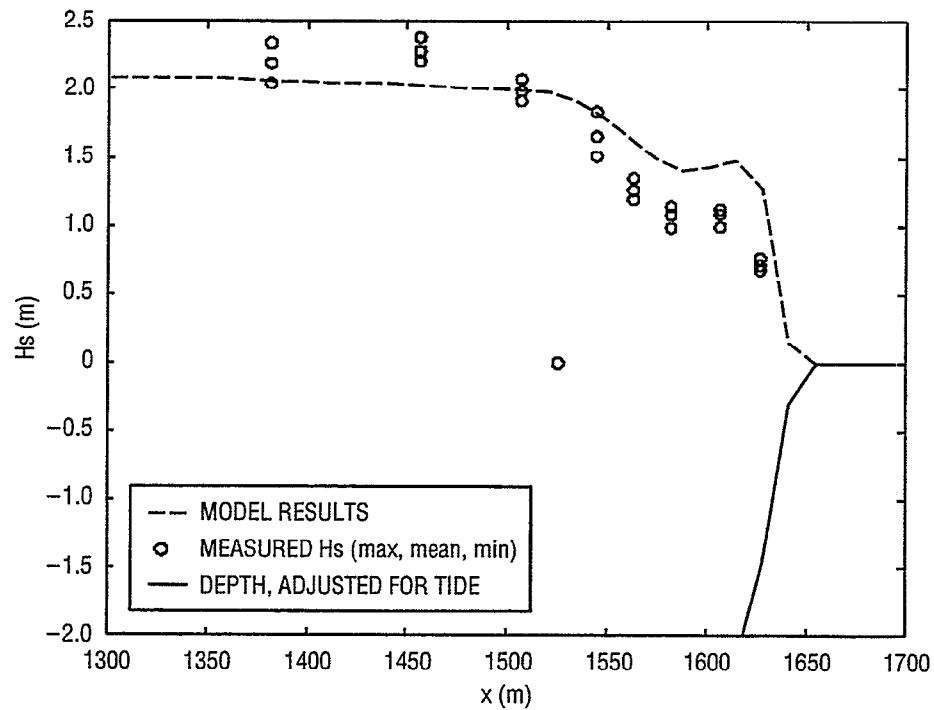


Fig. 5.11 — Comparison of significant wave heights from REF/DIF-S to the DELILAH experiment data for the time period beginning at 0100 EST, 10-13-90

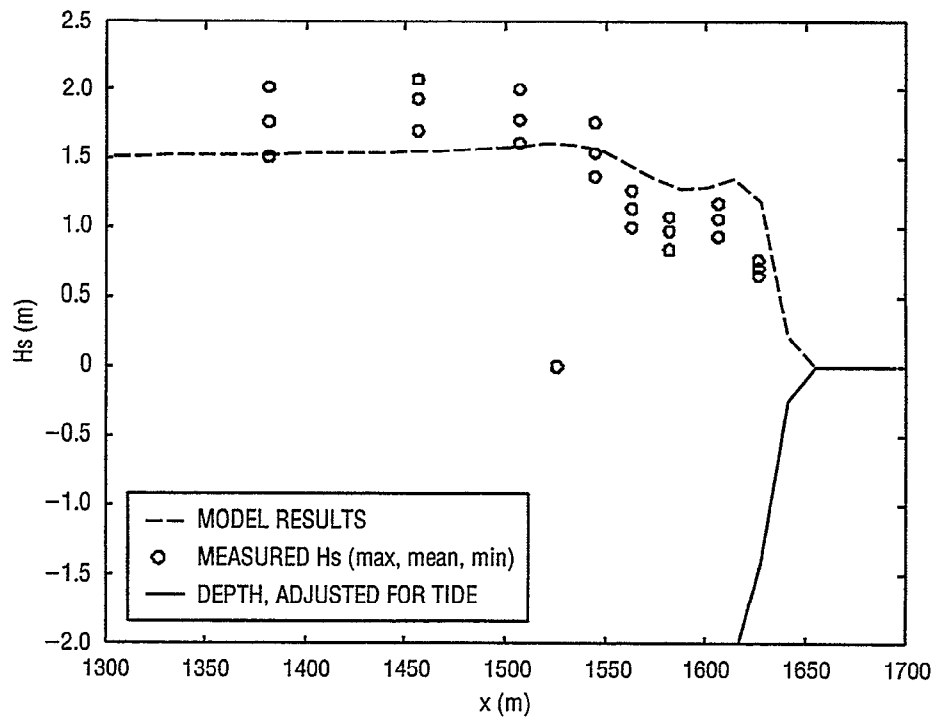


Fig. 5.12 — Comparison of significant wave heights from REF/DIF-S to the DELILAH experiment data for the time period beginning at 1600 EST, 10-13-90

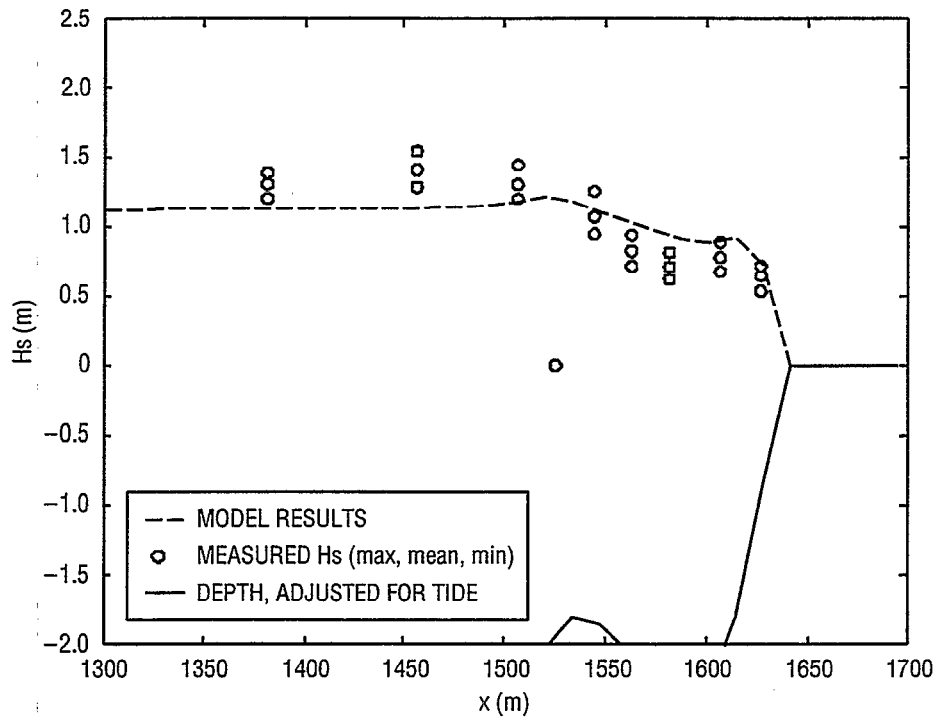


Fig. 5.13 — Comparison of significant wave heights from REF/DIF-S to the DELILAH experiment data for the time period beginning at 1900 EST, 10-14-90

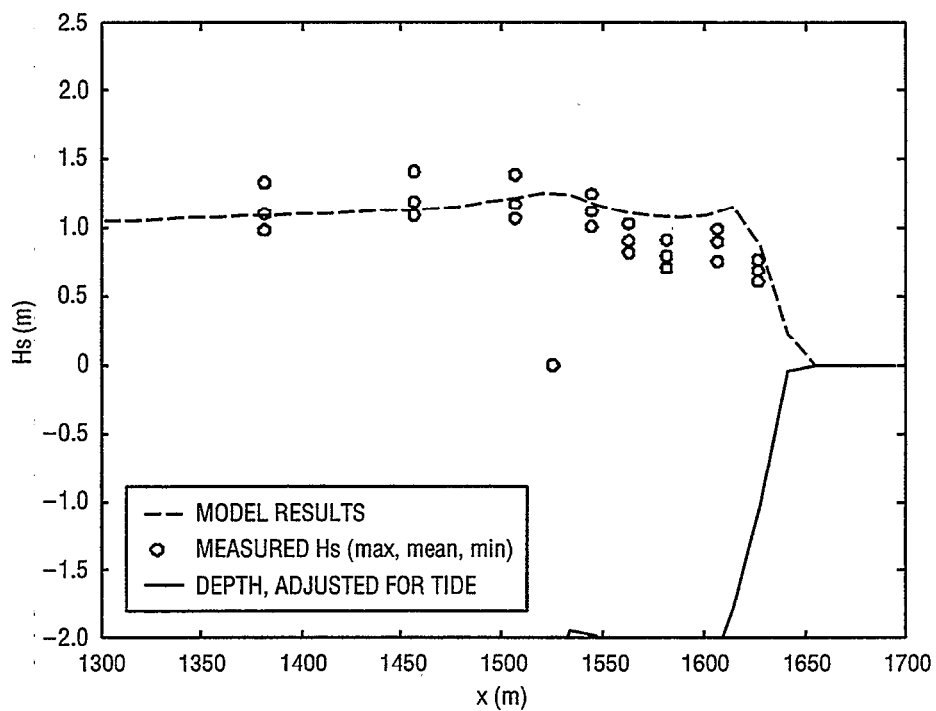


Fig. 5.14 — Comparison of significant wave heights from REF/DIF-S to the DELILAH experiment data for the time period beginning at 0100 EST, 10-15-90

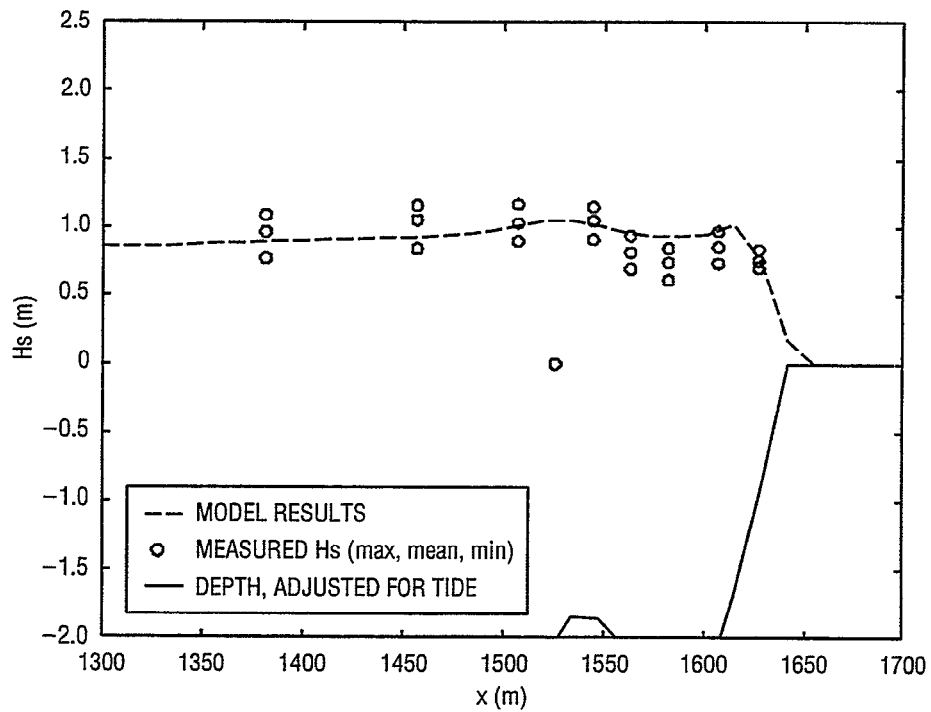


Fig. 5.15 — Comparison of significant wave heights from REF/DIF-S to the DELILAH experiment data for the time period beginning at 1300 EST, 10-15-90

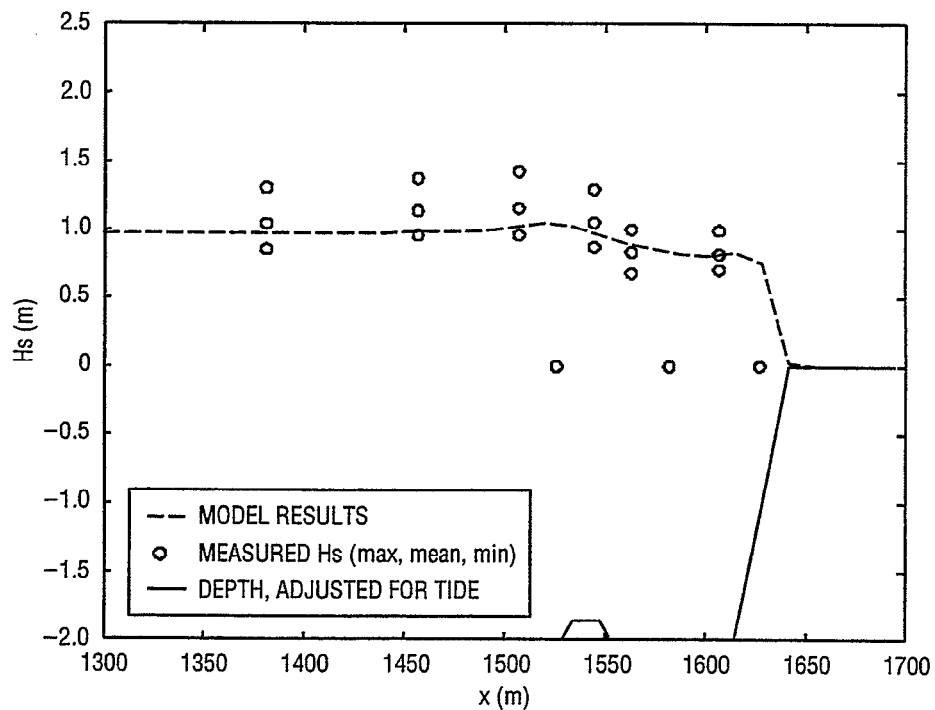


Fig. 5.16 — Comparison of significant wave heights from REF/DIF-S to the DELILAH experiment data for the time period beginning at 0100 EST, 10-16-90

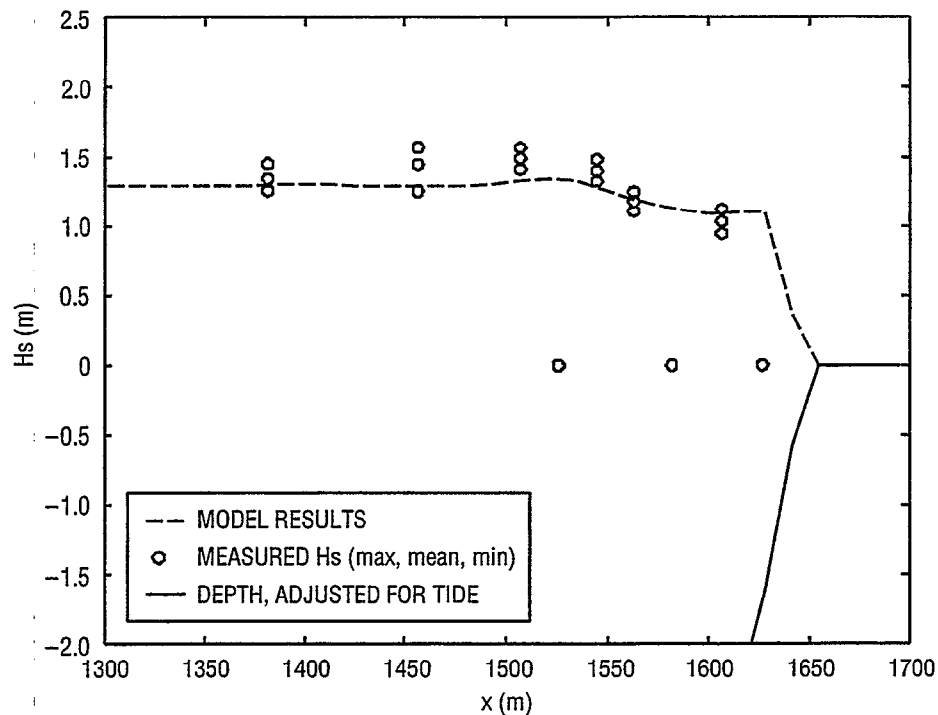


Fig. 5.17 — Comparison of significant wave heights from REF/DIF-S to the DELILAH experiment data for the time period beginning at 0400 EST, 10-16-90

5.2.3 Effect of Grid Resolution on Results from Uncorrected Model

As a test of the sensitivity of REF/DIF-S to grid resolution, the bathymetric spatial step was doubled. The resulting coarser bathymetric grid caused wave height output from REF/DIF-S to be significantly larger. This result is unexpected, as the Duck bathymetry seaward of the bar is fairly bland—not much information is lost by decreasing resolution by a factor of two in this region. Shoreward of the point where breaking occurs, the effect of using a different grid resolution is not as great. Figs. 5.18 and 5.19 show test results for several cases.

5.2.4 Effect of Increase in Number of Direction and Frequency Bins on Model Results

The sensitivity of REF/DIF-S to the number of directional and frequency bins was tested by increasing the number of frequency bins from 10 to 15 and the number of directional bins from 20 to 30. This change made very little difference in model output wave heights in the surf zone. However, using more components resulted in slightly lower wave heights seaward of the surf zone (Figs. 5.20 and 5.21).

5.2.5 Effect of Spectra Discretization Method on REF/DIF-S Results

All REF/DIF-S model runs described above were performed with the input spectra represented by bins of equal energy. As mentioned previously, an alternative method for representing spectra

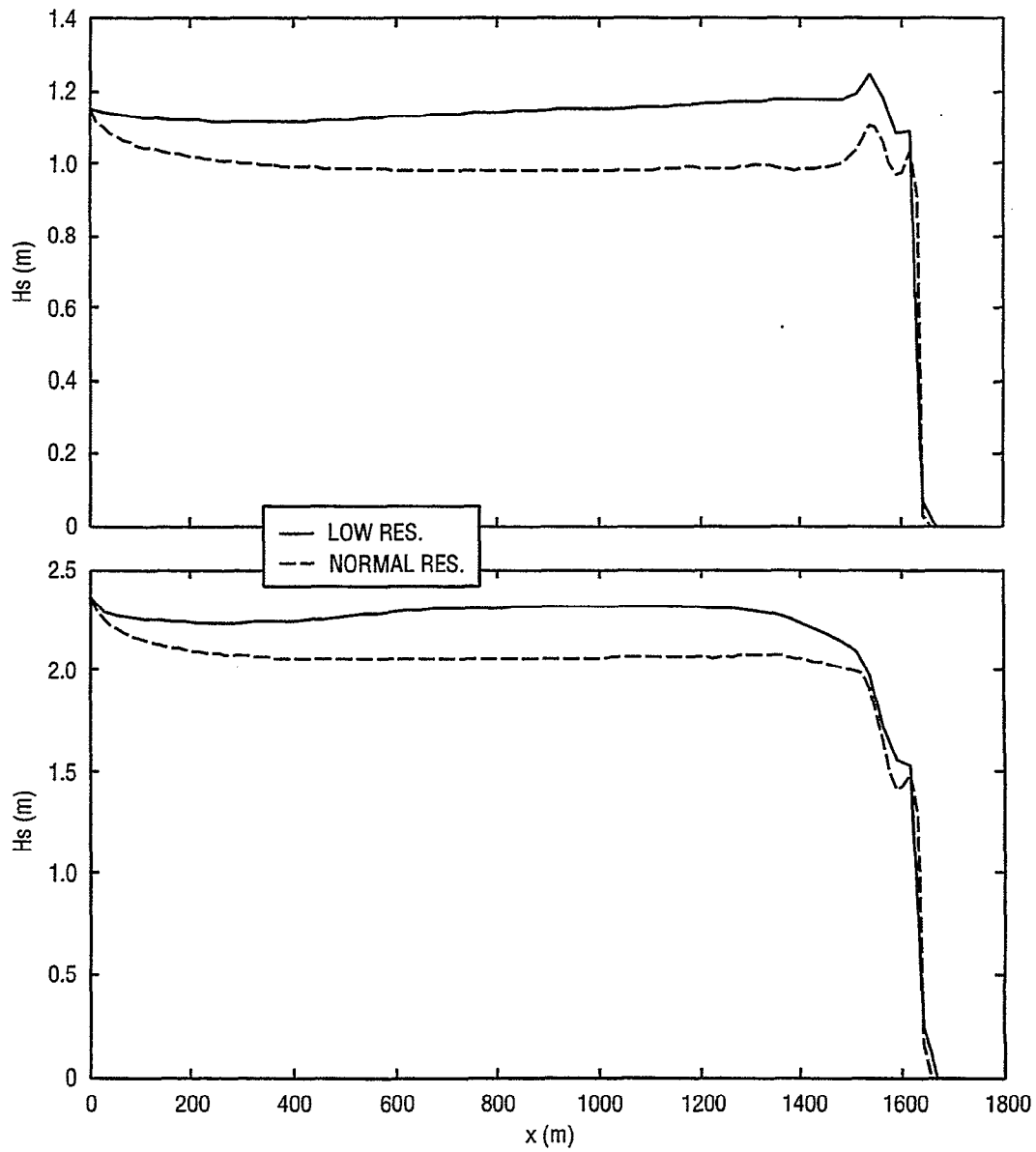


Fig. 5.18 — Comparison of uncorrected REF/DIF-S significant wave heights over low-resolution bathymetry and bathymetry at given resolution

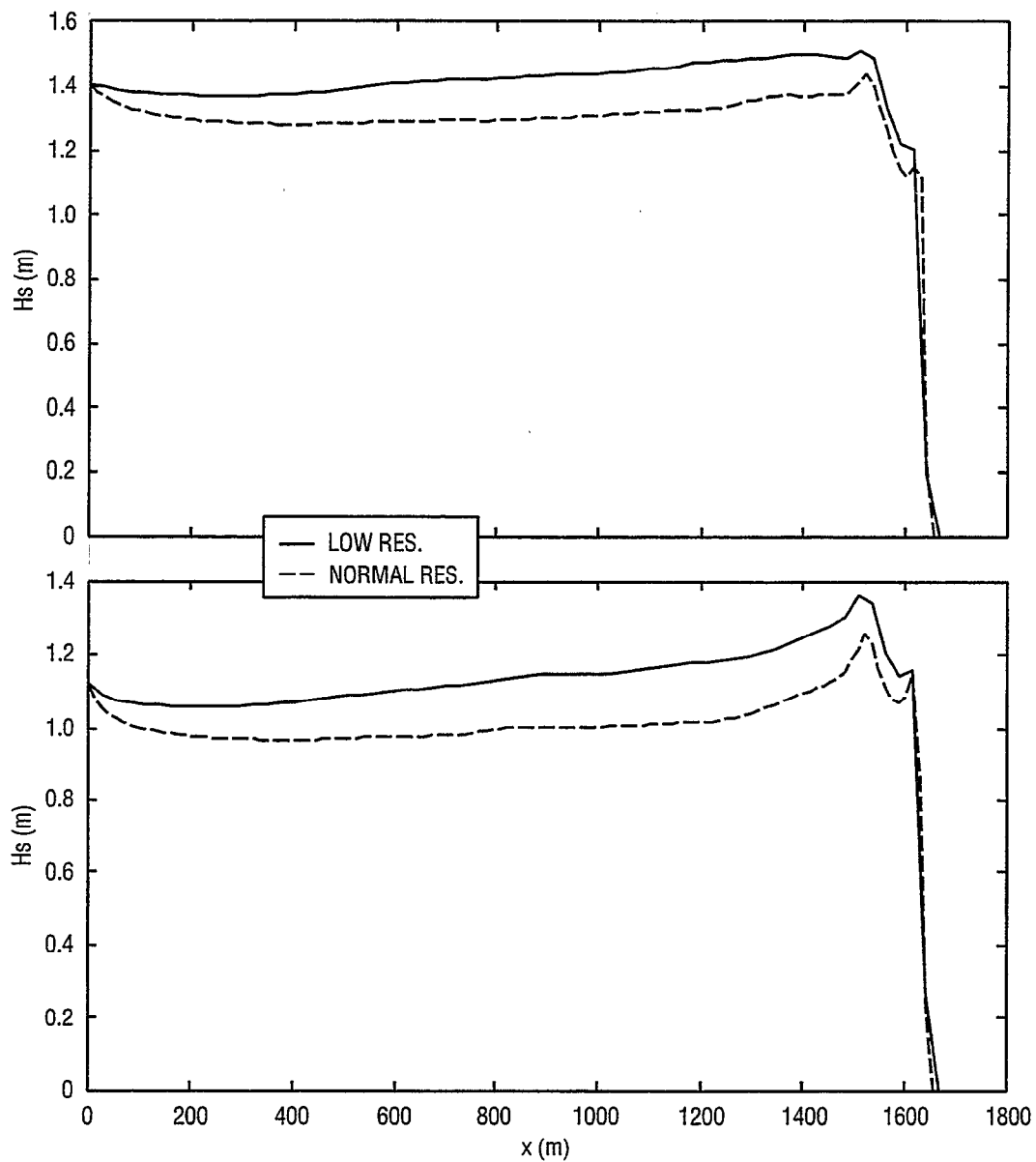


Fig. 5.19 — Comparison of uncorrected REF/DIF-S significant wave heights over low-resolution bathymetry and bathymetry at given resolution

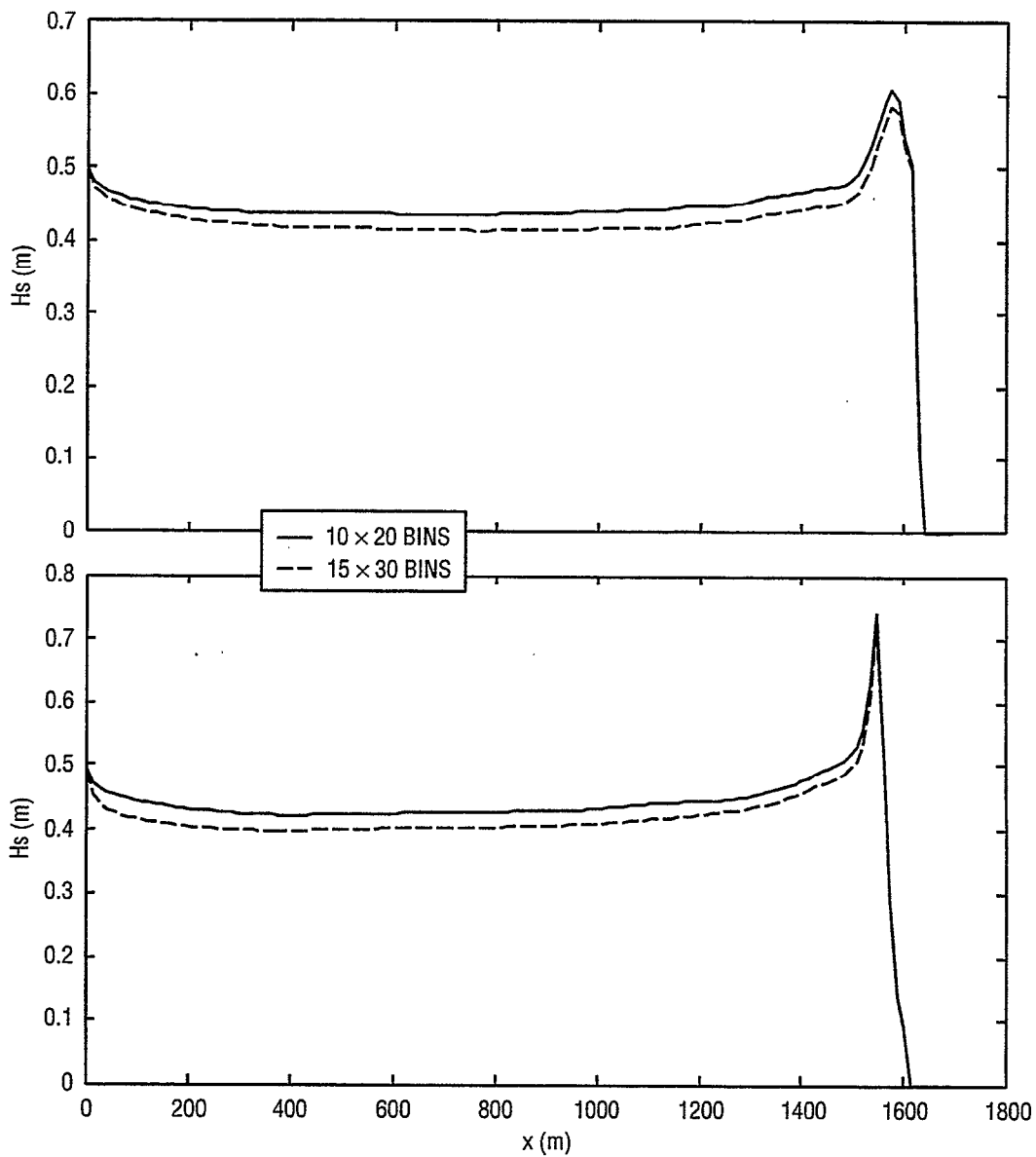


Fig. 5.20 — Comparison of uncorrected REF/DIF-S significant wave heights with different numbers of frequency and direction bins

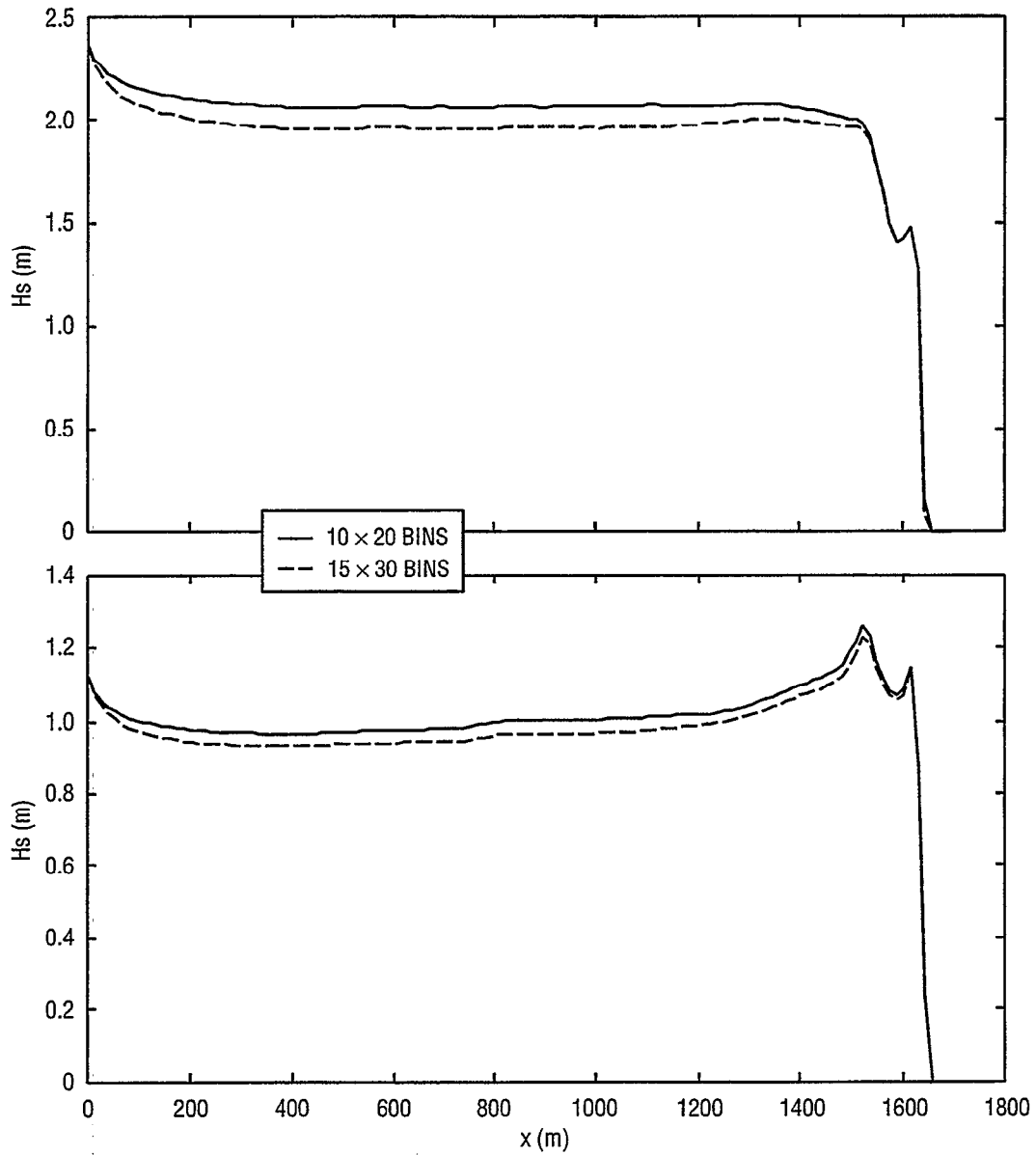


Fig. 5.21 — Comparison of uncorrected REF/DIF-S significant wave heights with different numbers of frequency and direction bins

is with bins of equal width (equal Δf and $\Delta\theta$). Both methods of discretization were tested using artificial wave spectral input and the Duck bathymetry. Four spectra types were tested:

- Narrow directional distribution, narrow frequency distribution
- Wide directional distribution, narrow frequency distribution
- Narrow directional distribution, wide frequency distribution
- Wide directional distribution, wide frequency distribution

The artificial spectra used were a combination of the TMA (Texel-Marsden-Arsloe) frequency spectrum (Hughes 1984) with the wrapped normal directional distribution (Borgman 1985). The TMA spectrum is:

$$E(f) = \frac{\alpha g^2}{(2\pi)^4 f^5} \left(-1.25 \left(\frac{f_p}{f} \right)^4 + (\ln \gamma) \exp \left(\frac{-(f-f_p)^2}{2\sigma^2 f^2} \right) \right) \Phi(f, h), \quad (5.1)$$

where $E(f)$ is the energy density spectrum, α is Phillips' constant ($= 0.0081$), and f_p is the peak frequency. The spectrum peakedness is controlled by γ : $\gamma = 20$ is used for narrow-banded frequency distributions and $\gamma = 2$ for broad-banded frequency distributions. The variable $\Phi(f, h)$ is:

$$\Phi(f, h) = \begin{cases} \frac{1}{2} \omega_h^2; & \omega_h \leq 1 \\ 1 - \frac{1}{2} (2 - \omega_h)^2; & \omega_h > 1 \end{cases}, \quad (5.2)$$

where

$$\omega_h = 2\pi f \left(\frac{h}{g} \right)^{\frac{1}{2}}. \quad (5.3)$$

The wrapped normal distribution is:

$$D(\theta) = \frac{1}{2\pi} + \frac{1}{\pi} \sum_{j=1}^J \exp \left[-\frac{(j\sigma_m)^2}{2} \right] \cos j(\theta - \theta_m). \quad (5.4)$$

Here, $D(\theta)$ is the directional spreading function, σ_m is the variance in the spectrum, and θ_m is the mean wave direction. The variance here dictates the directional distribution; $\sigma_m = 10$ for narrow spectra and $\sigma_m = 30$ for broad spectra.

This test was performed after a correction to the REF/DIF-S code was made and, thus, does not use the "uncorrected" model. Figures 5.22–5.25 show wave heights calculated from the model using the various spectrum characteristics listed above and the two different spectra discretization methods. It is apparent that differences between the two methods are minor. However, this conclusion is likely case-dependent; it is expected that spectra with a more symmetric directional distribution would be more sensitive to discretization method.

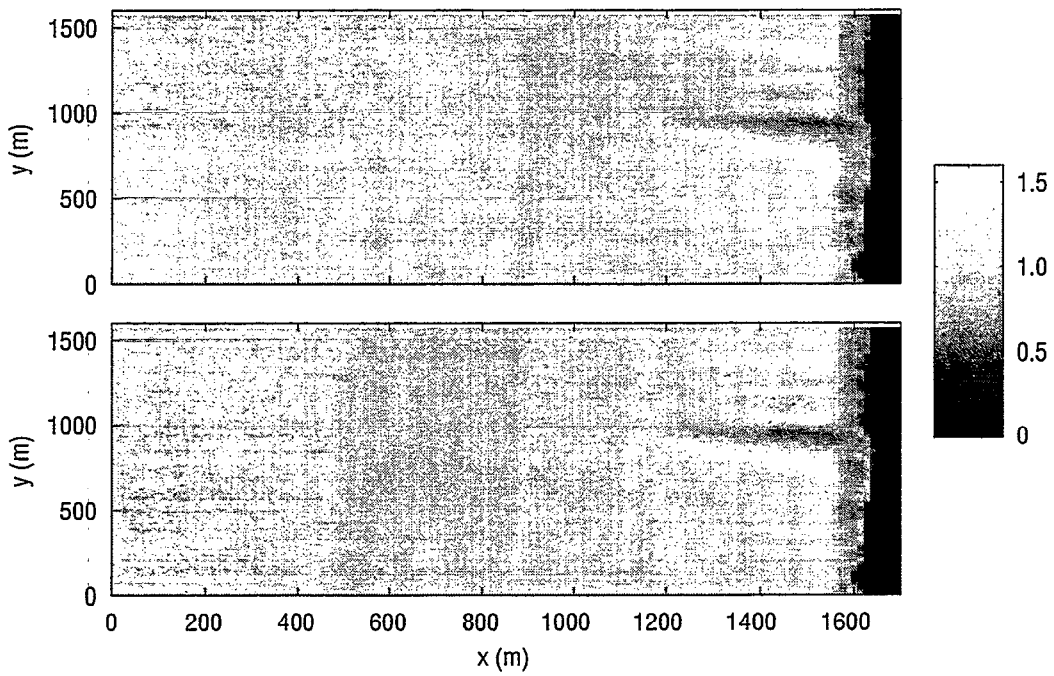


Fig. 5.22 — Comparison of REF/DIF-S results using different methods of spectra discretization, narrow frequency distribution, and narrow directional distribution

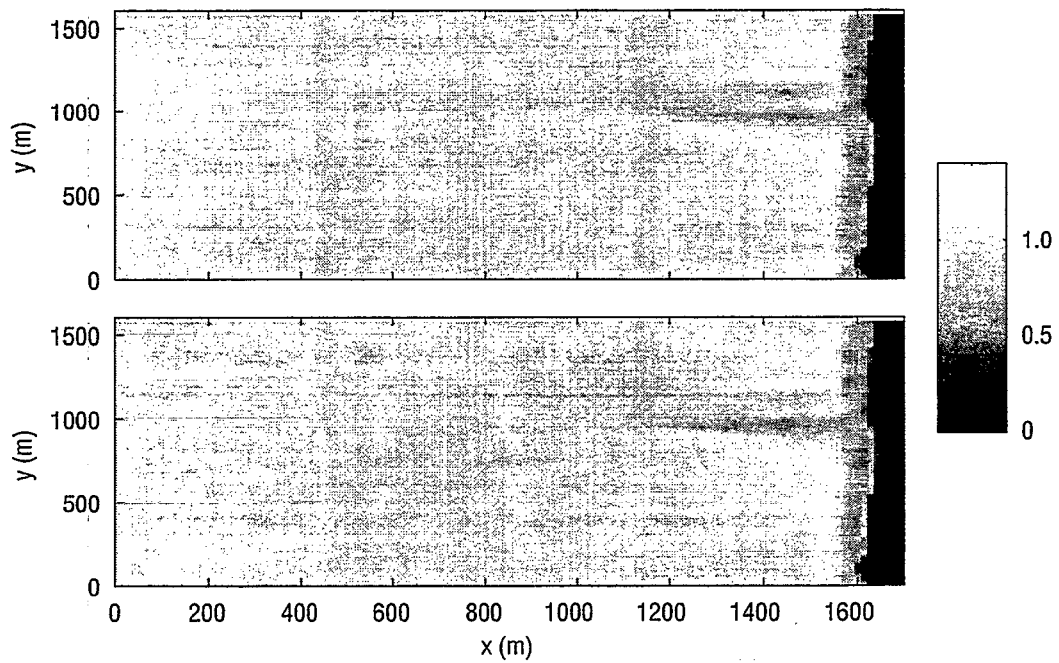


Fig. 5.23 — Comparison of REF/DIF-S results using different methods of spectra discretization, narrow frequency distribution, and broad directional distribution

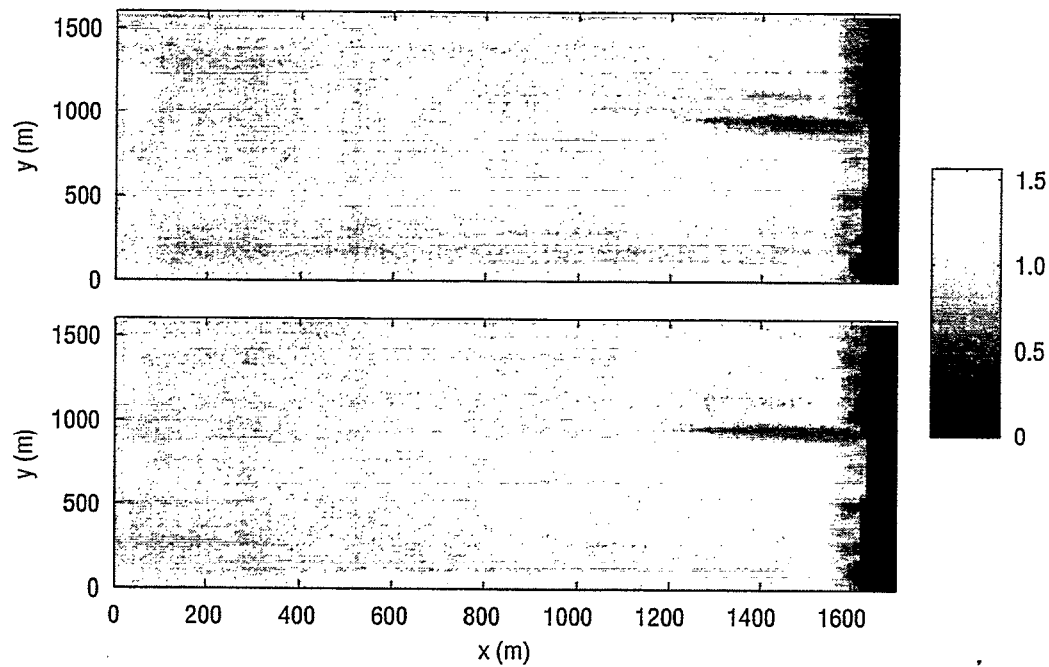


Fig. 5.24 — Comparison of REF/DIF-S results using different methods of spectra discretization, broad frequency distribution, and narrow directional distribution

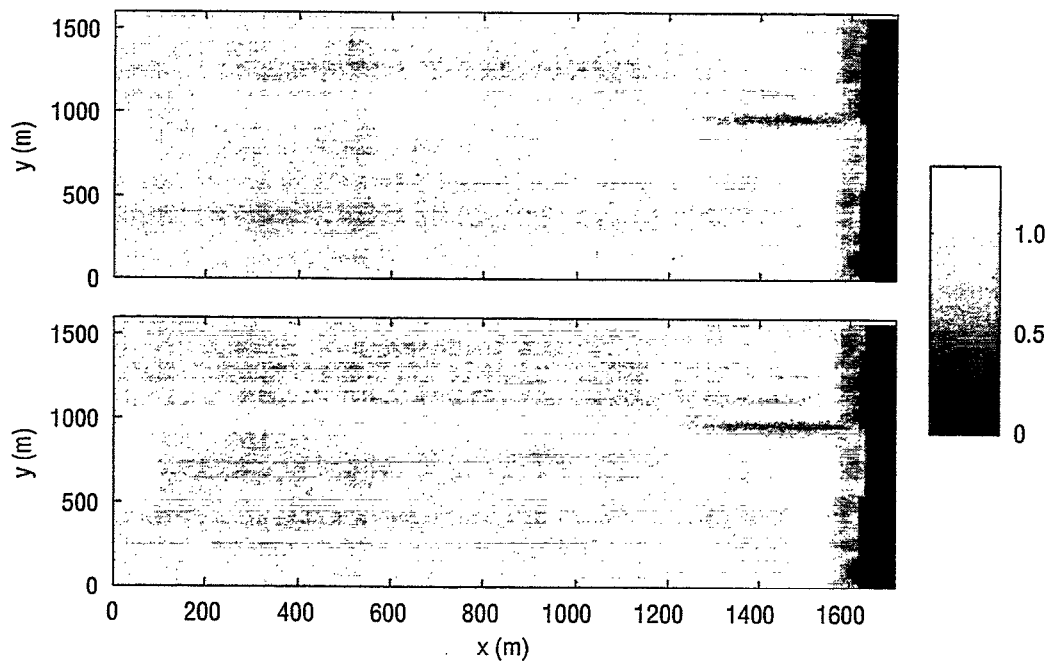


Fig. 5.25 — Comparison of REF/DIF-S results using different methods of spectra discretization, broad frequency distribution, and broad directional distribution

5.2.6 Comparison to RCPWAVE and REF/DIF1 Results

It is not uncommon for spectra to be approximated by a series of pseudo-monochromatic waves, particularly when many model runs need to be undertaken or when only integrated wave parameters from spectra (significant wave height, peak period, peak direction) are available. In this section, the effect of such an approximation is considered. For 22 of the DELILAH cases, the monochromatic models RCPWAVE and REF/DIF1 were run using the wave period at the spectral peak and peak direction associated with the offshore spectra; representative examples of these comparisons are shown in Figs. 5.26–5.43. For most of the DELILAH cases, RCPWAVE required much smoothing of the bathymetry to provide solution convergence at the grid resolution used. The amount of smoothing required was very sensitive to wave period; for the cases with the longest waves, RCPWAVE failed to converge even with a very large amount of bathymetry smoothing. For the cases for which smoothing was required, RCPWAVE and REF/DIF1 were run with the smoothed bathymetries and results were compared. Results from the two models were generally similar. The monochromatic models typically overpredicted wave heights offshore of the surf zone. The model output frequently exhibits a sharp peak in wave height prior to breaking; this peak is not seen in the data. The difference in the breaking patterns between the data and the model are due to the monochromatic nature of the models. With the irregular nature of the waves in nature, the surf zone is wider and the breaking point less pronounced than with monochromatic waves. This is because different waves in the spectrum have different breaking depths and the net effect is an overall smoothing of the decay. As mentioned in an earlier section, the model REF/DIF-S accounts for the irregular nature of the waves both outside and within the surf zone. For several DELILAH cases, no bathymetry smoothing was necessary to get useable RCPWAVE output; for these cases, all three models were run over the same unsmoothed bathymetry and compared. Oscillations are evident in some RCPWAVE output, likely due to slight convergence problems. It is felt that cases that do not converge offshore do not suffer detrimental effects on output for convergent grid rows farther inshore. REF/DIF-S output is typically more accurate than the other models offshore of the surf zone. Landward of the sand bar seen in many of the profiles, results are mixed; no one model gives the best results consistently. Figs. 5.44–5.47 show comparisons of wave angle as measured by the directional array to that from the three models. It is clear that no model does particularly well and a definitive conclusion is impossible.

5.3 Comparisons To Field Data—Conclusions

In this section, a few general conclusions concerning REF/DIF1, REF/DIF-S, and their agreement with the DELILAH data will be discussed. Note here that these are preliminary conclusions; the limited amount of data outside the surf zone precludes a more rigorous discussion.

In general, the models perform well in this field scenario. The surf zone component in the model replicates the wave height decay well, even simulating the wave reformation in the lee of the sand bar. The irregular wave model REF/DIF-S seems to do better than the monochromatic wave models REF/DIF1 and RCPWAVE, and neither of the REF/DIF models require bathymetric smoothing beforehand for convergence to occur. It can be argued that a truer representation of the irregular wave environment within the monochromatic wave models would be to run them repeatedly over the bathymetry with the discretized spectral components and add the results. However, using characteristic spectral parameters to represent the entire spectrum is a common technique in simulating a wave climate for a particular region.

To more fully validate the models in a field situation, it is necessary to have high quality directional wave data at several points outside the surf zone within a modeled domain. In particular,

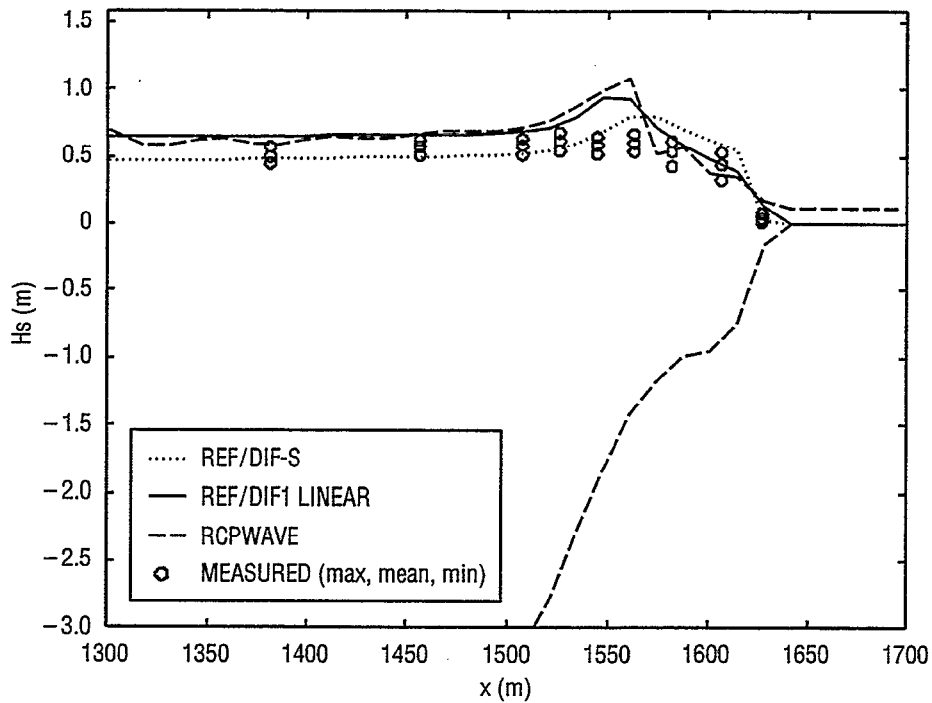


Fig. 5.26 — Comparison of significant wave heights from REF/DIF-S, REF/DIF1, and RCPWAVE to the DELILAH experiment data for the time period beginning at 2200 EST, 10-7-90

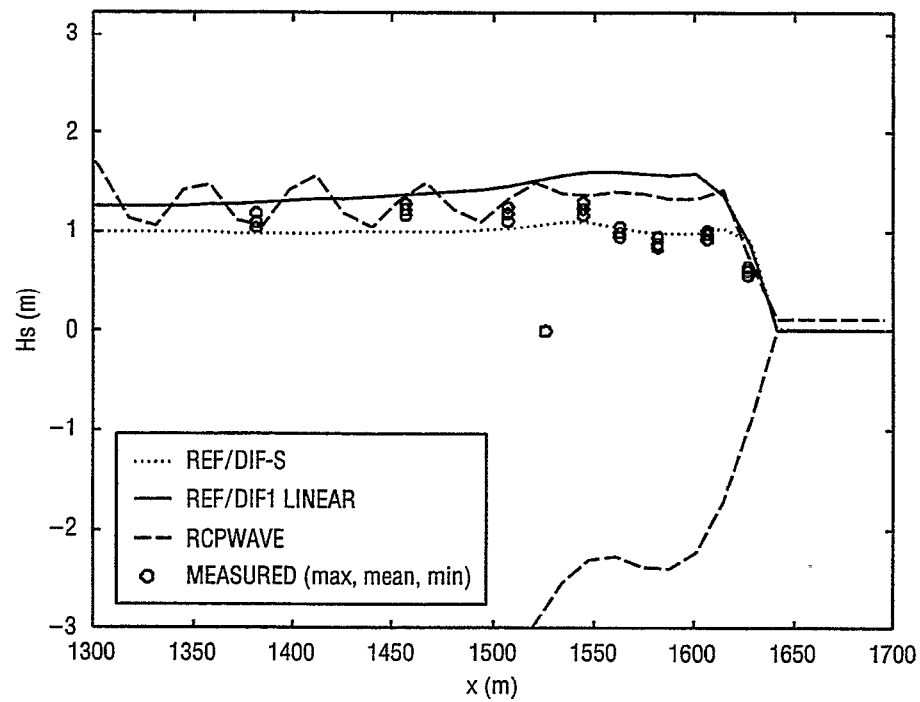


Fig. 5.27 — Comparison of significant wave heights from REF/DIF-S, REF/DIF1, and RCPWAVE to the DELILAH experiment data for the time period beginning at 0100 EST, 10-12-90

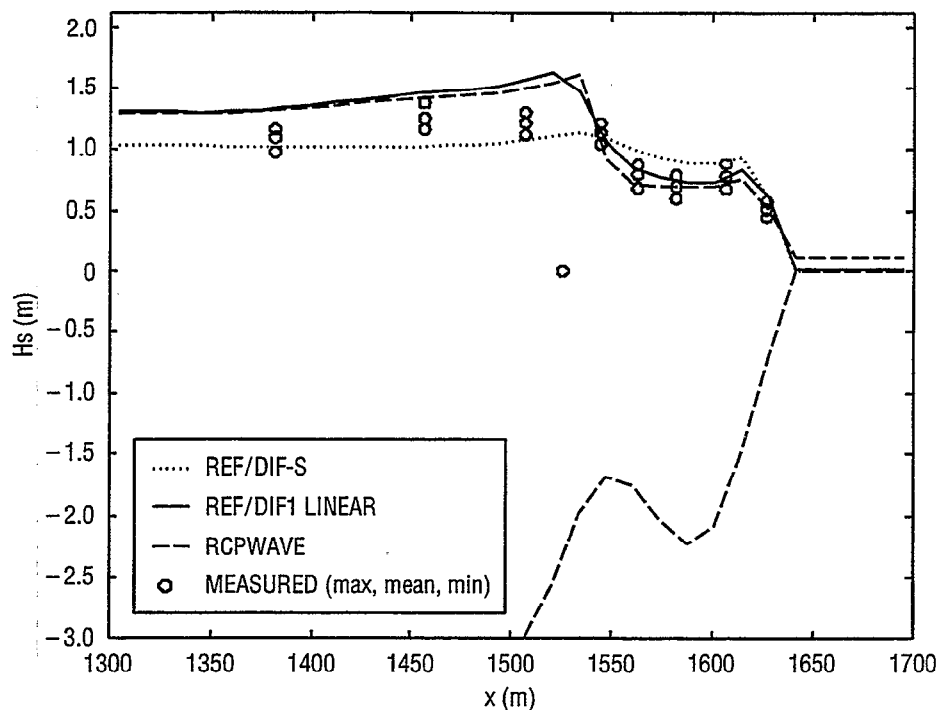


Fig. 5.28 — Comparison of significant wave heights from REF/DIF-S, REF/DIF1, and RCPWAVE to the DELILAH experiment data for the time period beginning at 0400 EST, 10-12-90

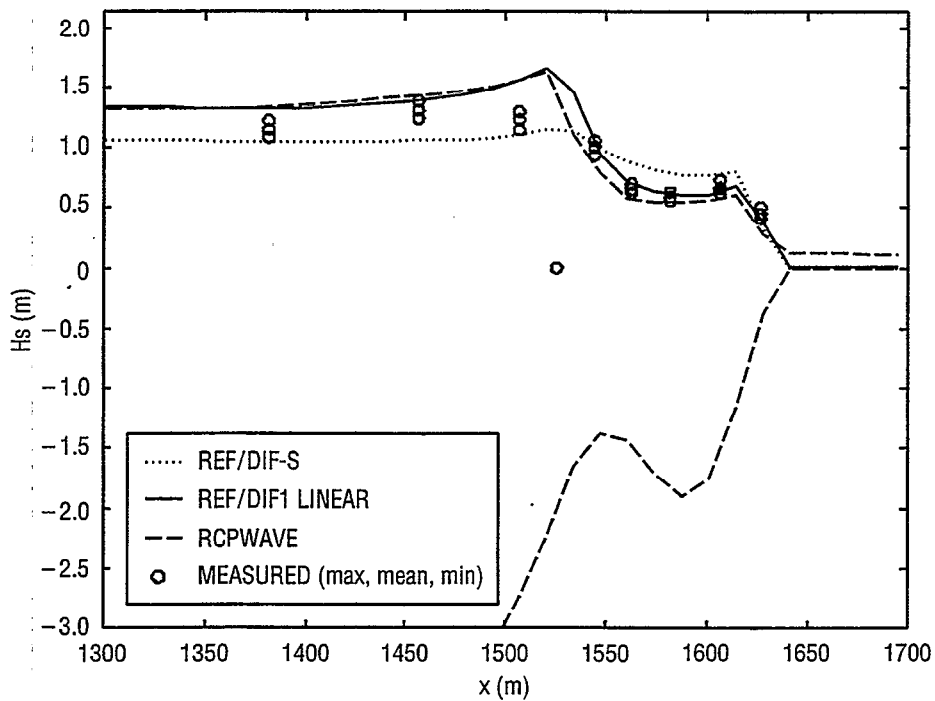


Fig. 5.29 — Comparison of significant wave heights from REF/DIF-S, REF/DIF1, and RCPWAVE to the DELILAH experiment data for the time period beginning at 0700 EST, 10-12-90

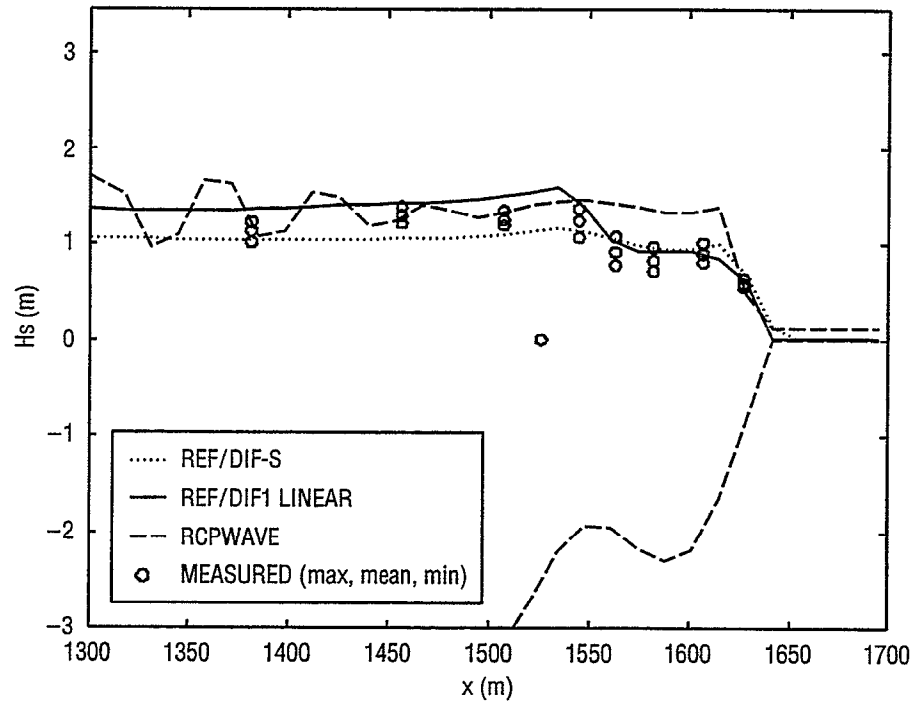


Fig. 5.30 — Comparison of significant wave heights from REF/DIF-S, REF/DIF1, and RCPWAVE to the DELILAH experiment data for the time period beginning at 1000 EST, 10-12-90

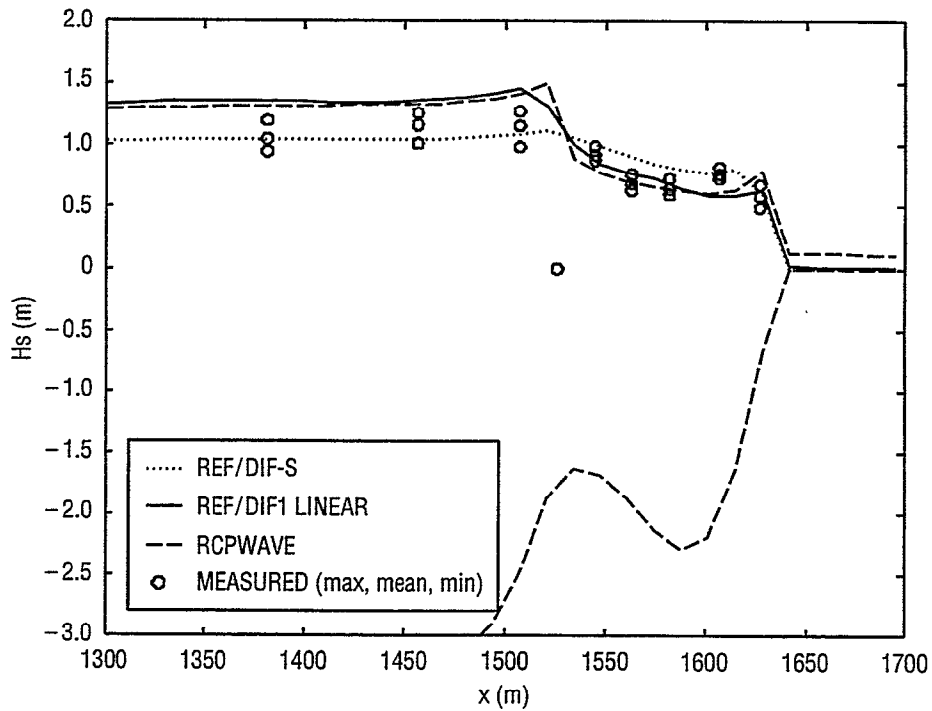


Fig. 5.31 — Comparison of significant wave heights from REF/DIF-S, REF/DIF1, and RCPWAVE to the DELILAH experiment data for the time period beginning at 1000 EST, 10-14-90

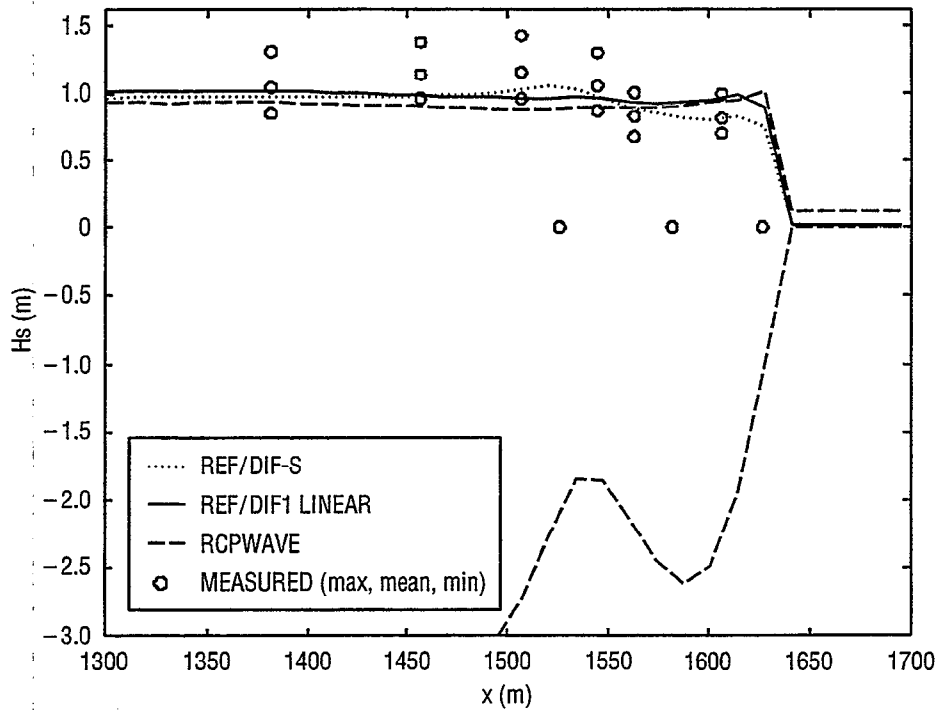


Fig. 5.32 — Comparison of significant wave heights from REF/DIF-S, REF/DIF1, and RCPWAVE to the DELILAH experiment data for the time period beginning at 0100 EST, 10-16-90

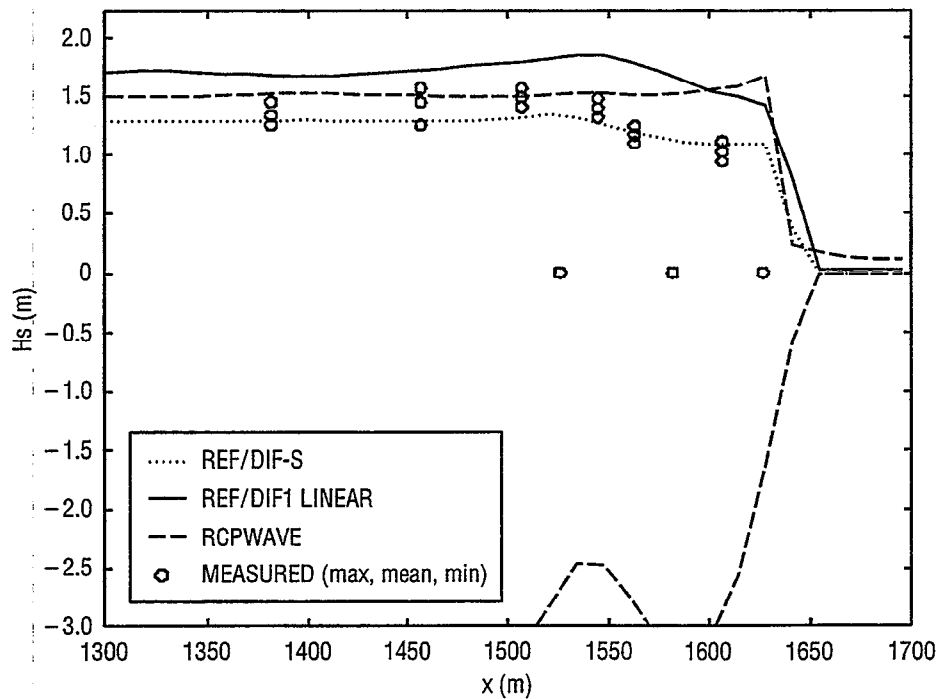


Fig. 5.33 — Comparison of significant wave heights from REF/DIF-S, REF/DIF1, and RCPWAVE to the DELILAH experiment data for the time period beginning at 0400 EST, 10-16-90

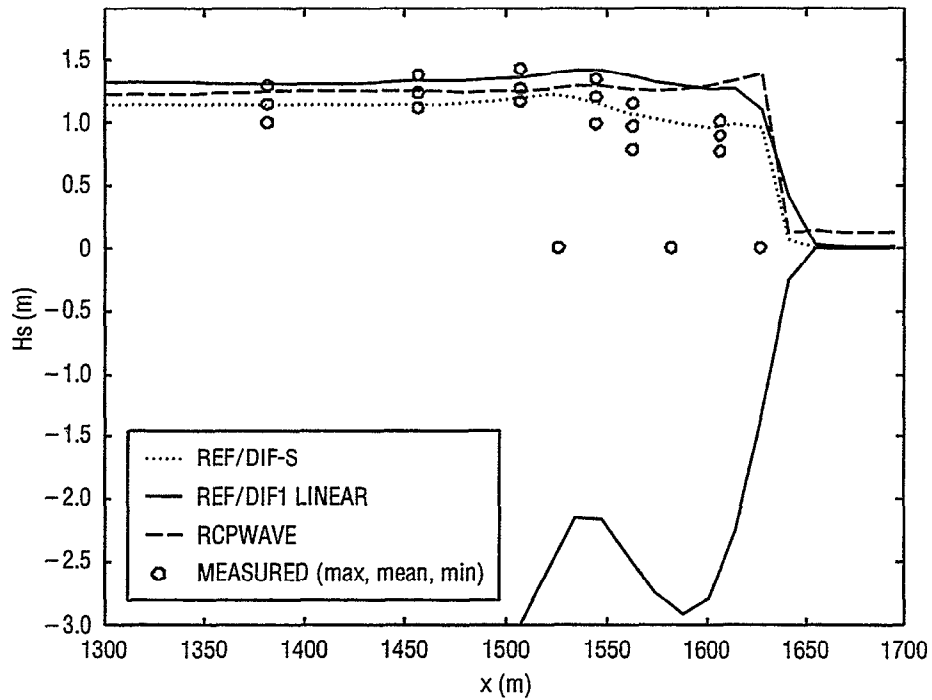


Fig. 5.34 — Comparison of significant wave heights from REF/DIF-S, REF/DIF1, and RCPWAVE to the DELILAH experiment data for the time period beginning at 0700 EST, 10-16-90

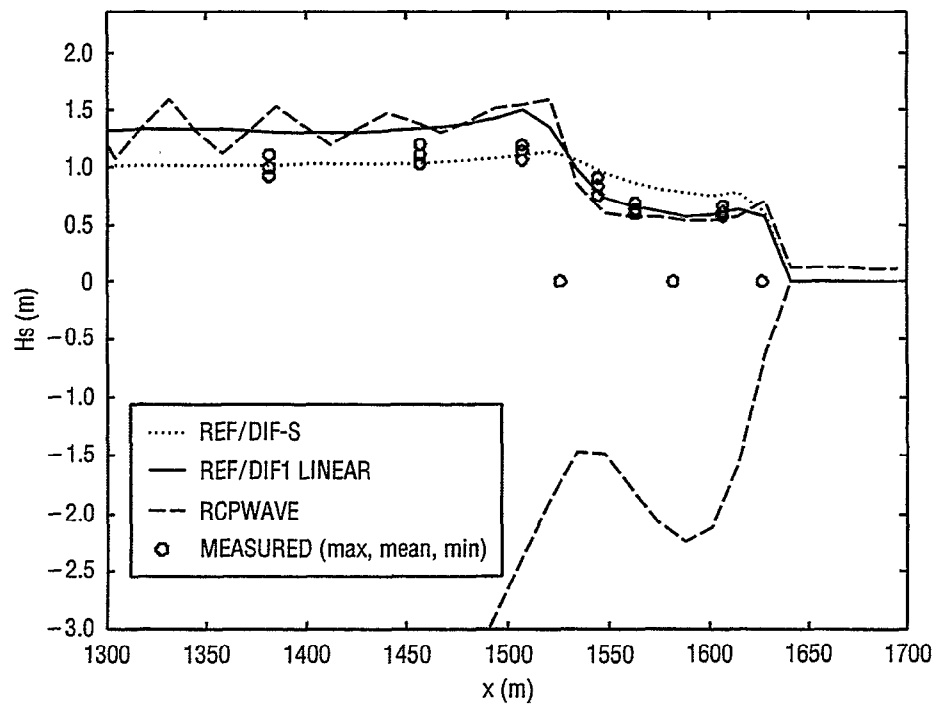


Fig. 5.35 — Comparison of significant wave heights from REF/DIF-S, REF/DIF1, and RCPWAVE to the DELILAH experiment data for the time period beginning at 1000 EST, 10-16-90

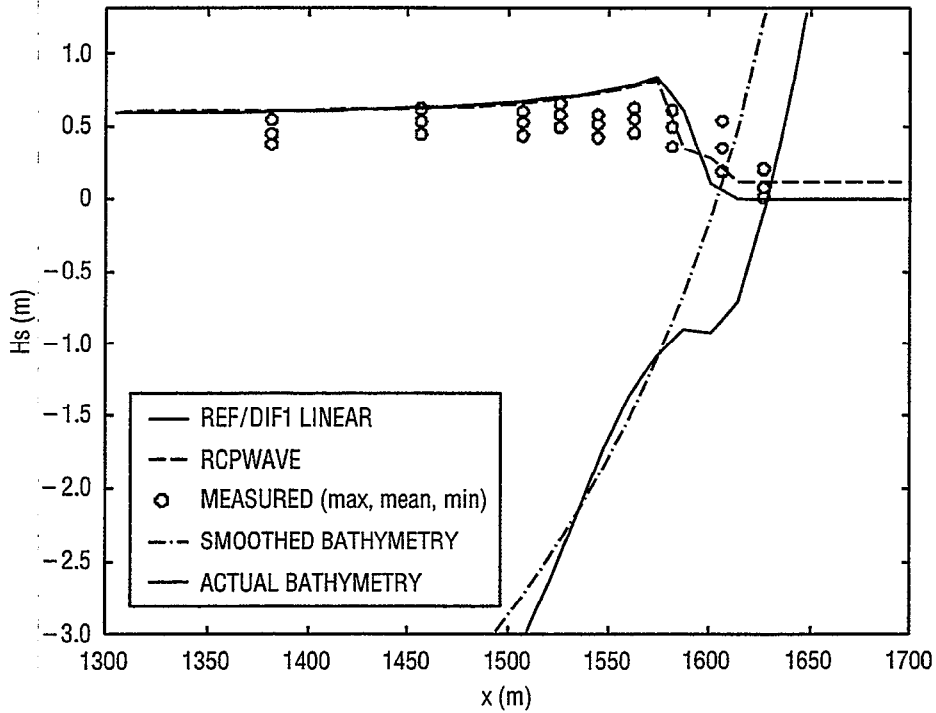


Fig. 5.36 — Comparison of significant wave heights from REF/DIF1 and RCPWAVE to the DELILAH experiment data for the time period beginning at 0400 EST, 10-6-90, with both models run over the smoothed bathymetry shown

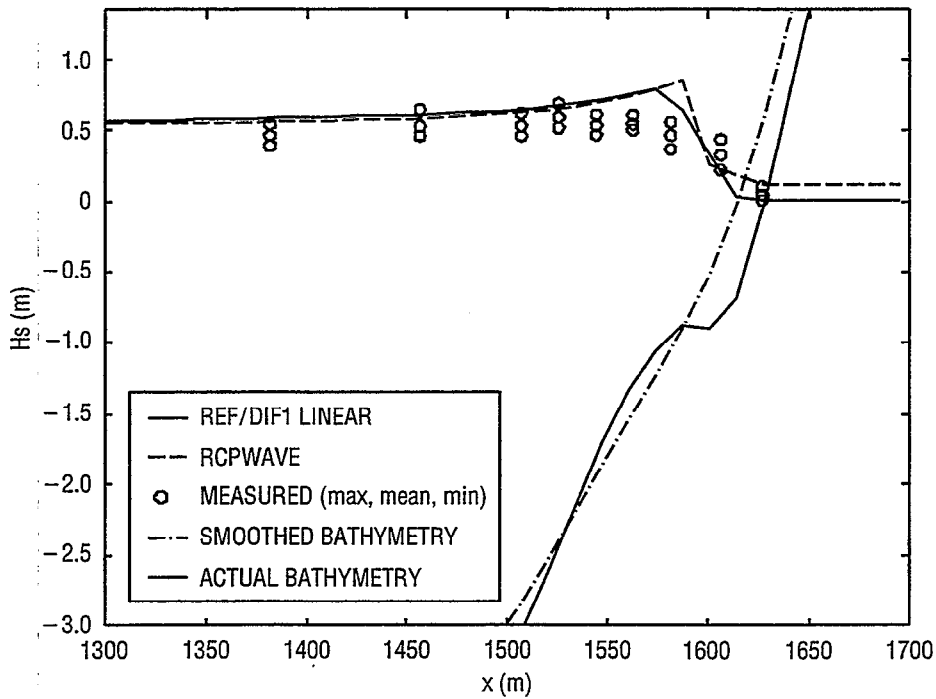


Fig. 5.37 — Comparison of significant wave heights from REF/DIF1 and RCPWAVE to the DELILAH experiment data for the time period beginning at 2200 EST, 10-6-90, with both models run over the smoothed bathymetry shown

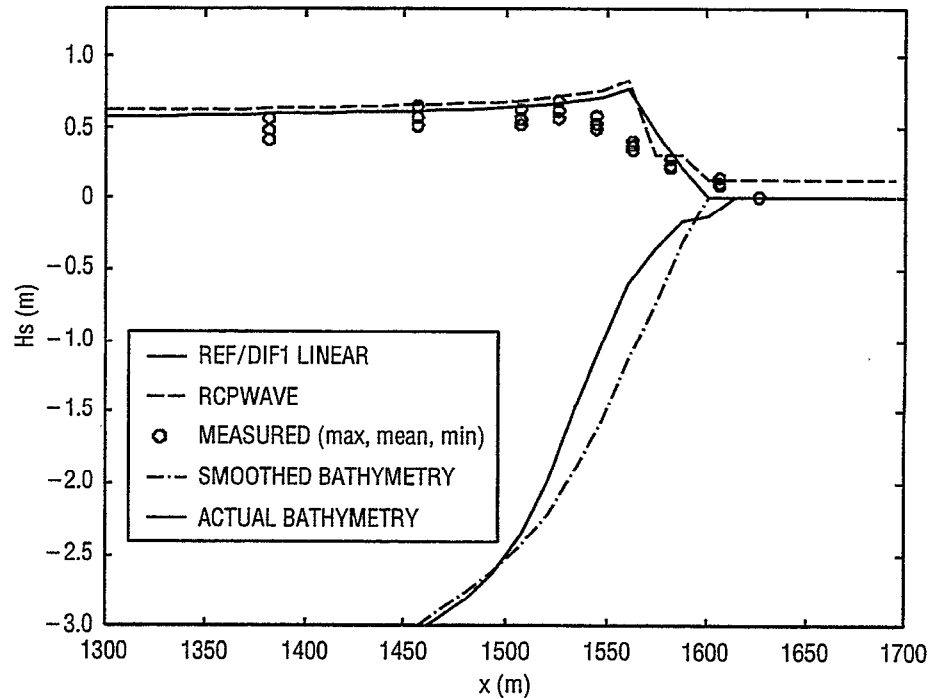


Fig. 5.38 — Comparison of significant wave heights from REF/DIF1 and RCPWAVE to the DELILAH experiment data for the time period beginning at 0100 EST, 10-7-90, with both models run over the smoothed bathymetry shown

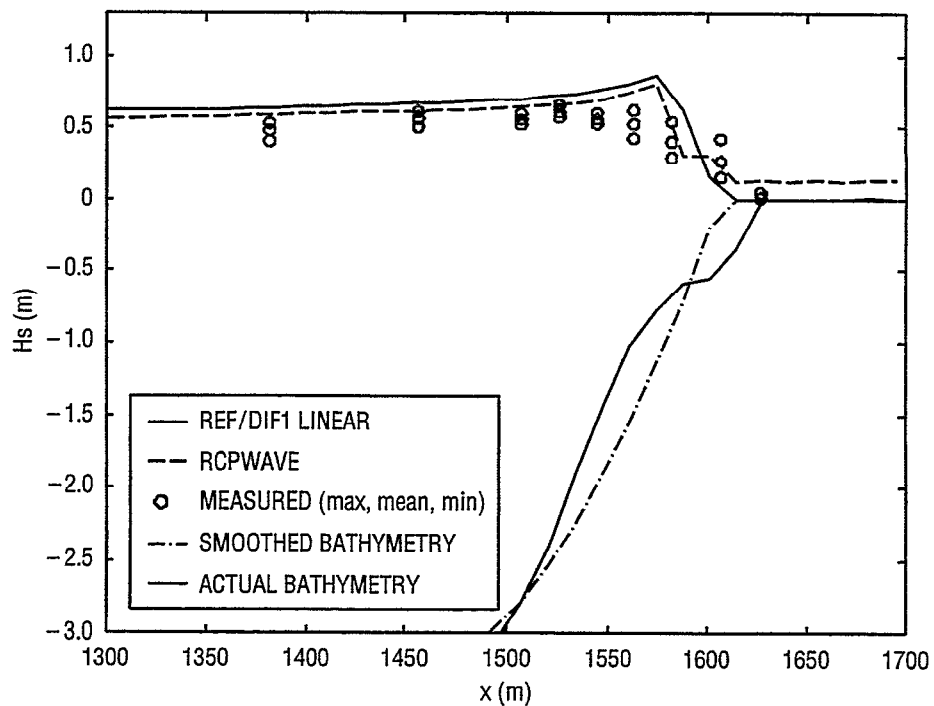


Fig. 5.39 — Comparison of significant wave heights from REF/DIF1 and RCPWAVE to the DELILAH experiment data for the time period beginning at 0400 EST, 10-7-90, with both models run over the smoothed bathymetry shown

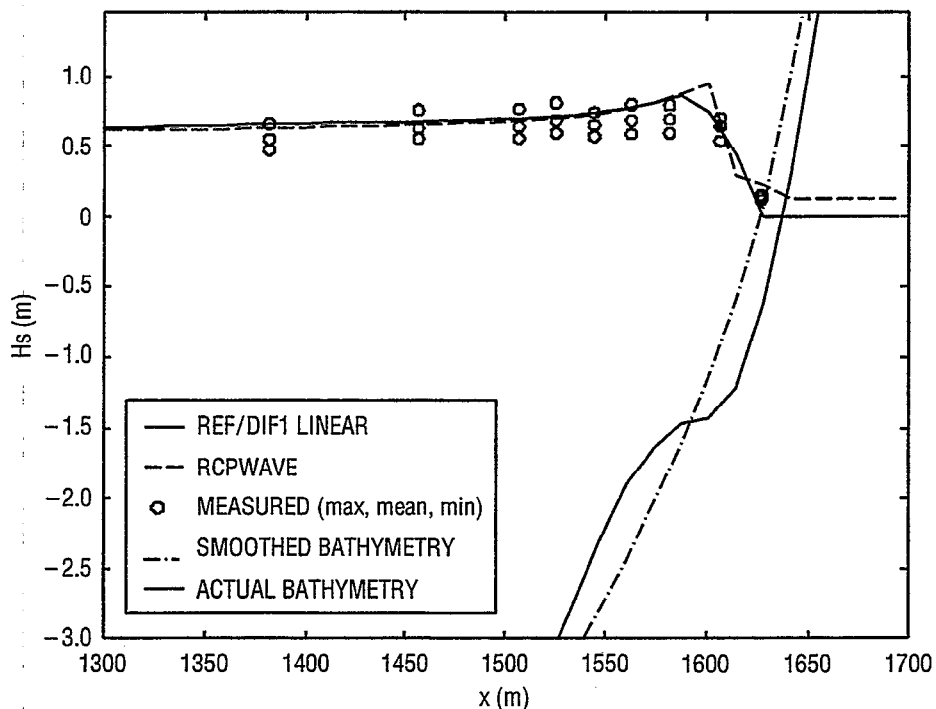


Fig. 5.40 — Comparison of significant wave heights from REF/DIF1 and RCPWAVE to the DELILAH experiment data for the time period beginning at 0700 EST, 10-7-90, with both models run over the smoothed bathymetry shown

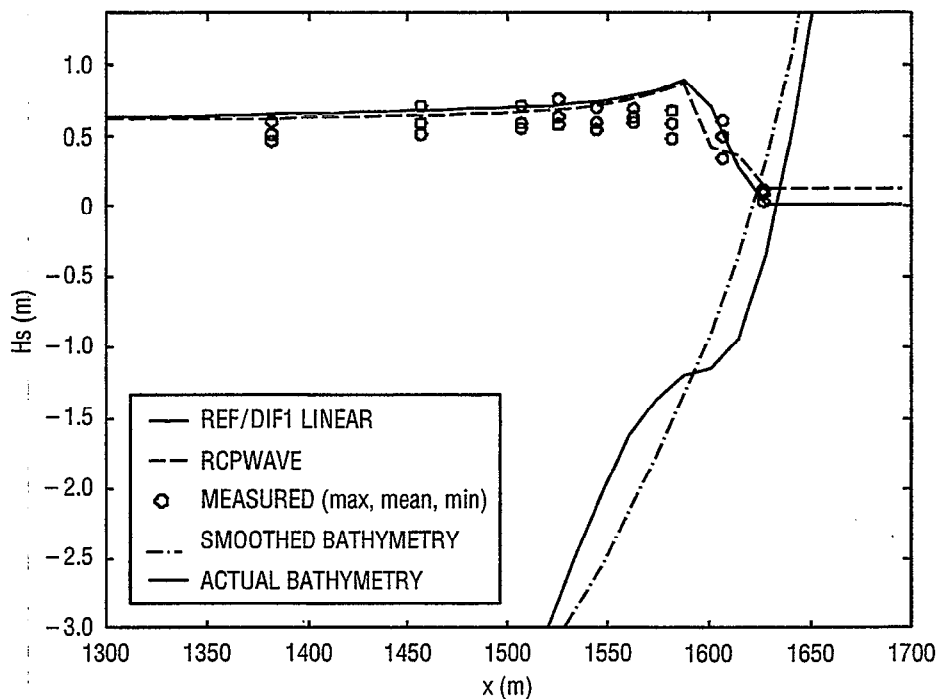


Fig. 5.41 — Comparison of significant wave heights from REF/DIF1 and RCPWAVE to the DELILAH experiment data for the time period beginning at 1000 EST, 10-7-90, with both models run over the smoothed bathymetry shown

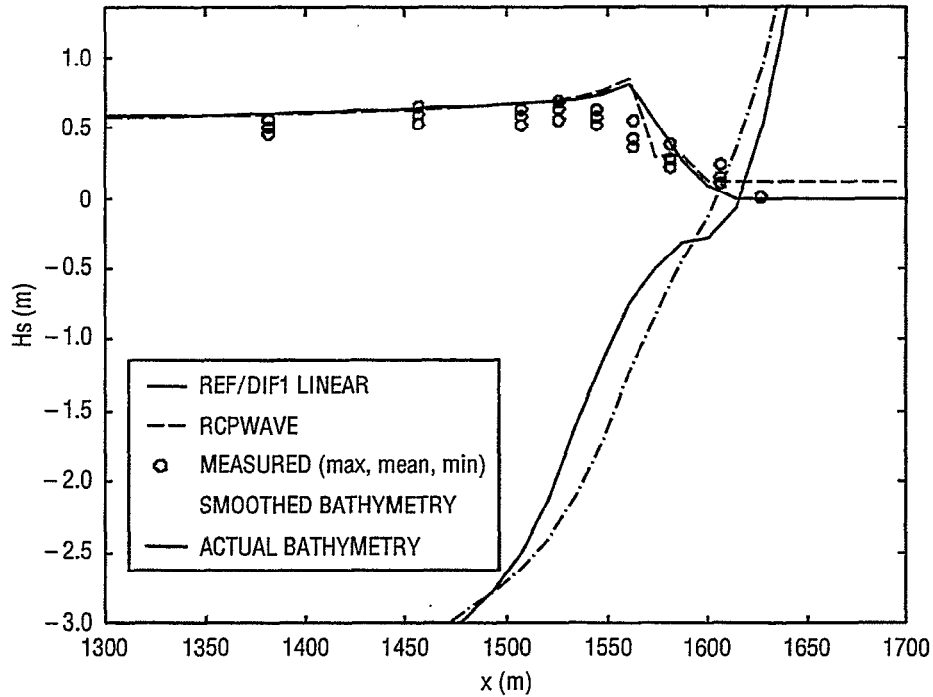


Fig. 5.42 — Comparison of significant wave heights from REF/DIF1 and RCPWAVE to the DELILAH experiment data for the time period beginning at 1300 EST, 10-7-90, with both models run over the smoothed bathymetry shown

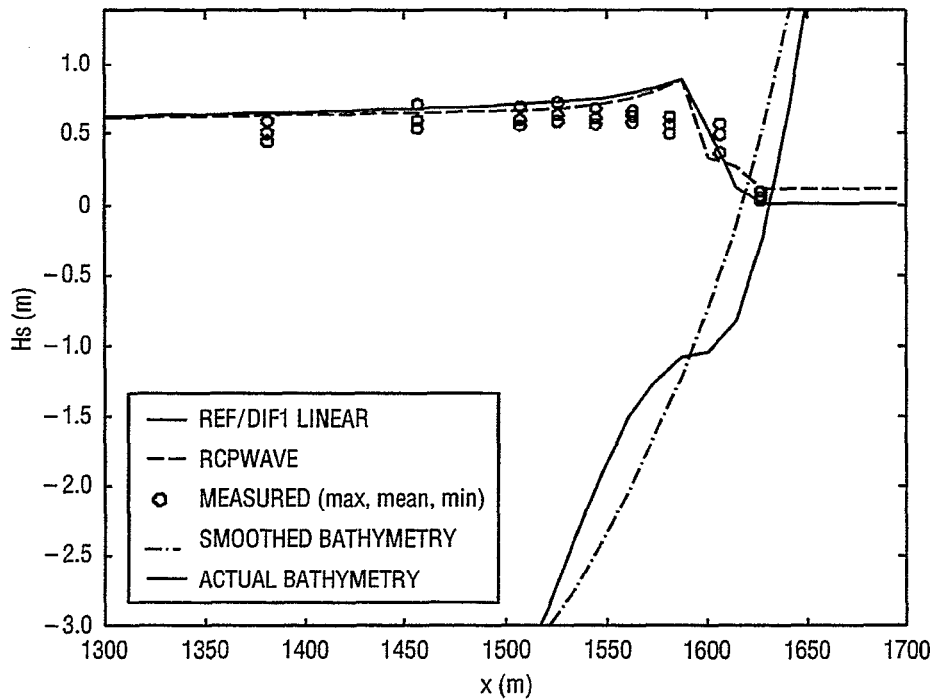


Fig. 5.43 — Comparison of significant wave heights from REF/DIF1 and RCPWAVE to the DELILAH experiment data for the time period beginning at 1900 EST, 10-7-90, with both models run over the smoothed bathymetry shown

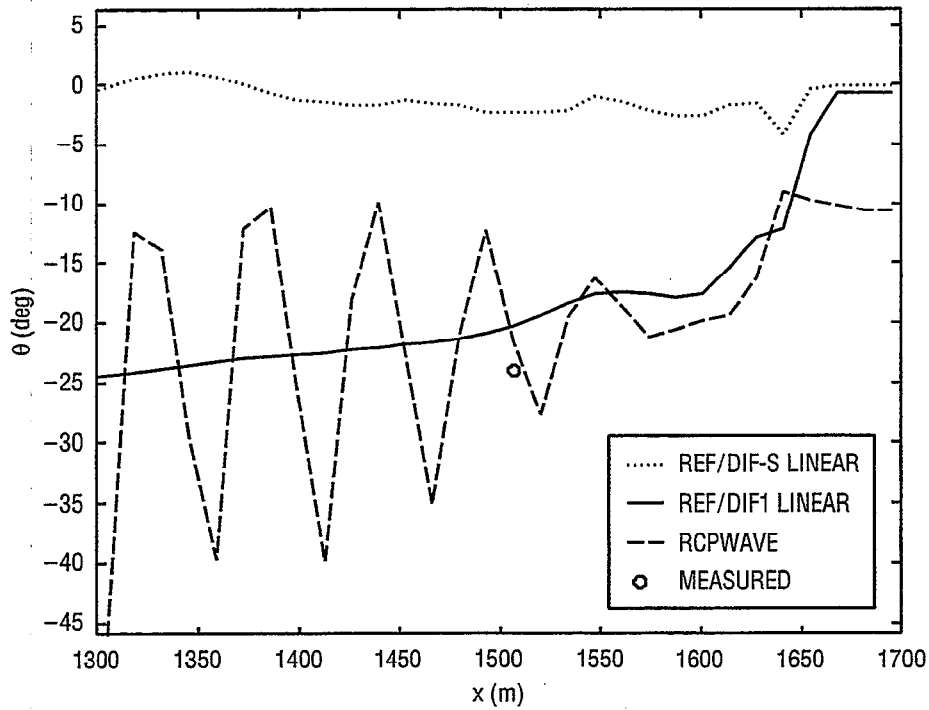


Fig. 5.44 — Comparison of wave angles from REF/DIF-S, REF/DIF1, and RCPWAVE to the DELILAH experiment data for the time period beginning at 0100 EST, 10-12-90

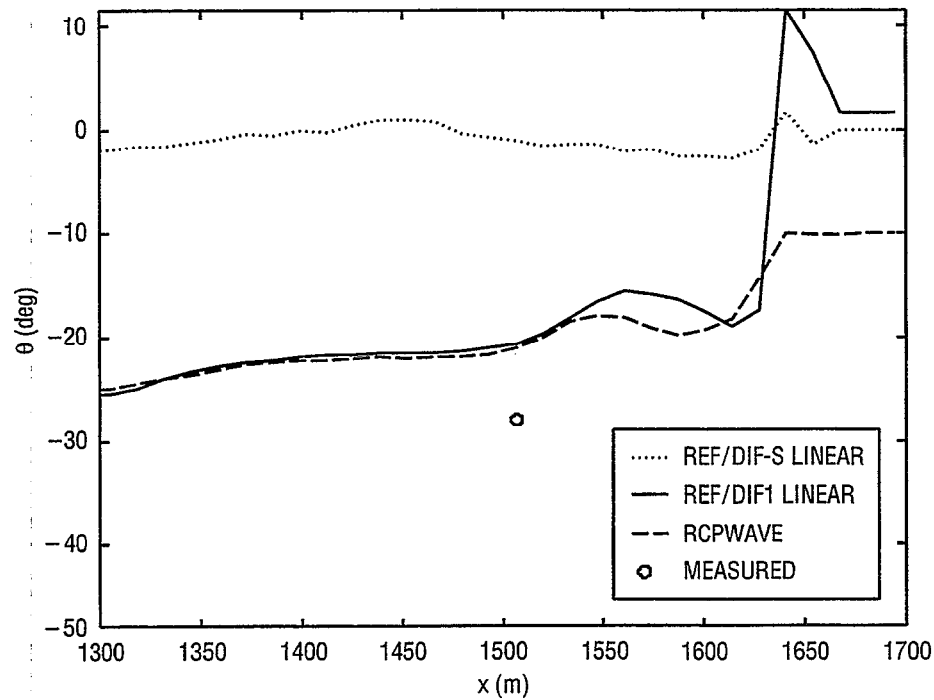


Fig. 5.45 — Comparison of wave angles from REF/DIF-S, REF/DIF1, and RCPWAVE to the DELILAH experiment data for the time period beginning at 0400 EST, 10-12-90

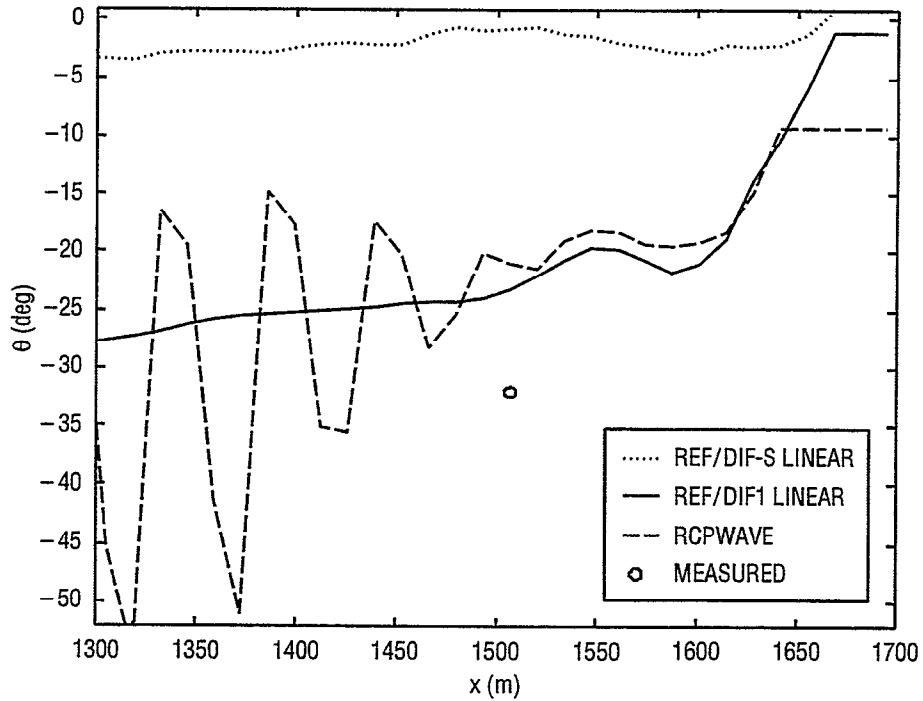


Fig. 5.46 — Comparison of wave angles from REF/DIF-S, REF/DIF1, and RCPWAVE to the DELILAH experiment data for the time period beginning at 1000 EST, 10-12-90

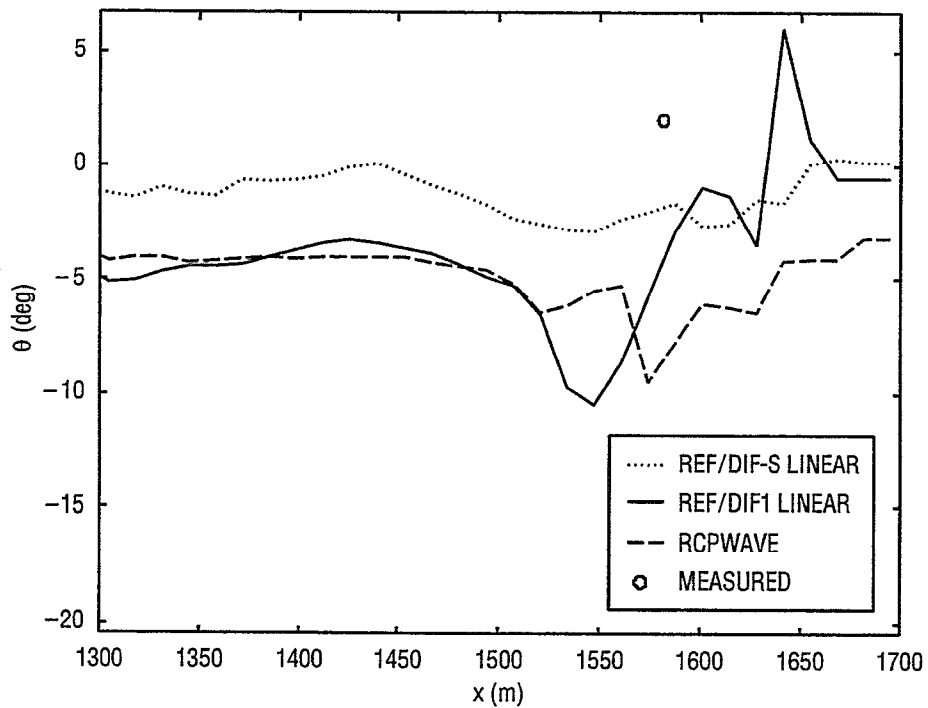


Fig. 5.47 — Comparison of wave angles from REF/DIF-S, REF/DIF1, and RCPWAVE to the DELILAH experiment data for the time period beginning at 1000 EST, 10-14-90

the wave angle calculation for REF/DIF-S has not been extensively validated at all due to a general lack of data. It is anticipated to obtain spectral wave data off the California coast in the near future; this will serve as a more rigorous test of the wave propagation characteristics of the models.

6.0 SENSITIVITY TO BATHYMETRIC UNCERTAINTY

The performance of the models discussed here are obviously quite dependent on input, either from bathymetry or initial wave conditions. This section will discuss the model sensitivity on uncertainty of bathymetric measurement.

Though the technologies used by boat surveyors have advanced greatly during the 20th century, error in depth measurement is still unavoidable. The wave models REF/DIF1 and REF/DIF-S were tested to determine how the deviation of bathymetric input from the "true" error-free bathymetry would affect model results. This deviation was created in a manner that would simulate the pattern of depth measurement errors that might occur during a boat survey where an echo sounder is used.

Similar model sensitivity studies have been done in the past. Brown et al. (1991) observed the effect of doubly periodic perturbations on wave ray models. Holthuijsen and Booij (1994) used calculations of wave height standard deviations to quantify the response of a wave model to a randomly perturbed bathymetry. Guo and Dalrymple (1996) made similar quantifications using bathymetries perturbed by uniformly and Gaussian distributed noise.

In the interest of simplicity, the simulated sounding data points were evenly spaced on a rectangular grid. Two tests were conducted.

6.1 Perturbed Planar Slope

For the first test, the planar beach used in the linear theory comparisons of Sec. 2.1 was utilized here as the idealized error-free bathymetry (slope = 0.009, offshore depth = 7 m). Six random realizations of the perturbed bathymetry (error-free bathymetry with random realizations of error superimposed) were generated on an 800 × 800 m grid with 50-m resolution. This coarse grid was then mapped onto a finer grid (3 m spacing) for use as wave model bathymetric input. This interpolation made use of "kriging," an advanced interpolation technique that makes use of statistical probability of the realization of interpolated depths. Three wave periods were used for this test: $T = 2.5$ s (deep water at the offshore boundary); $T = 5$ s (intermediate depth); and $T = 22$ s (shallow water). Both REF/DIF models were used with the composite nonlinear dispersion feature.

Error was calculated at each gridpoint using a statistical parameter, σ_e , and a Gaussian distribution. Error at each point was completely random (i.e., no correlation between errors at different data points). The British Royal Navy (1990) has suggested a standard for depth measurement that boat surveyors are expected to achieve:

$$2\sigma_e = \pm 0.5 \text{ m} \pm 0.009 h. \quad (6.1)$$

This is the error at the $2\sigma_e$ level; 95% of the error values should fall within this range.

6.1.2 REF/DIF1

Figure 6.1 shows an example of input and output from one of the realizations. The top figure (a) shows a realization of the bathymetry (perturbed with the error) and the bottom figure (b) shows the resulting wave height field for the $T = 5$ s case.

Six realizations of random perturbations of the bathymetry were generated, the wave model was run for the wave conditions given over each realization, and then the standard deviations of both the bathymetry and the wave height field over all the realizations were calculated. It is expected that as more realizations were generated, the average of these realizations would approach the unperturbed original bathymetry. Figure 6.2 shows the standard deviation fields of both the bathymetry and the wave heights for $T = 2.5$ s. Figure 6.3 shows the standard deviation fields for the wave

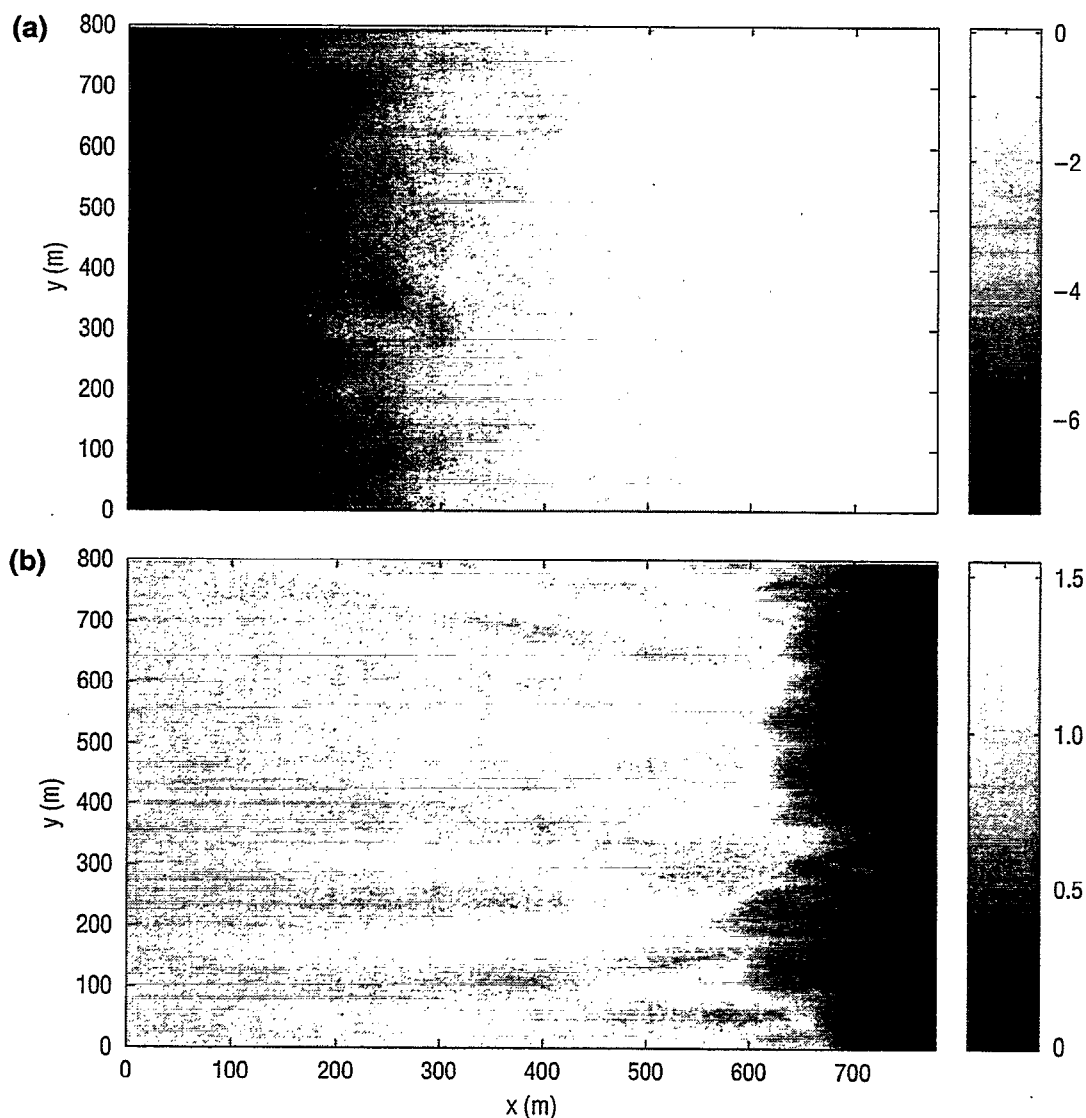


Fig. 6.1 — Results of a single realization of 100% random error distributed over linear slope, (a) bathymetry and (b) wave heights from REF/DIF1 for a 5 s wave

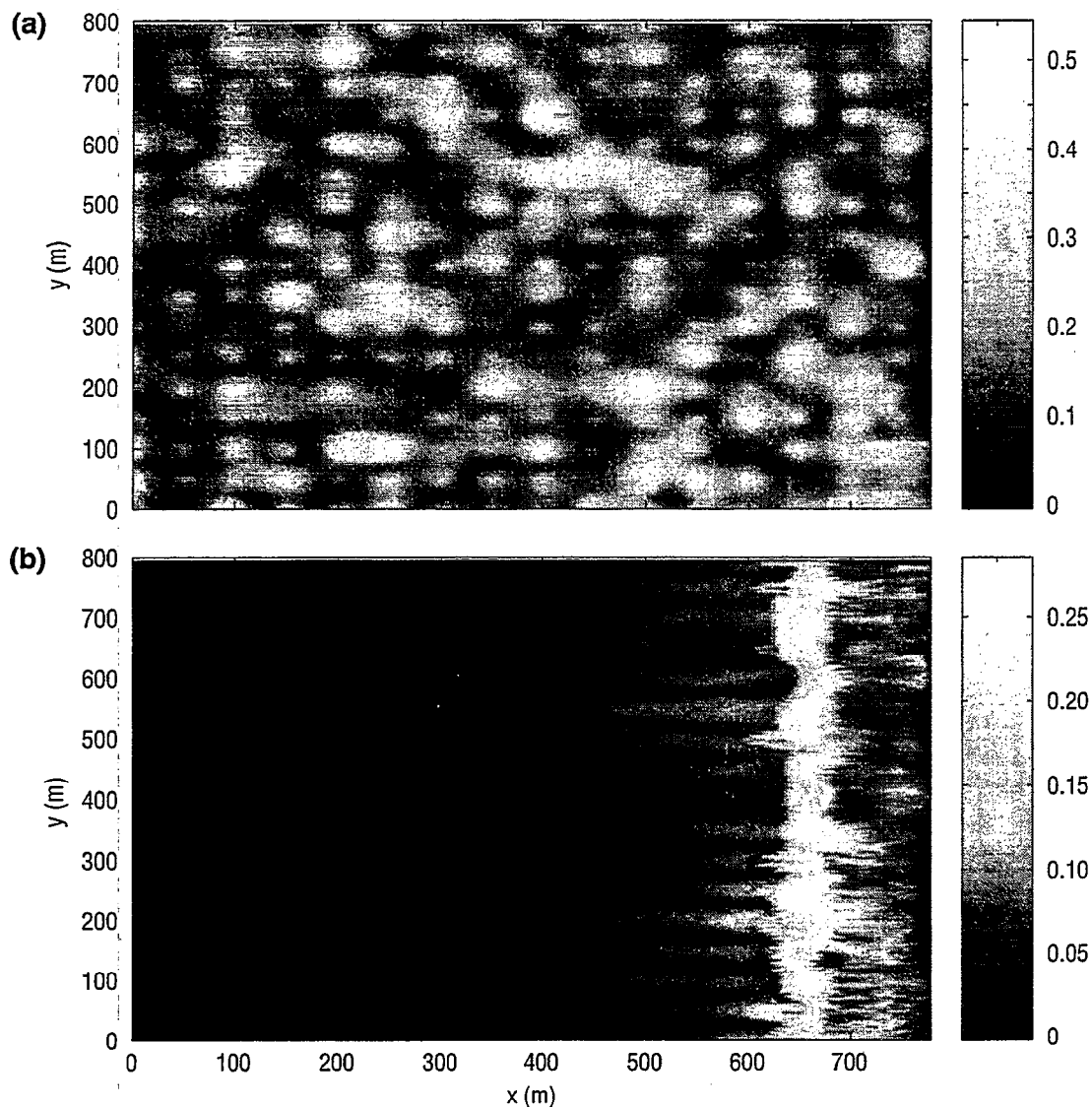


Fig. 6.2 — Results of analysis for six realizations of 100% random error distributed over linear slope, (a) standard deviation of depths and (b) standard deviation of wave heights from REF/DIF1, $T = 2.5$ s

heights with $T = 5$ s and $T = 22$ s. Figures 6.4–6.9 depict the standard deviations of both the bathymetry and the wave height field along various x - and y -wise transects. For the $T = 2.5$ s case, a region of high wave height standard deviation exists near the surf zone, likely due to variability of breaking location from one realization to the other. The wave height standard deviation is greater in the offshore regions for the 5 s case than it is for the other cases; the reason for this is not clear. The perturbation of the bathymetry caused unrealistically high wave heights landward of the surf zone for the $T = 22$ s. This resulted in very high variance at these locations. It may be that the dissipation mechanism in the model has difficulty with excessive bathymetric variations on scales of less than 1 wavelength.

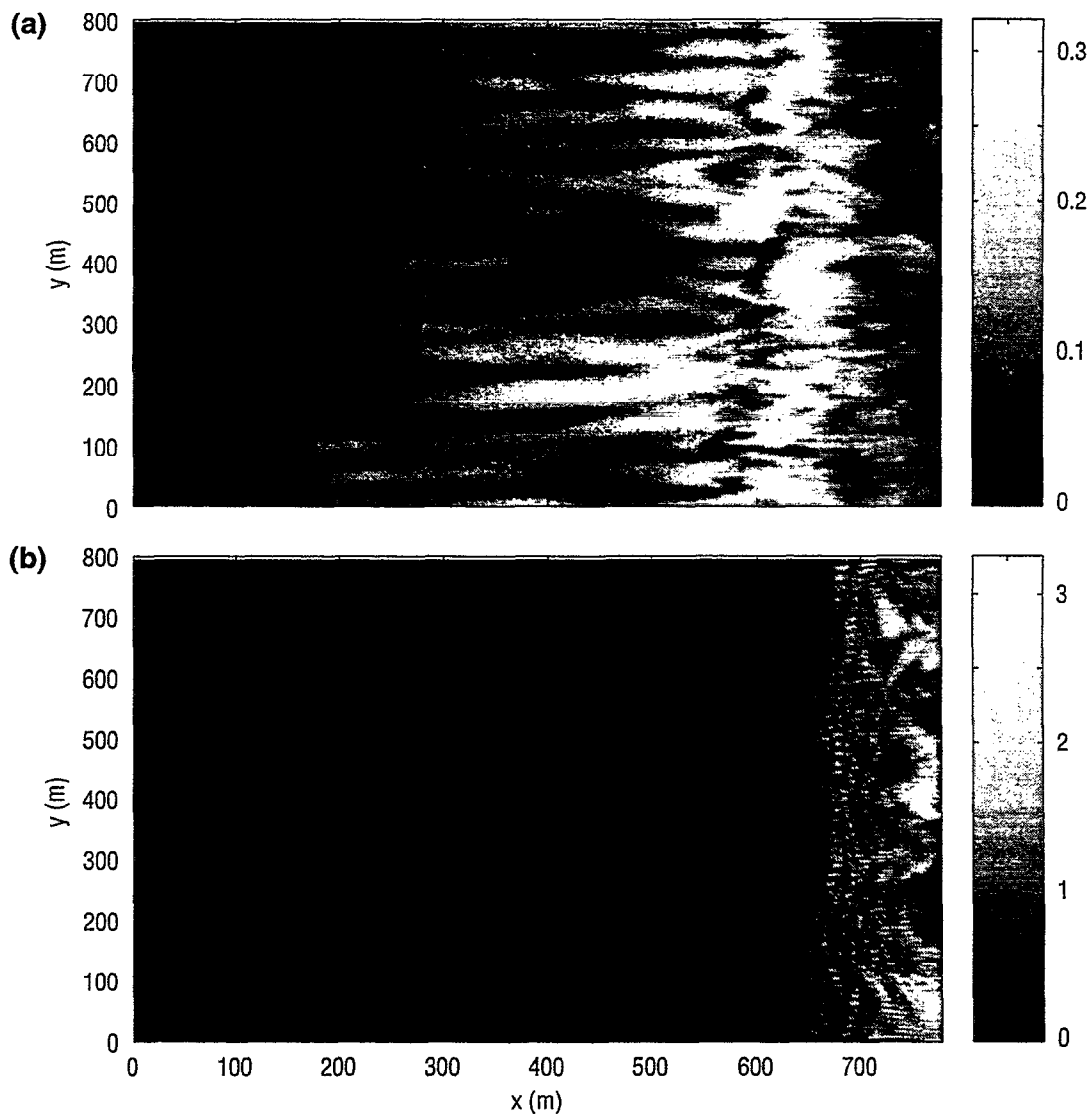


Fig. 6.3 — Results of analysis for six realizations of 100% random error distributed over linear slope, (a) standard deviation of wave heights from REF/DIF1, $T = 5$ s and (b) standard deviation of wave heights from REF/DIF1, $T = 22$ s

6.1.3 REF/DIF-S

The same six bathymetric realizations were used with REF/DIF-S. REF/DIF-S was run with similar wave conditions ($\theta_{mean} = 0$, $T_{peak} = 2.5$ s, 5 s, 22 s). Two different spectral modes were employed: (1) narrow directional spectrum ($\sigma = 10$), narrow frequency spectrum ($\gamma = 20$) and (2) broad directional spectrum ($\sigma = 30$), broad frequency spectrum ($\gamma = 2$). Figures 6.10–6.13 show the spatial distributions of bathymetric standard deviations and wave height fields for both the narrow frequency, narrow direction and broad frequency, broad direction cases. Figures 6.14–6.25 show the results along transects as before. The resulting wave height standard deviations are typically smaller than those calculated from REF/DIF1 output. The shape of the wave spectra (broad or narrow frequency/direction distributions) seems to have had little effect on σ_H , the wave height

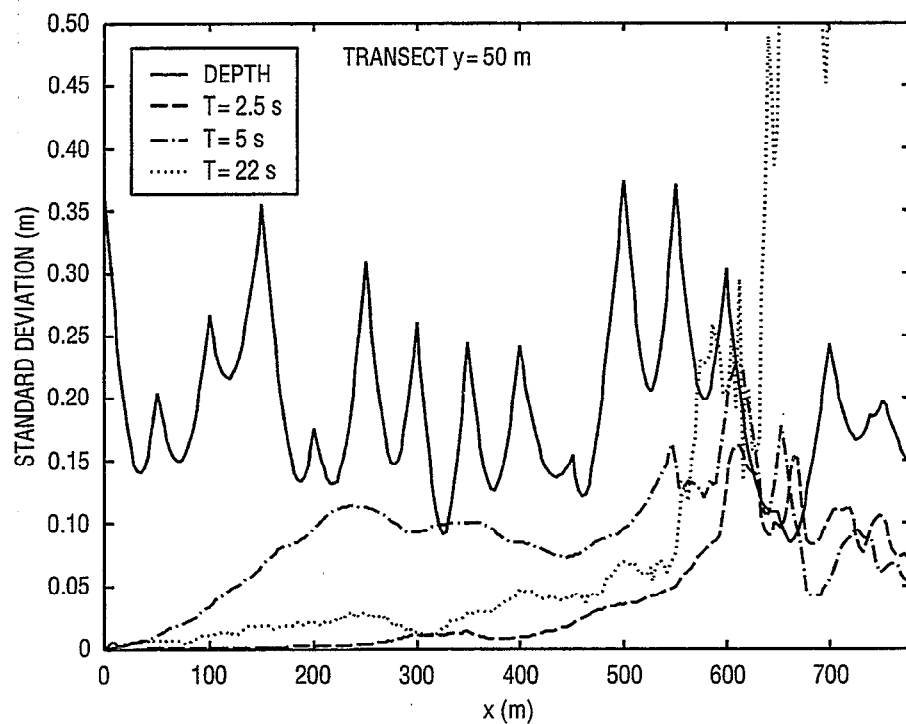


Fig. 6.4 — Comparison of standard deviations of depths to standard deviations of wave heights from REF/DIF1 for slice along $y = 50$ m

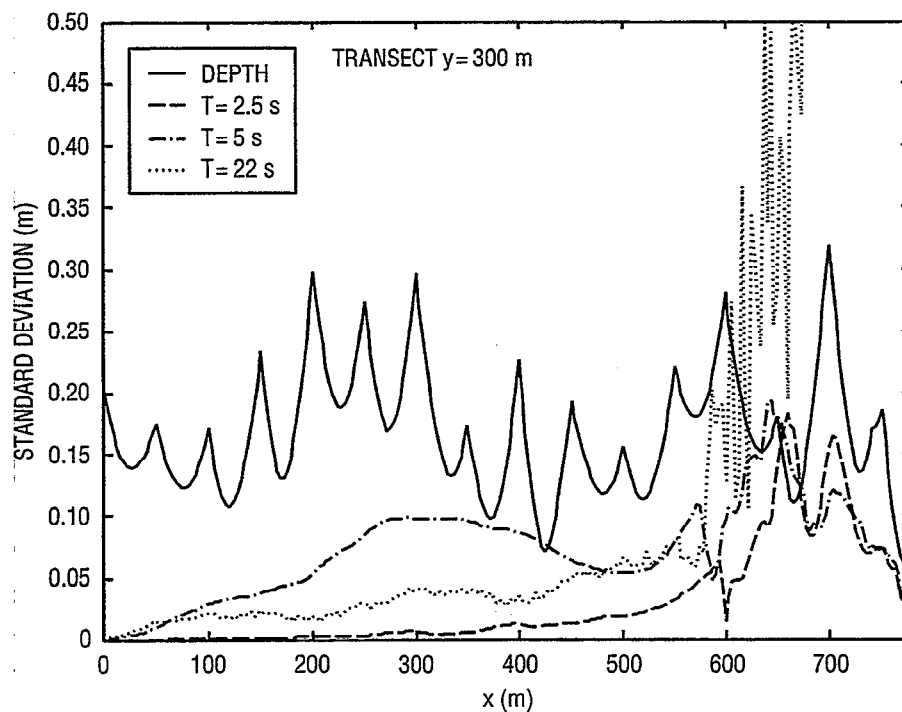


Fig. 6.5 — Comparison of standard deviations of depths to standard deviations of wave heights from REF/DIF1 for slice along $y = 300$ m

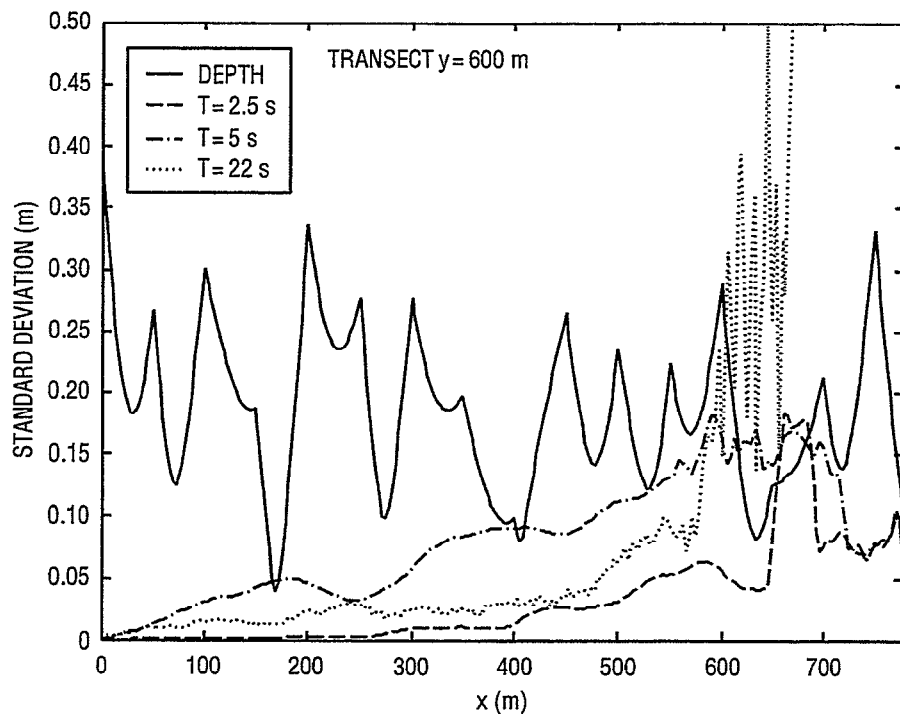


Fig. 6.6 — Comparison of standard deviations of depths to standard deviations of wave heights from REF/DIF1 for slice along $y = 600$ m

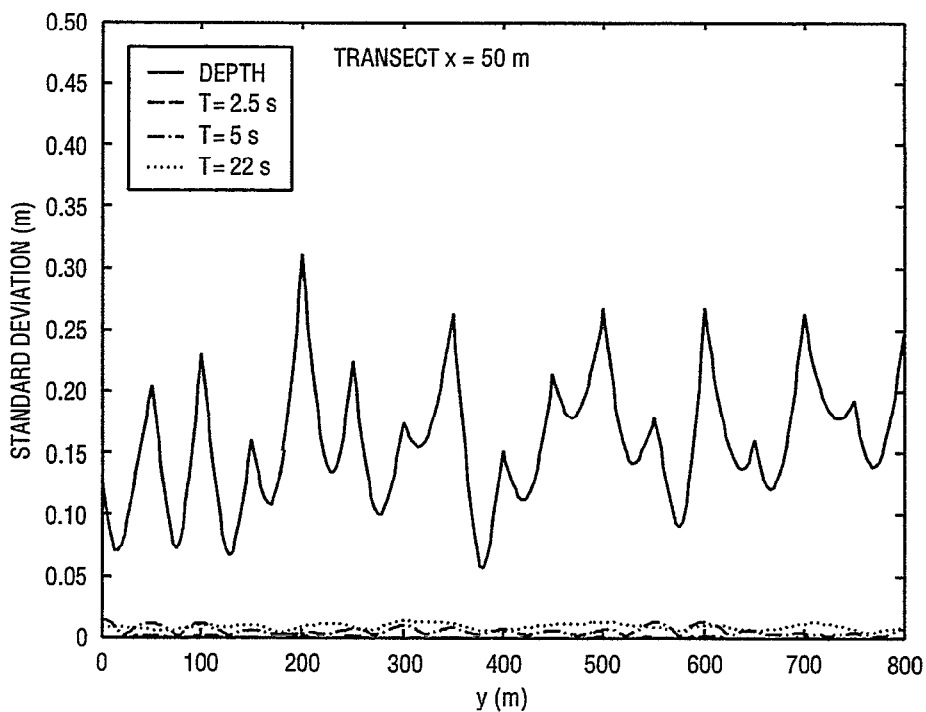


Fig. 6.7 — Comparison of standard deviations of depths to standard deviations of wave heights from REF/DIF1 for slice along $x = 50$ m

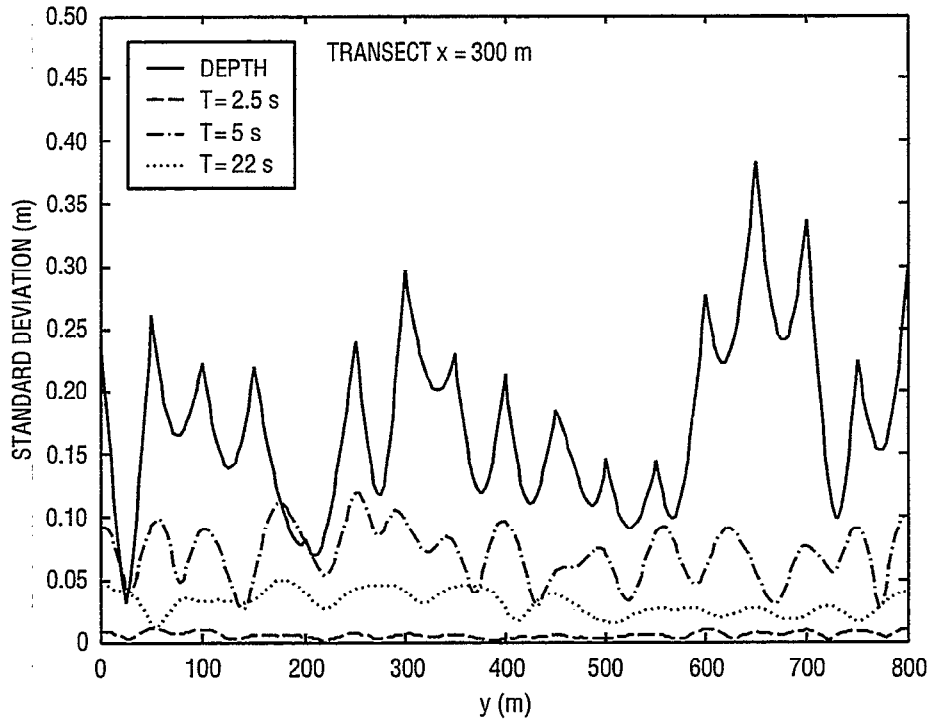


Fig. 6.8 — Comparison of standard deviations of depths to standard deviations of wave heights from REF/DIF1 for slice along $x = 300$ m

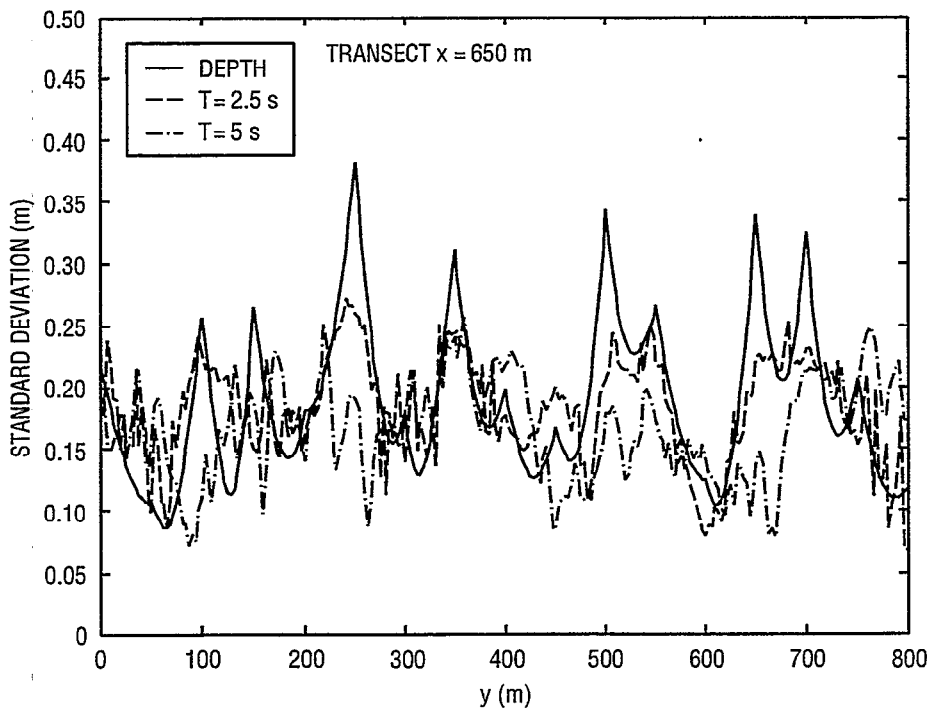


Fig. 6.9 — Comparison of standard deviations of depths to standard deviations of wave heights from REF/DIF1 for slice along $x = 650$ m

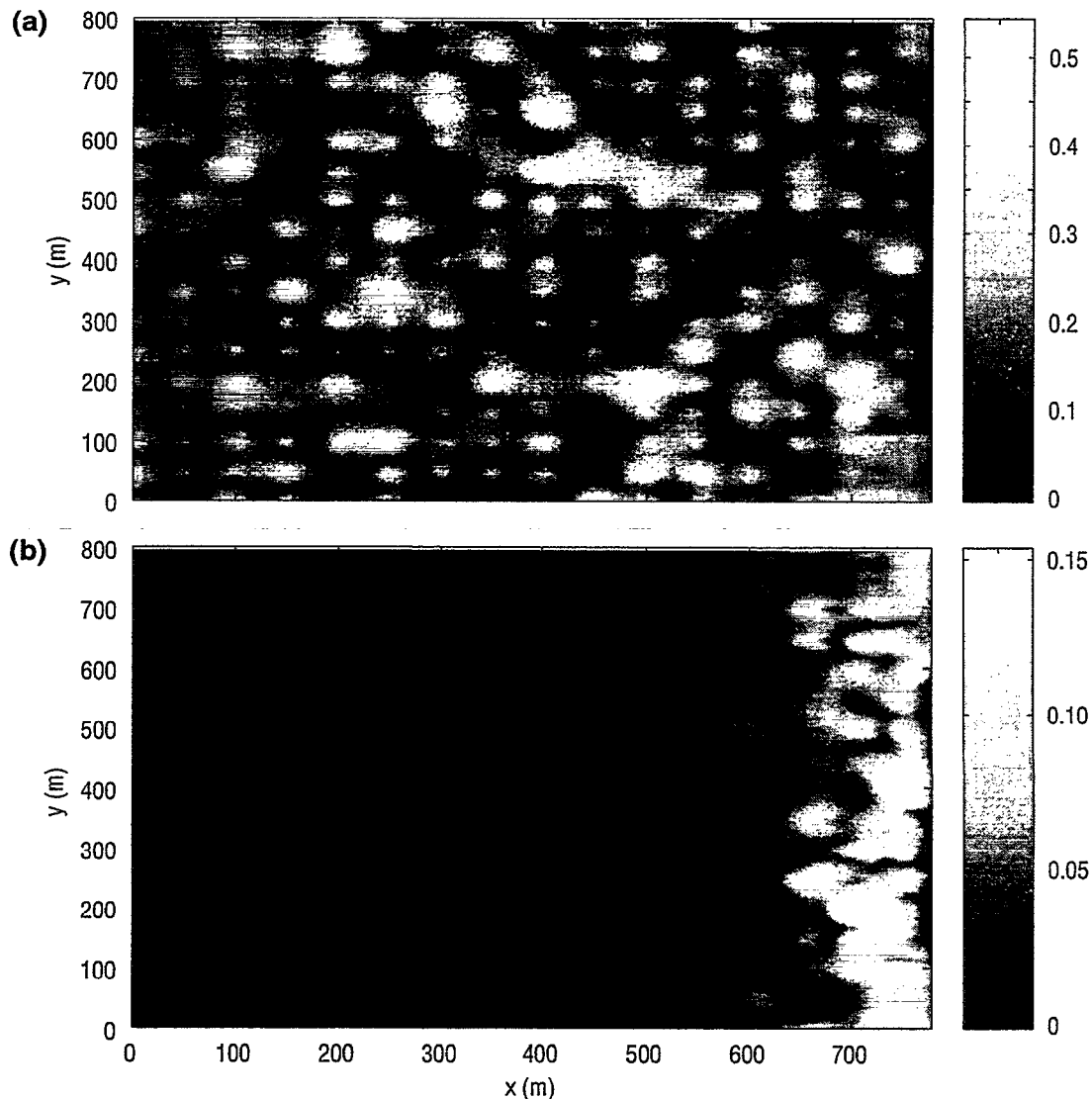


Fig. 6.10 — Results of analysis for six realizations of 100% random error distributed over linear slope, (a) standard deviation of depths and (b) standard deviation of wave heights from REF/DIF-S, $T_p = 2.5$ s, narrow frequency distribution, narrow directional distribution

standard deviation. The long waves (high peak period) seem to have smaller wave height standard deviations than the shorter waves. No unrealistically high wave heights were observed in the REF/DIF-S output. This is likely due to the dissipation mechanism in REF/DIF-S. The spectral dissipation model has no set breaking point; instead, the wave height decay is smooth, which is likely to account for smaller standard deviations in the surf zone than seen in the REF/DIF1 model. With the REF/DIF1 results, the locations of wave breaking differ with the different bathymetric realizations, which causes greater standard deviations in the wave height field in the surf zone because the point of breaking appears as a discontinuity in the wave height field. Since the location of this discontinuity shifts with the bathymetric realization, the standard deviation of the wave height field close to breaking is expected to be relatively high near the surf zone.

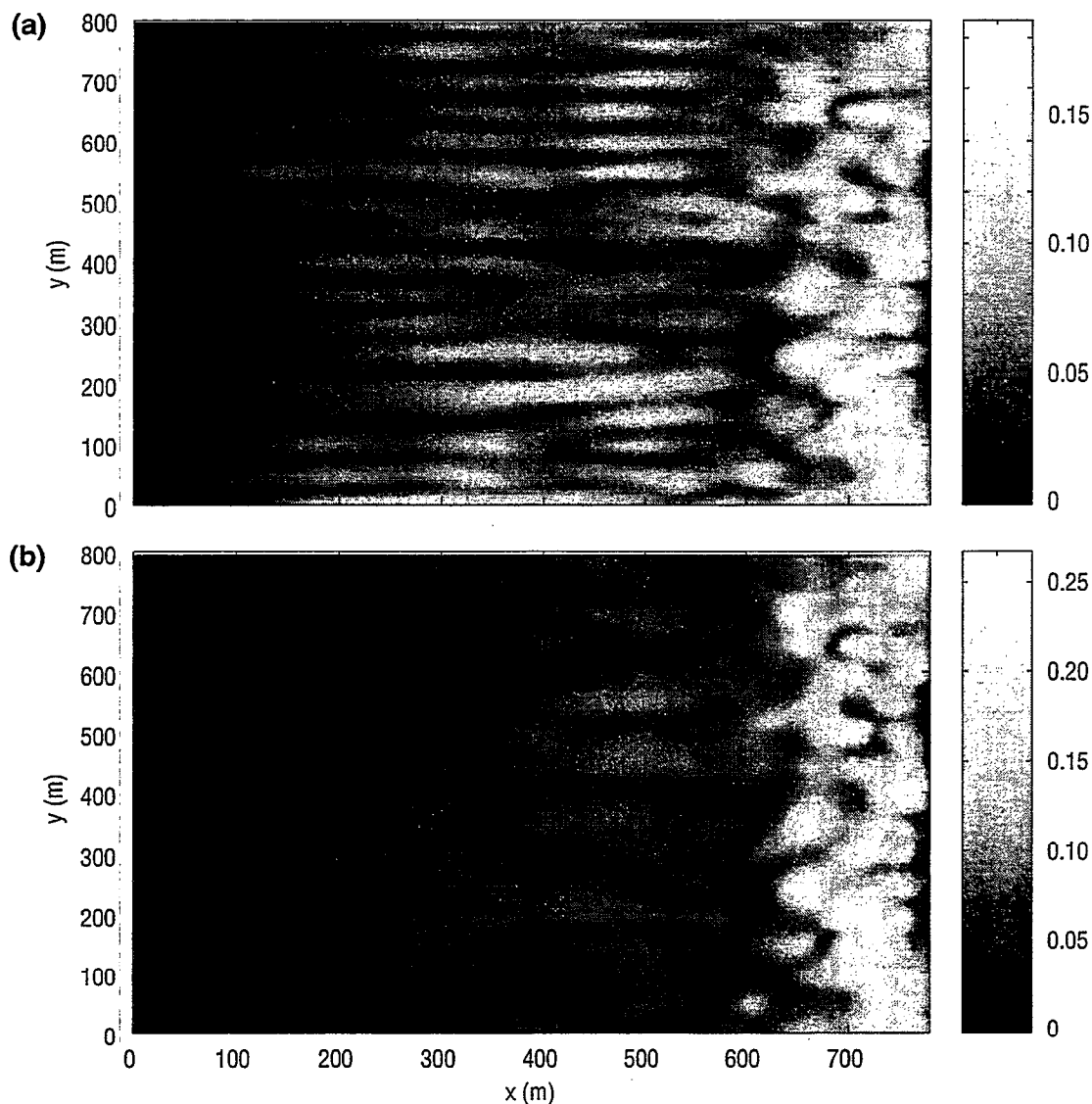


Fig. 6.11 — Results of analysis for six realizations of 100% random error distributed over linear slope, (a) standard deviation of wave heights from REF/DIF-S, $T_p = 5$ s, narrow frequency distribution, narrow directional distribution and (b) standard deviation of wave heights from REF/DIF1, $T_p = 22$ s, narrow frequency distribution, narrow directional distribution

6.2 Bathymetric Shoal

The second test involved the use of a more realistic distribution of error than the planar slope test, as well as a “true” (unperturbed) bathymetry that would cause wave refraction and diffraction. The Berkhoff-Booij-Radder bathymetry of Sec. 4.1 was used, scaled up to prototype: depths, horizontal distances, and input wave height were multiplied by 20. To insure a wave response to the bathymetry similar to that seen in the original laboratory experiment, a wave period was used so that $kh_{prototype} = kh_{laboratory}$ at the offshore boundary. Only REF/DIF1 was used in this test, run in linear mode. The following modeling parameters were used:

$$T = 4.47 \text{ s}$$

$$H_o = 0.928 \text{ m}$$

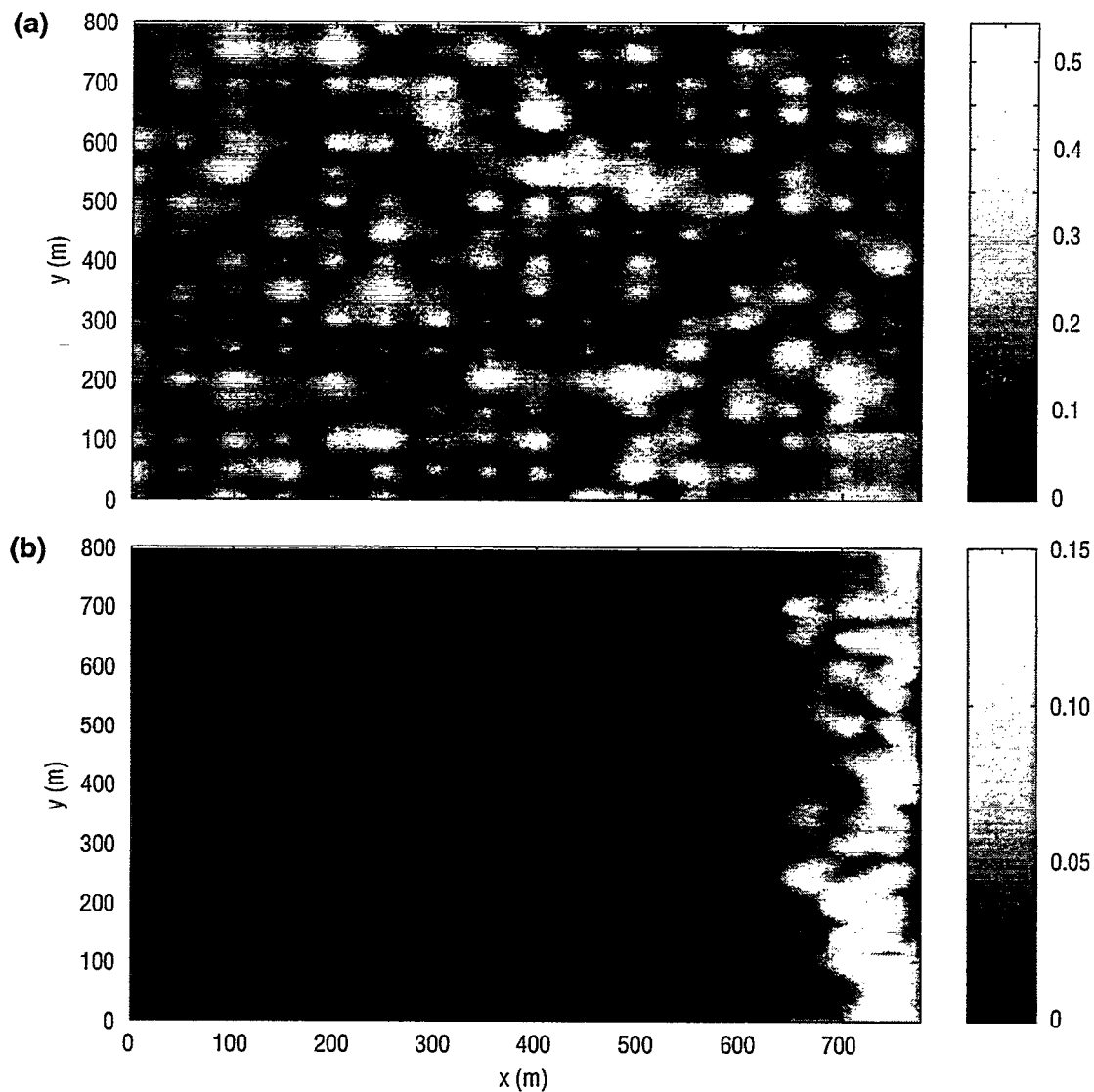


Fig. 6.12 — Results of analysis for six realizations of 100% random error distributed over linear slope, (a) standard deviation of depths and (b) standard deviation of wave heights from REF/DIF-S, $T_p = 2.5$ s, broad frequency distribution, broad directional distribution

$$h_o = 9 \text{ m}$$

$$\theta_o = 0$$

Grid resolution: $\Delta x = \Delta y = 5$ m

Domain size: 490×490 m

Because surveyors tend to measure known bathymetric features with greater thoroughness, a “survey point” grid spacing of 10 m was used here. Survey error was simulated in a more realistic fashion; this better reflects the many causes of error expected to occur during a boat survey. A total standard deviation $\sigma_e = 0.25$ m was used, which is similar to the error used for the planar beach cases. However, this error was split into three parts, each with a standard deviation of:

$$\sigma_e = 0.25 \text{ m} \sqrt{\frac{1}{3}} . \quad (6.2)$$

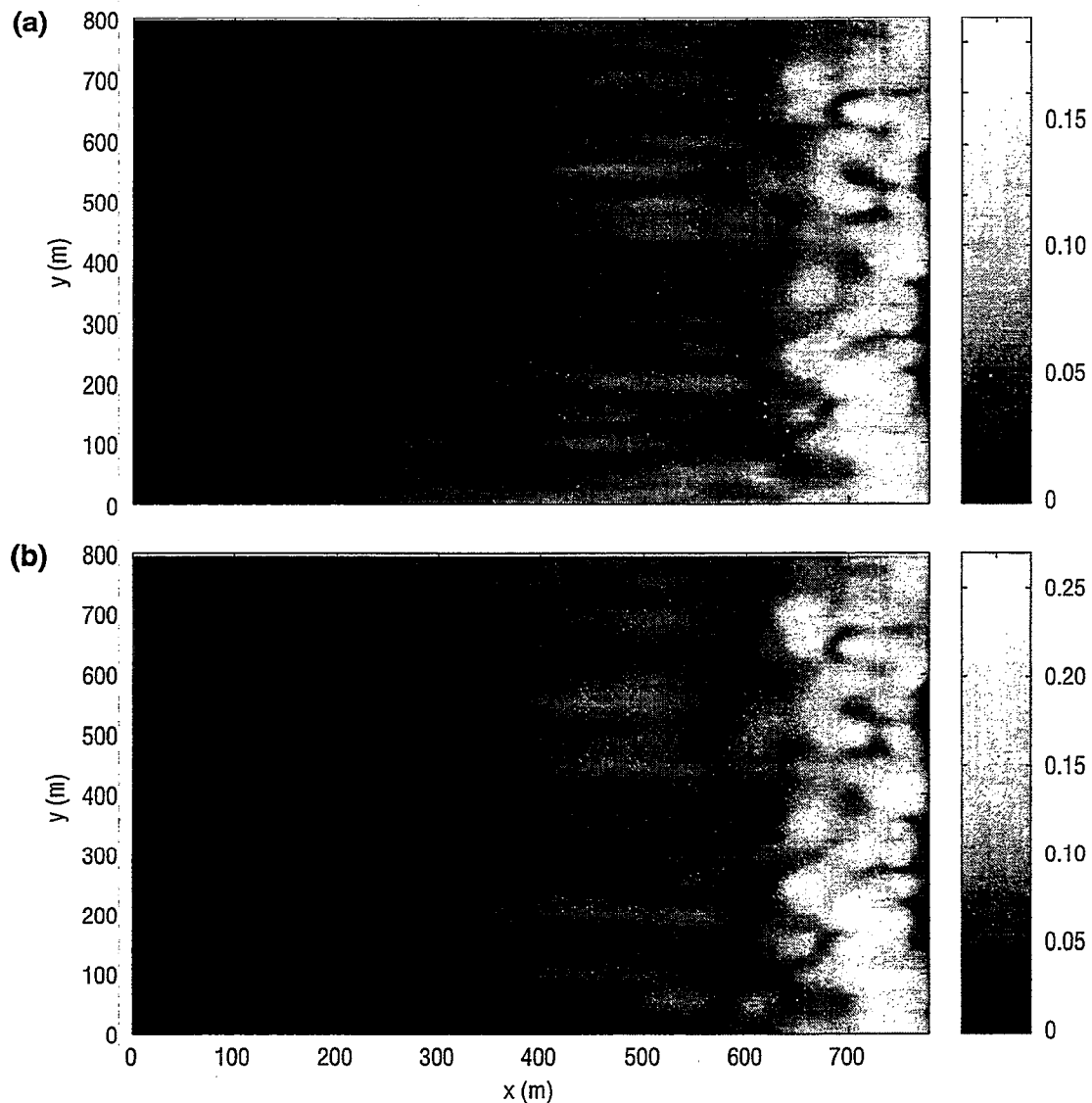


Fig. 6.13 — Results of analysis for six realizations of 100% random error distributed over linear slope, (a) standard deviation of wave heights from REF/DIF-S, $T_p = 5$ s, broad frequency distribution, broad directional distribution and (b) standard deviation of wave heights from REF/DIF1, $T_p = 22$ s, broad frequency distribution, broad directional distribution

The total error consisted of the following:

- Random error
- Systematic error, which was random but constant over the entire bathymetry
- Systematic error at each point that was directly proportional to the “true” depth at the data point

All error was determined using a Gaussian distribution. Thirty random realizations of the bathymetry were created, each with a different, randomly determined systematic error and constant of proportionality (for determining the proportional systematic error). REF/DIF1 was run with these bathymetries. Figure 6.26 shows the bathymetry and wave height field (normalized by the offshore wave height) of the average of all 30 realizations; it can be seen that both are similar to the original (laboratory

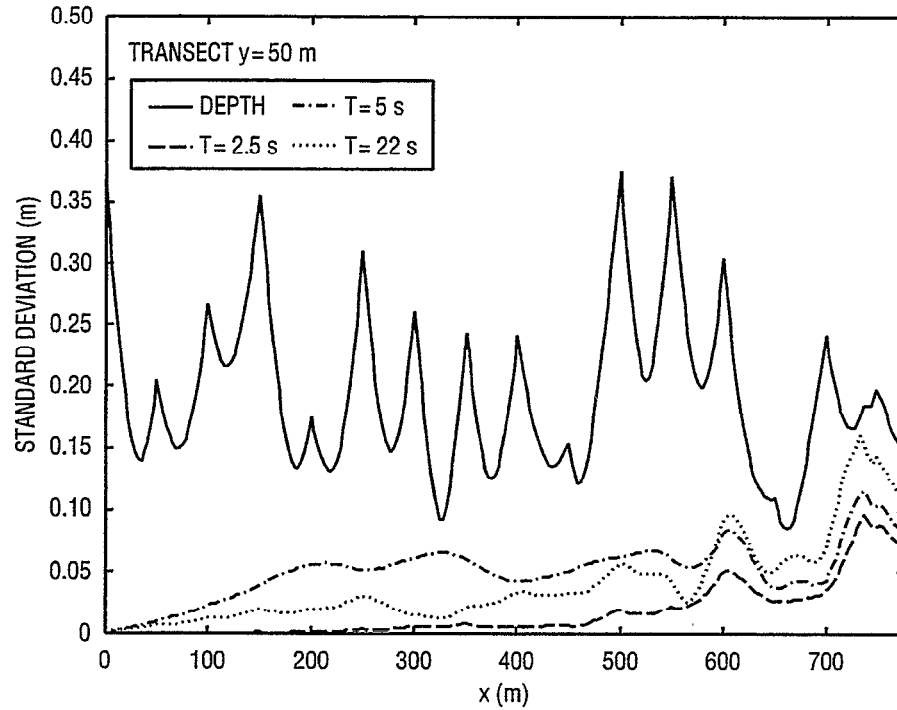


Fig. 6.14 — Comparison of standard deviations of depths to standard deviations of wave heights from REF/DIF-S, narrow frequency distribution, narrow directional distribution, for slice along $y = 50$ m

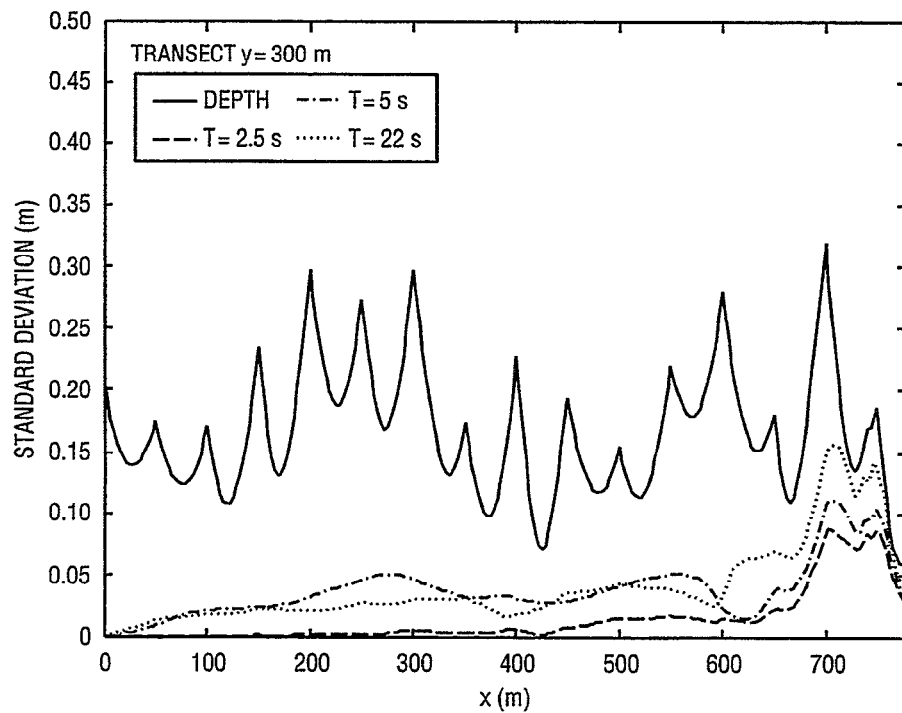


Fig. 6.15 — Comparison of standard deviations of depths to standard deviations of wave heights from REF/DIF-S, narrow frequency distribution, narrow directional distribution, for slice along $y = 300$ m

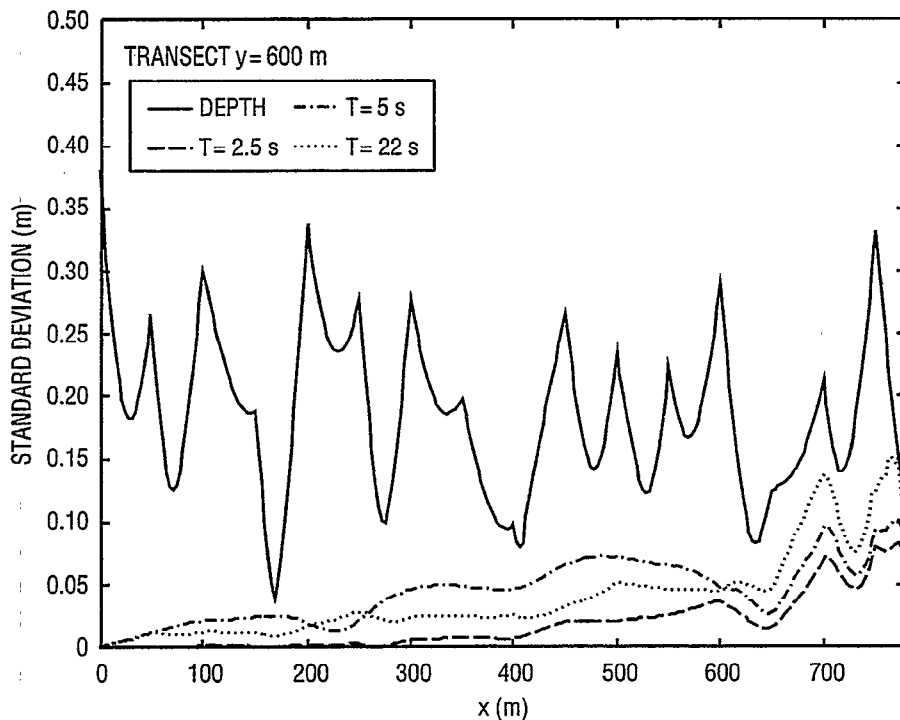


Fig. 6.16 — Comparison of standard deviations of depths to standard deviations of wave heights from REF/DIF-S, narrow frequency distribution, narrow directional distribution, for slice along $y = 600$ m

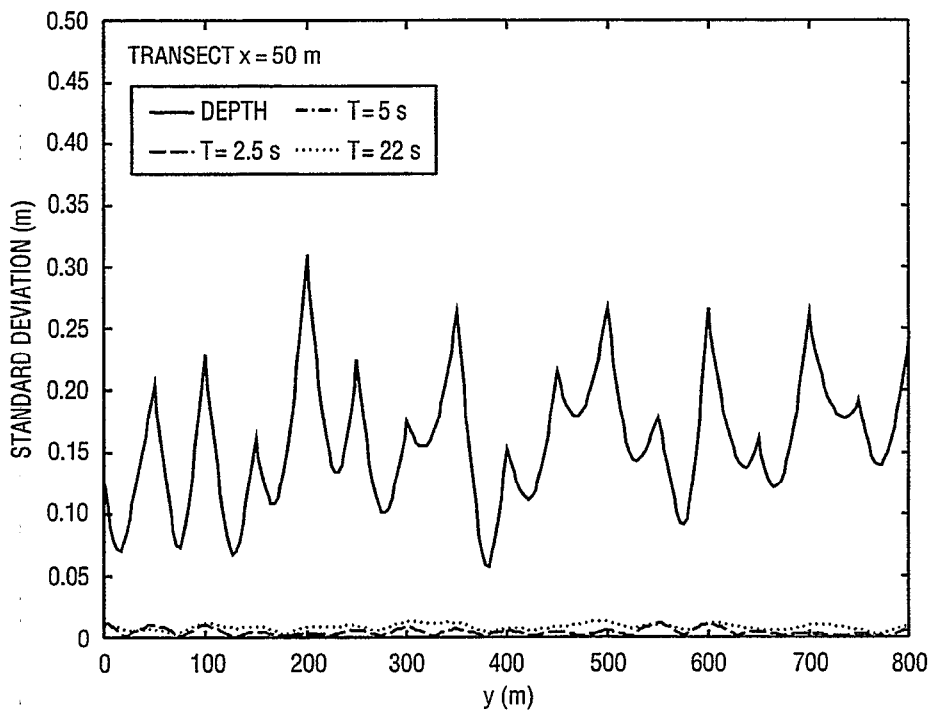


Fig. 6.17 — Comparison of standard deviations of depths to standard deviations of wave heights from REF/DIF-S, narrow frequency distribution, narrow directional distribution, for slice along $x = 50$ m

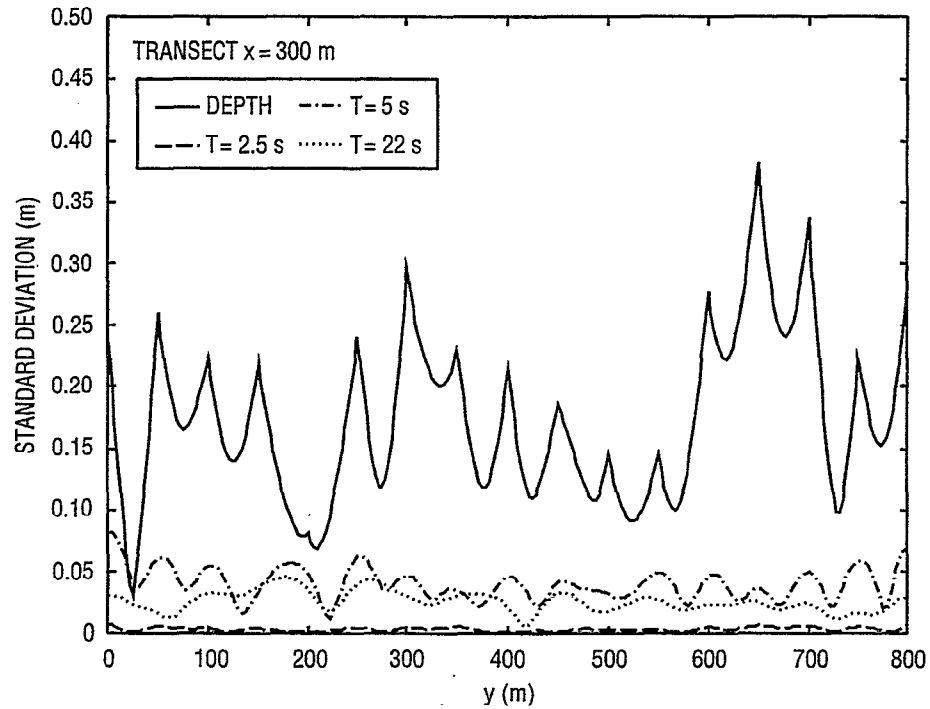


Fig. 6.18 — Comparison of standard deviations of depths to standard deviations of wave heights from REF/DIF-S, narrow frequency distribution, narrow directional distribution, for slice along $x = 300$ m

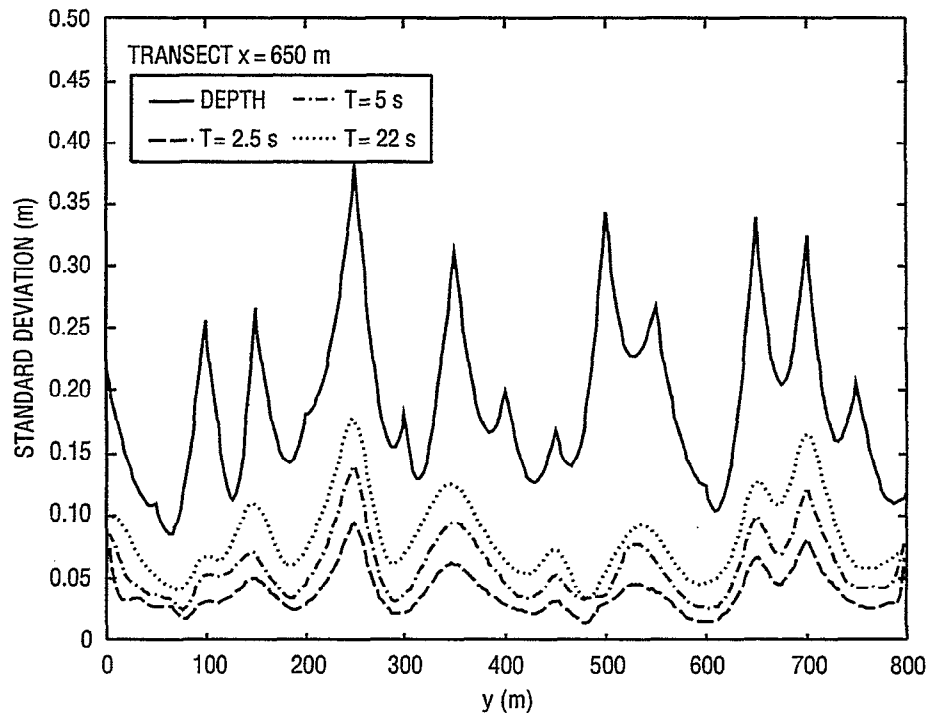


Fig. 6.19 — Comparison of standard deviations of depths to standard deviations of wave heights from REF/DIF-S, narrow frequency distribution, narrow directional distribution, for slice along $x = 600$ m

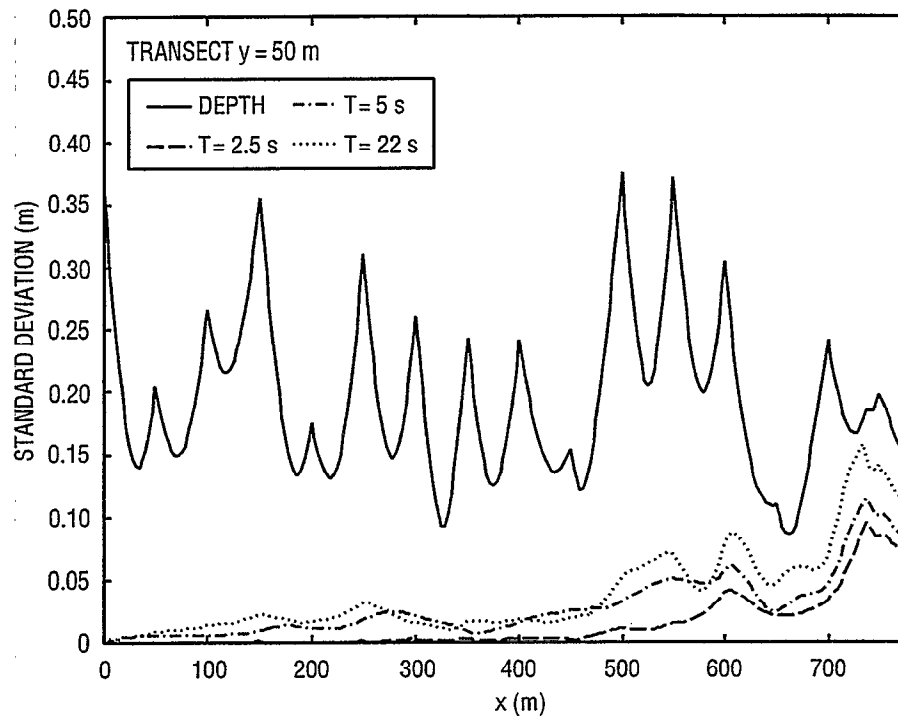


Fig. 6.20 — Comparison of standard deviations of depths to standard deviations of wave heights from REF/DIF-S, broad frequency distribution, broad directional distribution, for slice along $y = 50$ m

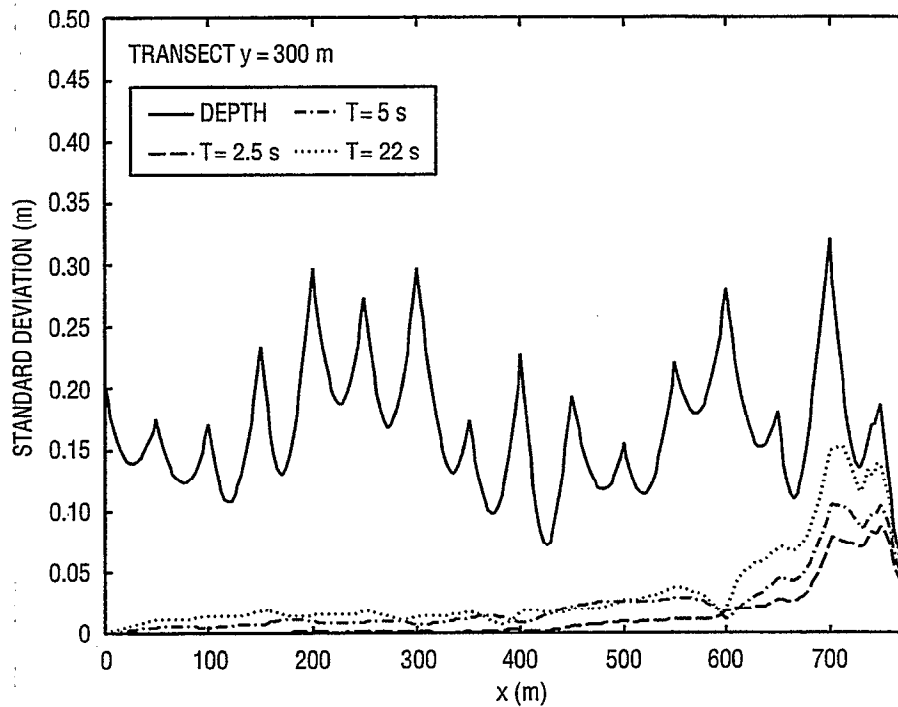


Fig. 6.21 — Comparison of standard deviations of depths to standard deviations of wave heights from REF/DIF-S, broad frequency distribution, broad directional distribution, for slice along $y = 300$ m

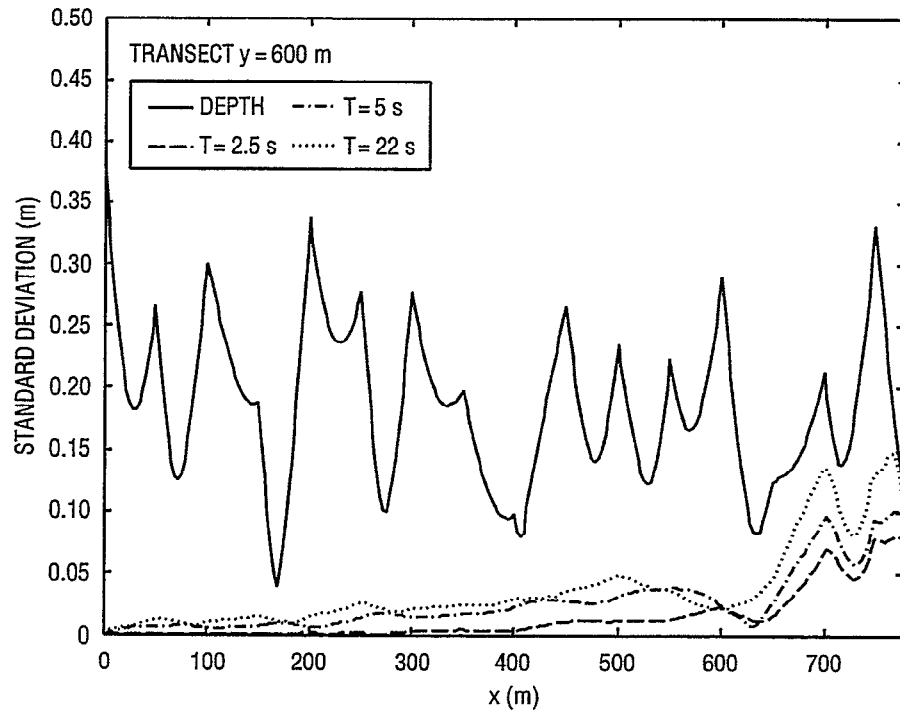


Fig. 6.22 — Comparison of standard deviations of depths to standard deviations of wave heights from REF/DIF-S, broad frequency distribution, broad directional distribution, for slice along $y = 600$ m

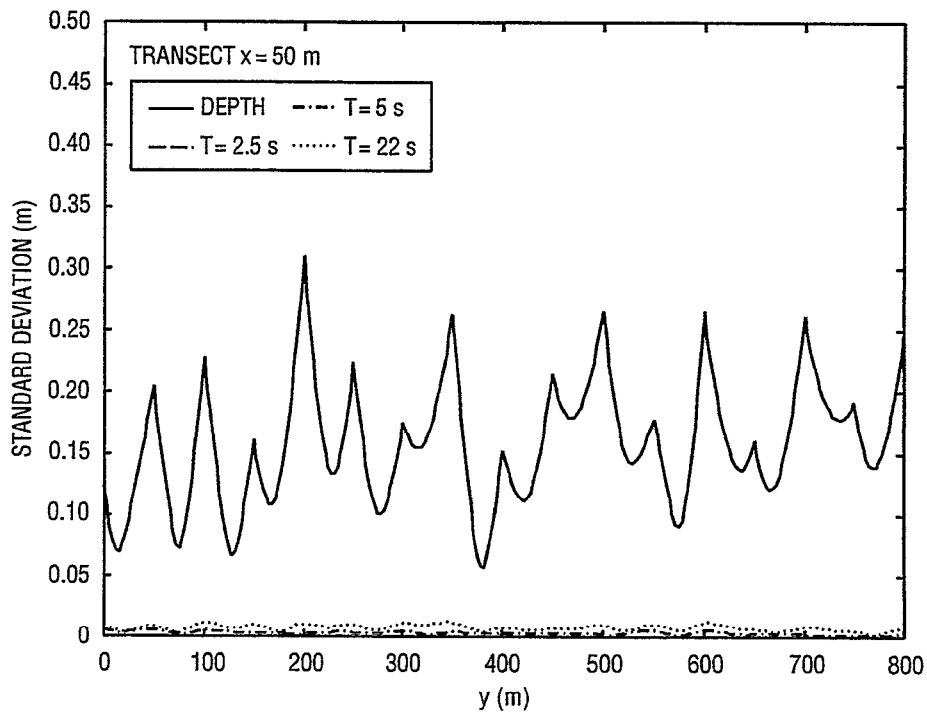


Fig. 6.23 — Comparison of standard deviations of depths to standard deviations of wave heights from REF/DIF-S, broad frequency distribution, broad directional distribution, for slice along $x = 50$ m

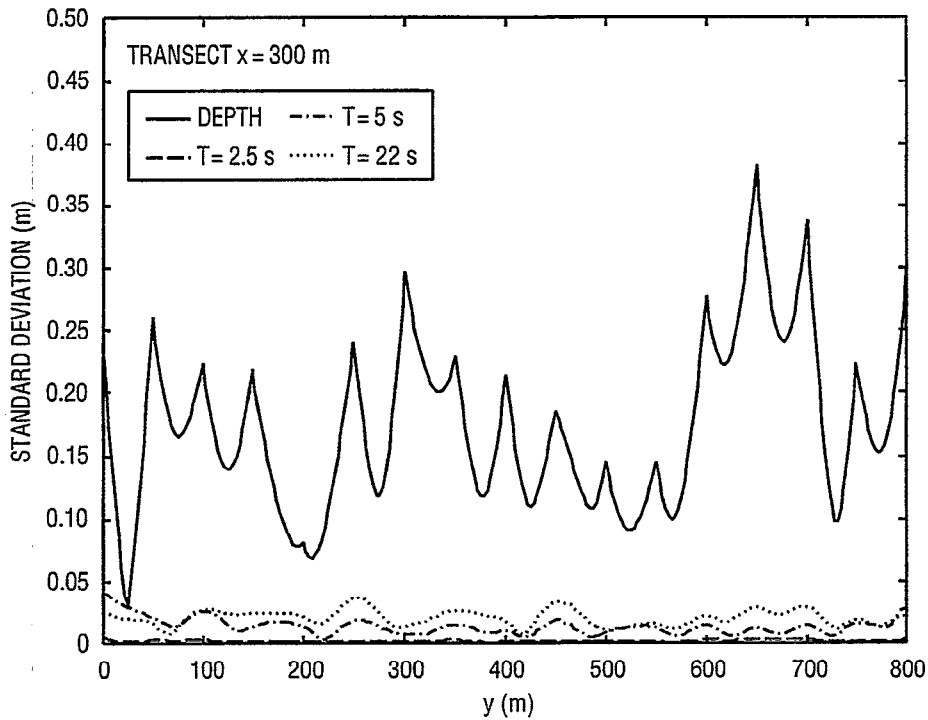


Fig. 6.24 — Comparison of standard deviations of depths to standard deviations of wave heights from REF/DIF-S, broad frequency distribution, broad directional distribution, for slice along $x = 300$ m

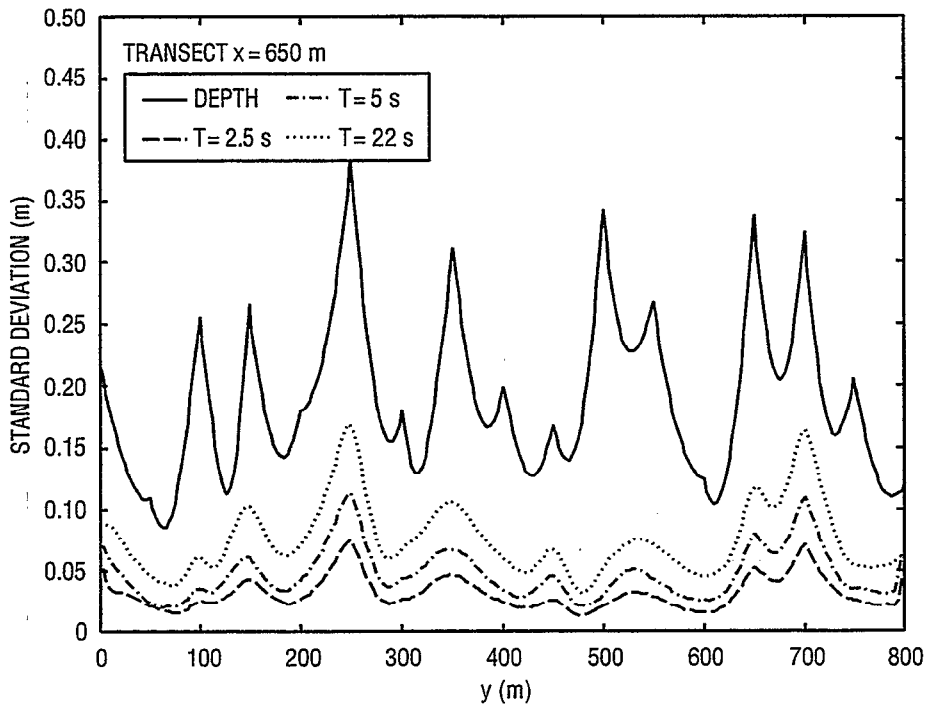


Fig. 6.25 — Comparison of standard deviations of depths to standard deviations of wave heights from REF/DIF-S, broad frequency distribution, broad directional distribution, for slice along $x = 600$ m

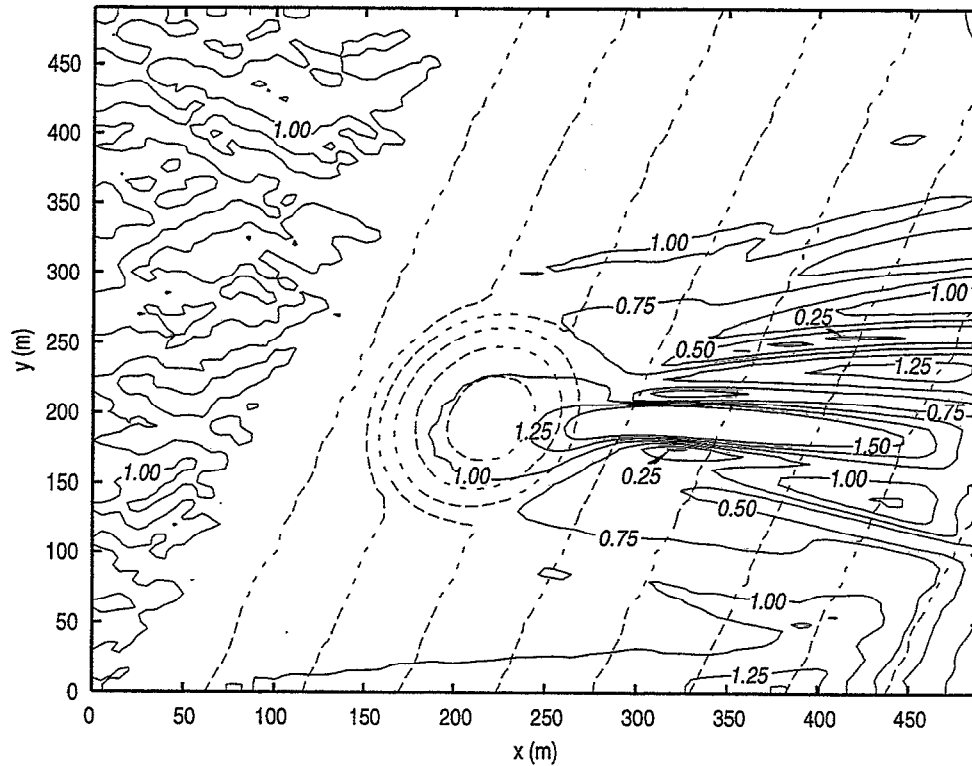


Fig. 6.26 — Average of 30 realizations of depths and normalized wave heights, BBR shoal

scale) shoal and the resulting wave height field. The standard deviation of depth σ_h and standard deviation of wave height σ_H was determined for each gridpoint as with the planar slope tests. Figure 6.27 shows the spatial distributions of both σ_h and σ_H for the 30 realizations. Except in the direct lee of the shoal, σ_H is less than σ_h , implying that the model is not overly sensitive to bathymetric uncertainty. The standard deviation of wave heights is largest behind the shoal; this is likely due to the variation in the locations of the diffraction lobes from realization to realization.

6.3 Other Issues Regarding Bathymetric Uncertainty

An actual bathymetric data set is unlikely to consist of survey data points that are regularly spaced over the survey region; spatial distribution is likely to be somewhat irregular. In areas where depths are less than 2 m, bathymetric data may have been taken with a rod and level, survey sled, or similar method. This type of data typically has a much finer x -wise resolution and very small random error, resulting in very different spatial distributions of error.

Not all bathymetric uncertainty is due to errors in the measurement and calculation of depths and locations during local surveys. Sediment transport can cause a bathymetric data set to become obsolete, especially in the shallower water depths. (This is one reason why bathymetry in the mini-grid of the DELILAH experiment was taken daily.) This type of data uncertainty is, of course, very site-specific. Interpolation of depths between data points can also be problematic. When data resolution is coarse, as in the planar bathymetry tests, irregular variation between data points can cause significant error in the interpolated depths. This is particularly true with rod and level surveys, which tend to be clustered in linear, cross-shore stripes. When interpolated onto a regularly spaced

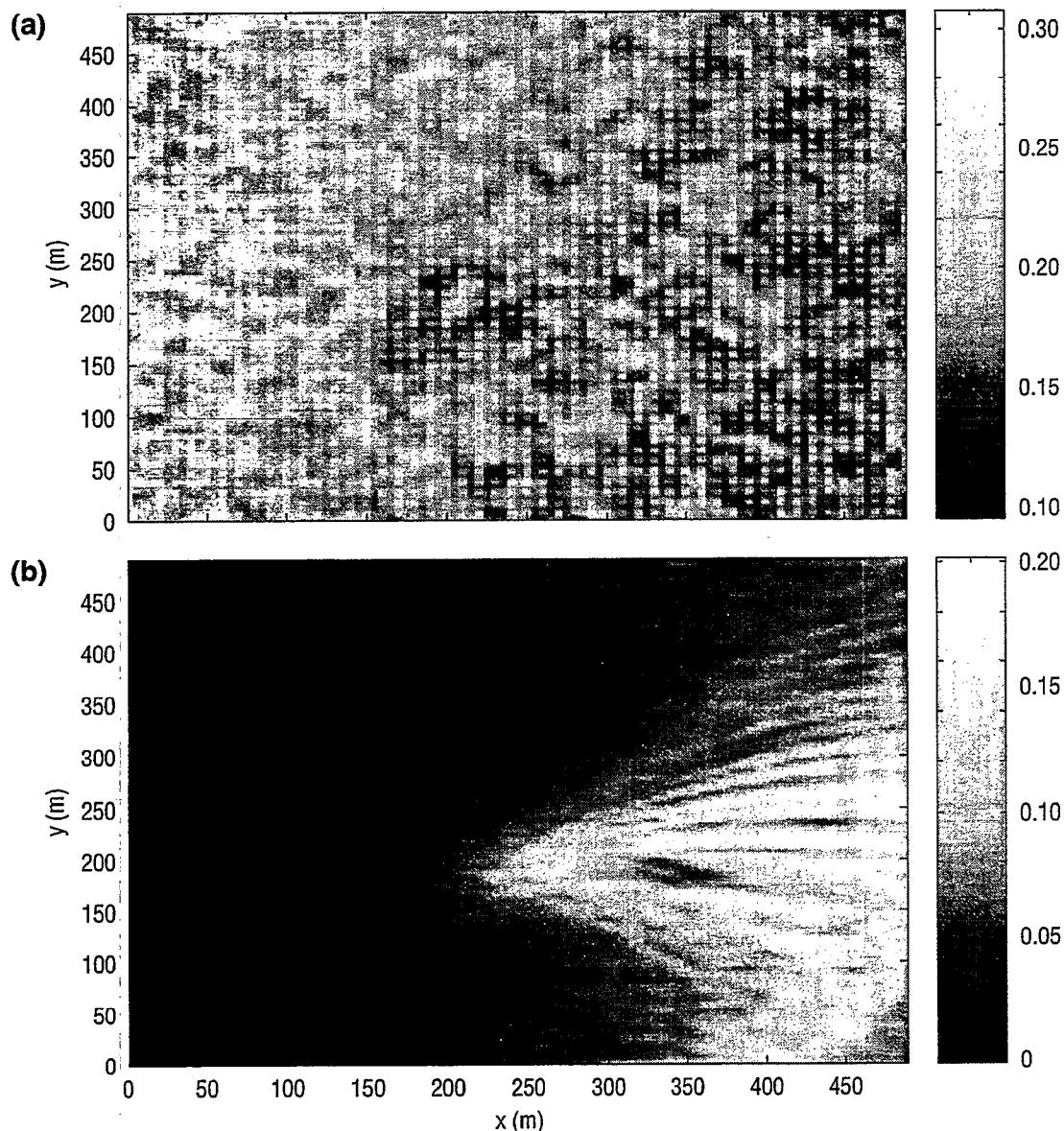


Fig. 6.27 — Results of analysis for 30 realizations of error distributed over BBR shoal, (a) standard deviations of depth and (b) standard deviations of wave heights

grid, these stripes often caused scallop-shaped bathymetric variations to occur. These nonphysical features can have deleterious effects on model performance.

7.0 WAVE SHOALING AND BREAKING WITH REF/DIF-S

As mentioned in Part 1, the model REF/DIF-S uses the Thornton and Guza (1983) dissipation mechanism. This dissipation mechanism is always in effect, but only becomes significant where breaking occurs. REF/DIF-S output was compared to REF/DIF1 output for the planar slope bathymetry and wave periods used in the linear wave theory comparisons. Both models were run in linear

mode. Two wave spectra were used as input for REF/DIF-S: (1) narrow directional distribution ($\sigma = 10$), narrow frequency distribution ($\gamma = 20$) and broad directional distribution ($\sigma = 30$), broad frequency distribution ($\gamma = 2$). The REF/DIF1 runs were initiated with the wave parameters used in Sec. 2.1. The REF/DIF-S model was run with the breaking left on and turned off (this was done inside the code and is not an option in the model). Results are shown in Figs. 7.1–7.3. Clearly, the dissipation mechanism causes significant wave height decrease prior to the breaking point predicted by the monochromatic REF/DIF1 model; this is most noticeable with the short waves. There is also a more noticeable difference between the REF/DIF1 and REF/DIF-S results for the broad frequency, broad direction case; this difference seems to be independent of the dissipation mechanism in REF/DIF-S.

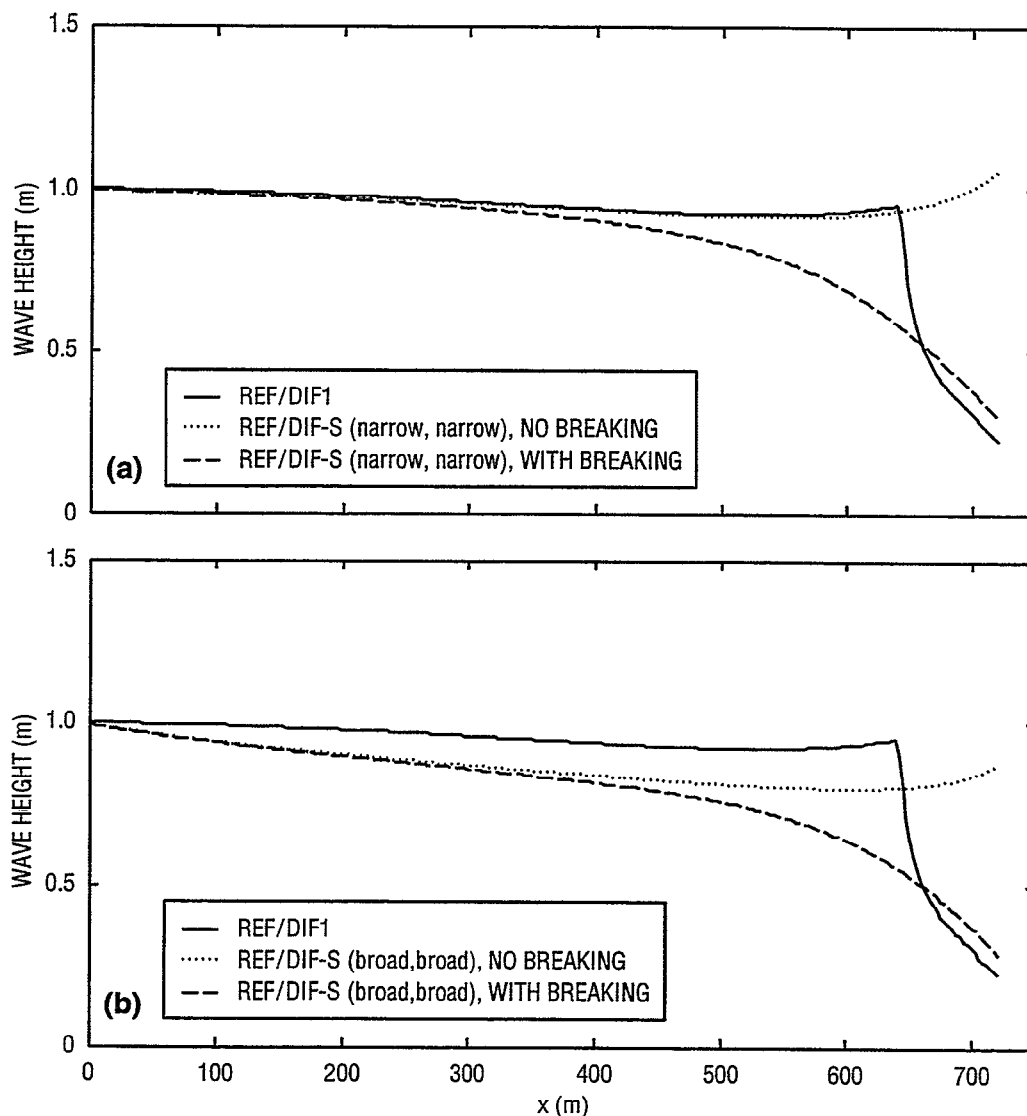


Fig. 7.1 — Comparison of wave heights from REF/DIF1 and REF/DIF-S with and without breaking, $T = 3$ s, (a) narrow frequency distribution, narrow directional distribution and (b) broad frequency distribution, broad directional distribution

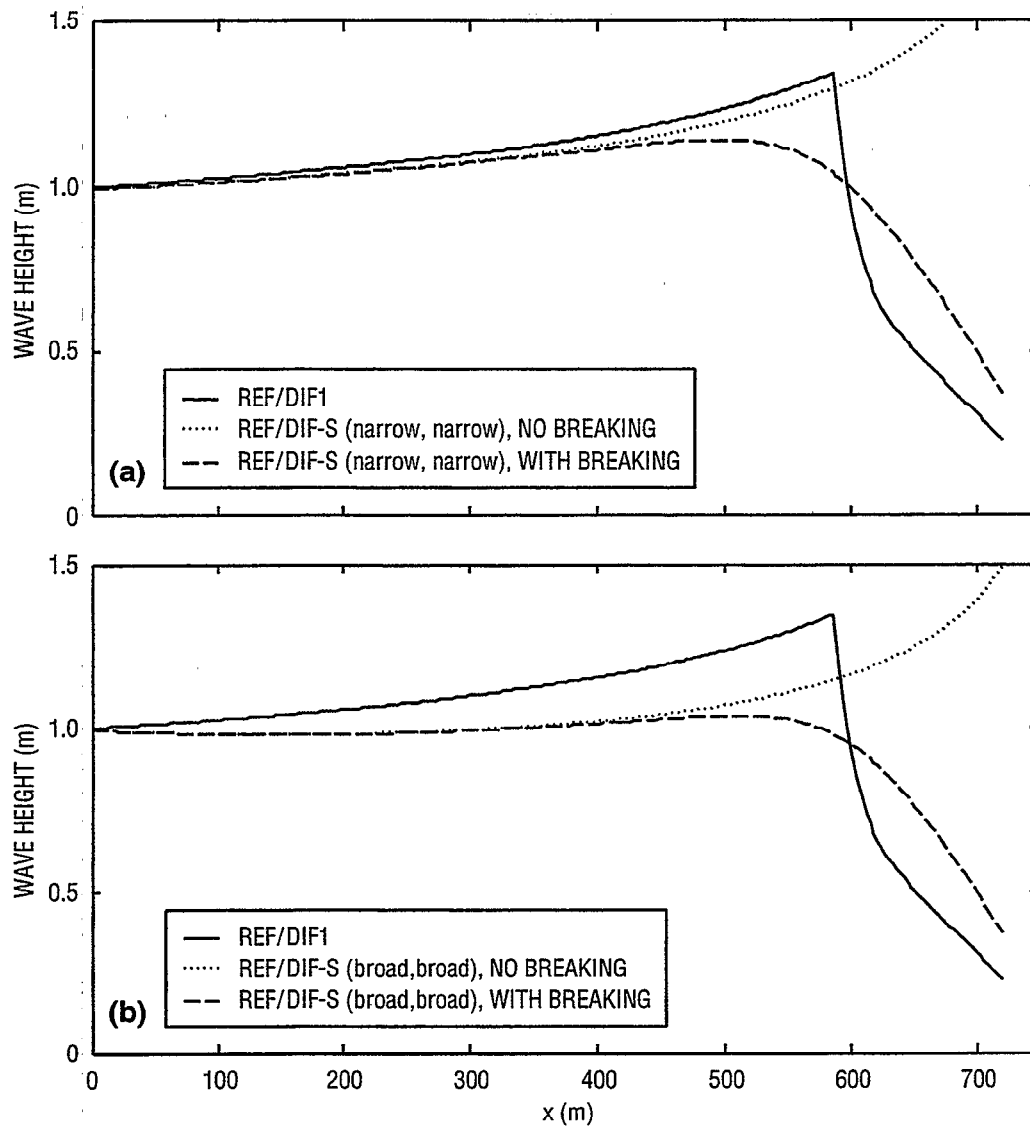


Fig. 7.2 — Comparison of wave heights from REF/DIF1 and REF/DIF-S with and without breaking, $T = 10$ s, (a) narrow frequency distribution, narrow directional distribution and (b) broad frequency distribution, broad directional distribution

8.0 CORRECTIONS TO REF/DIF-S

In the course of the investigation of the REF/DIF-S model, a few problems have arisen that have been addressed and corrected. These problems had become most apparent during the attempt to revise the model to calculate and output directional spectra. This discussion is only germane to the model version 1.2, which differs from version 1.1 in (among other aspects) the use of makefiles and namelists.

8.1 Wave Number Dimensioning Correction

In the subroutine MODEL, the second "DIMENSION" statement includes the variable xk , which is dimensioned $xk(iyr, ncomp)$. This should be $xk(iy, ncomp)$ to make it consistent with similar

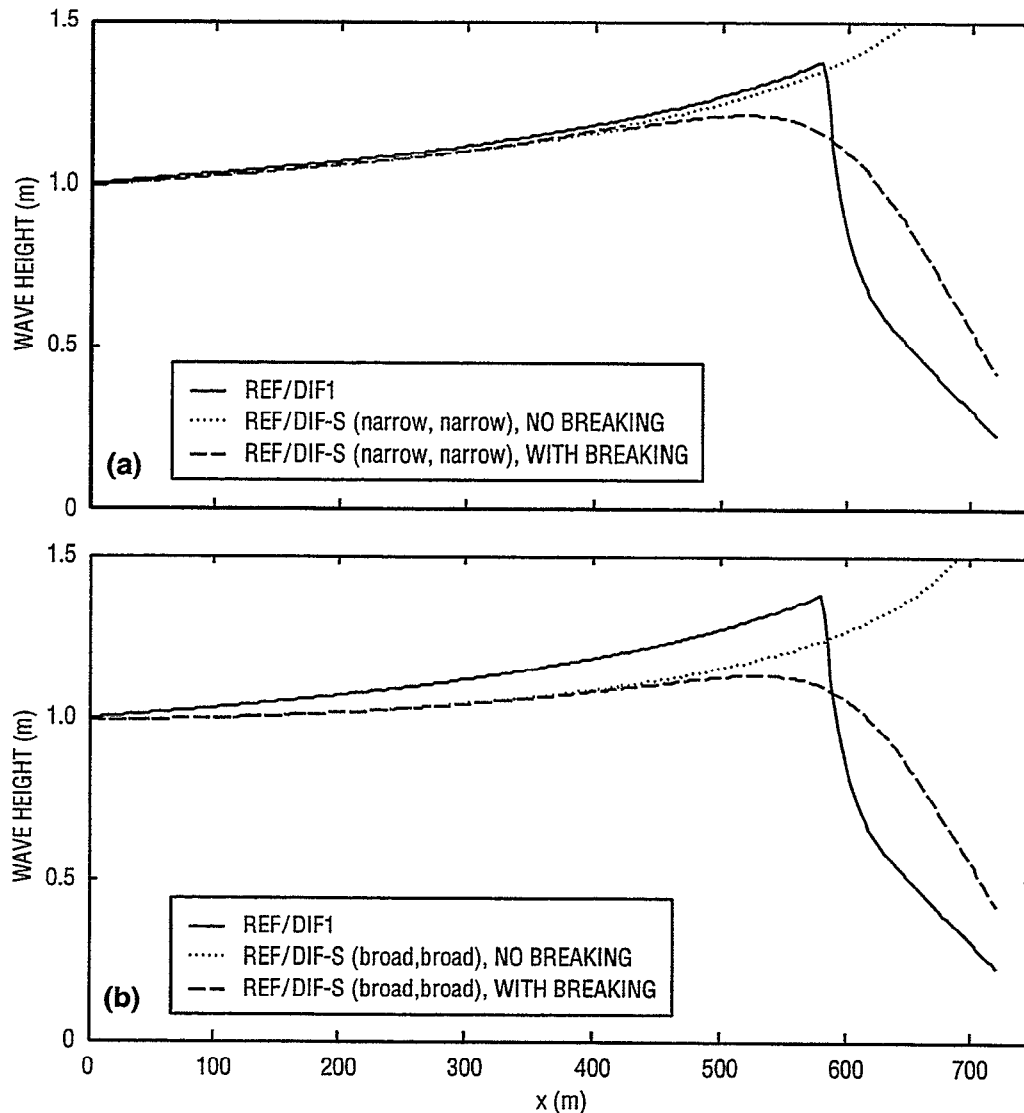


Fig. 7.3 — Comparison of wave heights from REF/DIF1 and REF/DIF-S with and without breaking, $T = 17$ s, (a) narrow frequency distribution, narrow directional distribution and (b) broad frequency distribution, broad directional distribution

dimension statements in other parts of the model. The result of the error was that a significant number of 0 wave numbers were returned from subroutine VWNUM. These wave numbers were used in calculating the y -averaged wave numbers for the phase function integration. The 0 wave numbers caused much of the energy to propagate at 0° . The correction of this error allowed directional spectra to be reliably calculated from the complex amplitudes in the model (discussed further in a later section). Figures 8.1–8.8 show the effect of the wave number dimensioning correction on the REF/DIF-S model results. There is improvement in the predictions of wave height in many cases. More significantly, the large decrease in significant wave height seen near the offshore row with the uncorrected model (Fig. 5.4) is no longer seen with the corrected model. Additionally, the effect of the number of bins (Figs. 5.20 and 5.21) and the grid resolution (Figs. 5.18 and 5.19) on the quality of the predictions are no longer apparent; this can be seen in Figs. 8.9 and 8.10.

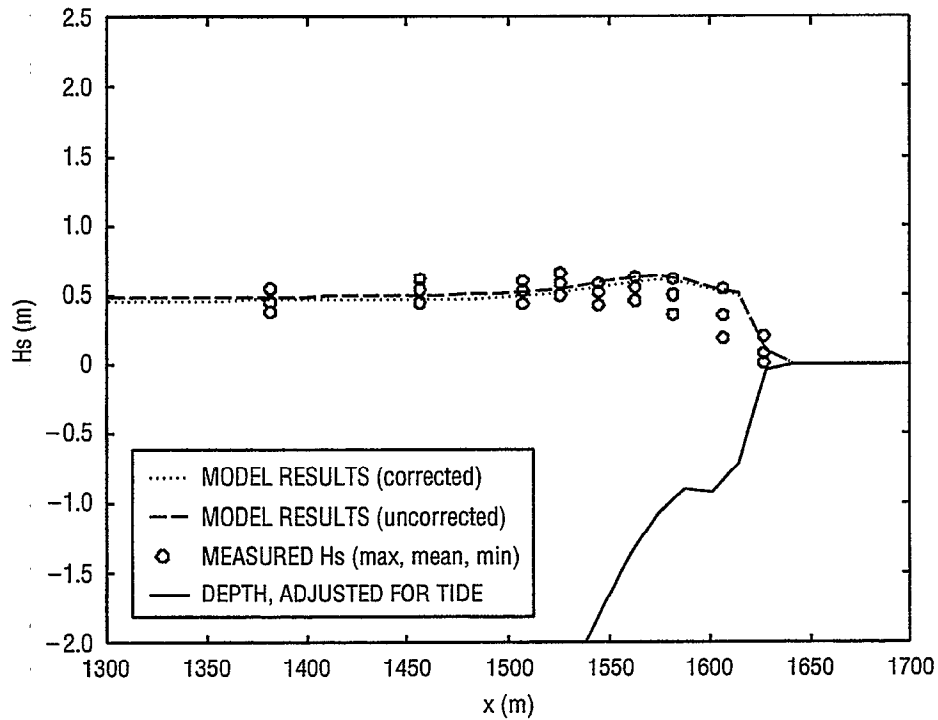


Fig. 8.1 — Comparison of wave heights from both corrected and uncorrected REF/DIF-S, the DELILAH experiment data for the time period beginning at 0400 EST, 10-6-90

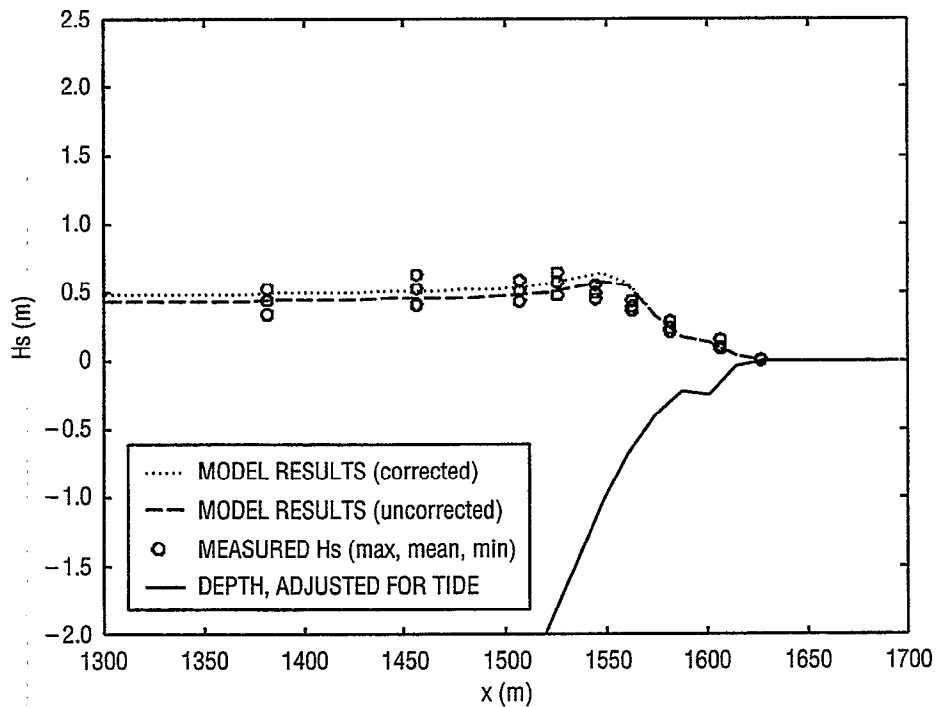


Fig. 8.2 — Comparison of wave heights from both corrected and uncorrected REF/DIF-S, the DELILAH experiment data for the time period beginning at 1300 EST, 10-6-90

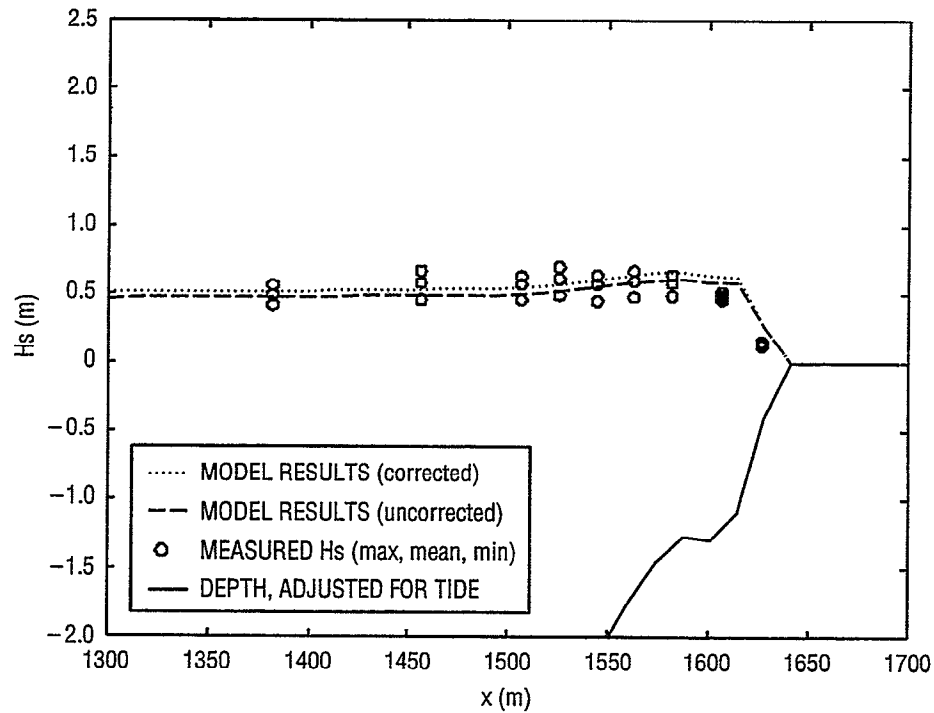


Fig. 8.3 — Comparison of wave heights from both corrected and uncorrected REF/DIF-S, the DELILAH experiment data for the time period beginning at 1900 EST, 10-6-90

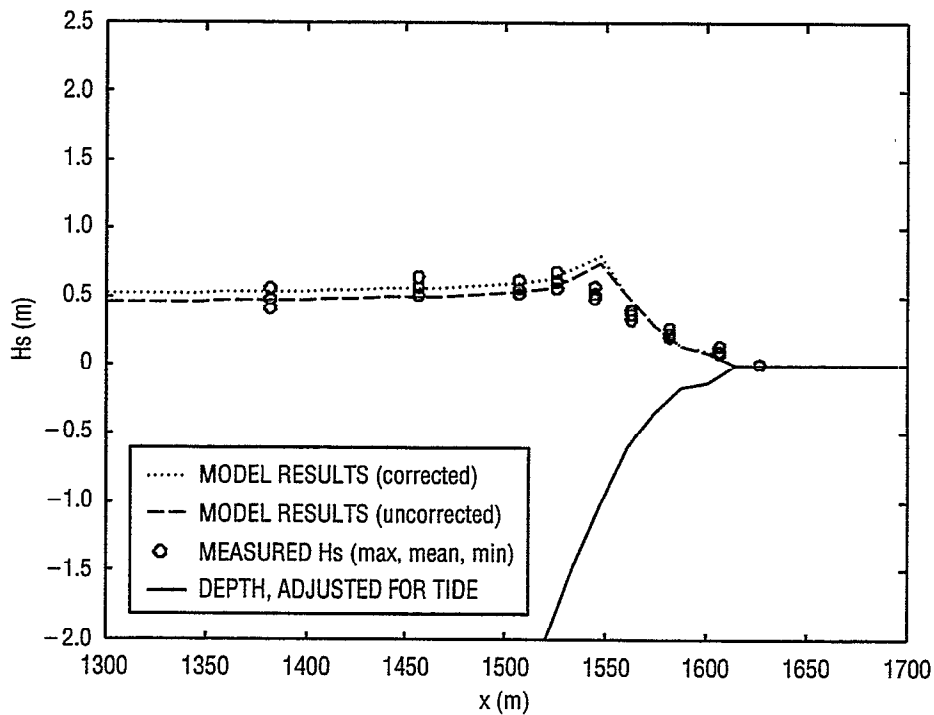


Fig. 8.4 — Comparison of wave heights from both corrected and uncorrected REF/DIF-S, the DELILAH experiment data for the time period beginning at 0100 EST, 10-7-90

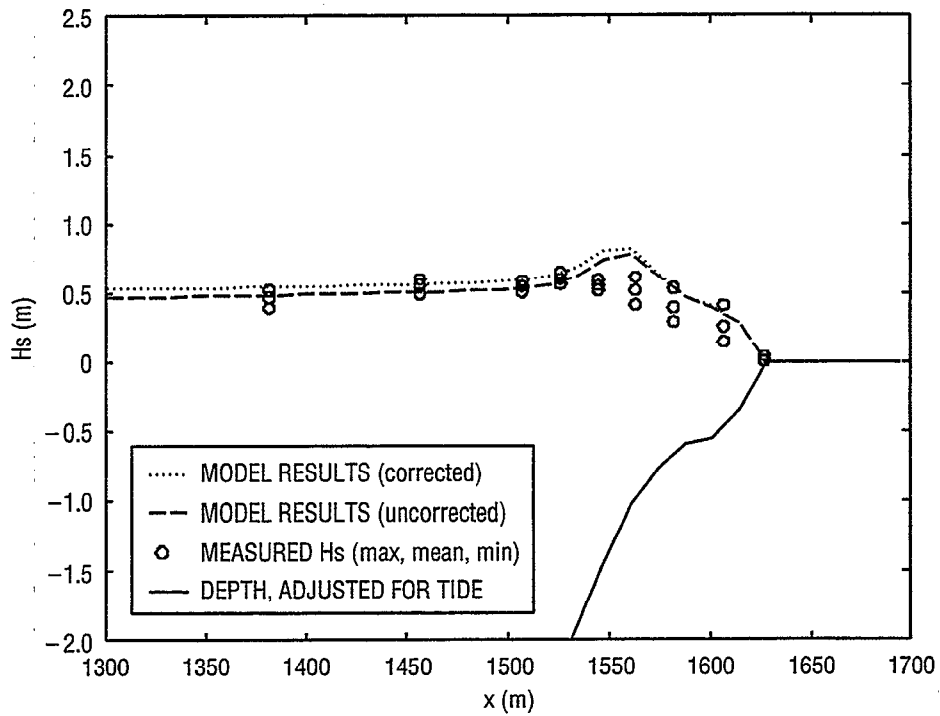


Fig. 8.5 — Comparison of wave heights from both corrected and uncorrected REF/DIF-S, the DELILAH experiment data for the time period beginning at 0400 EST, 10-7-90

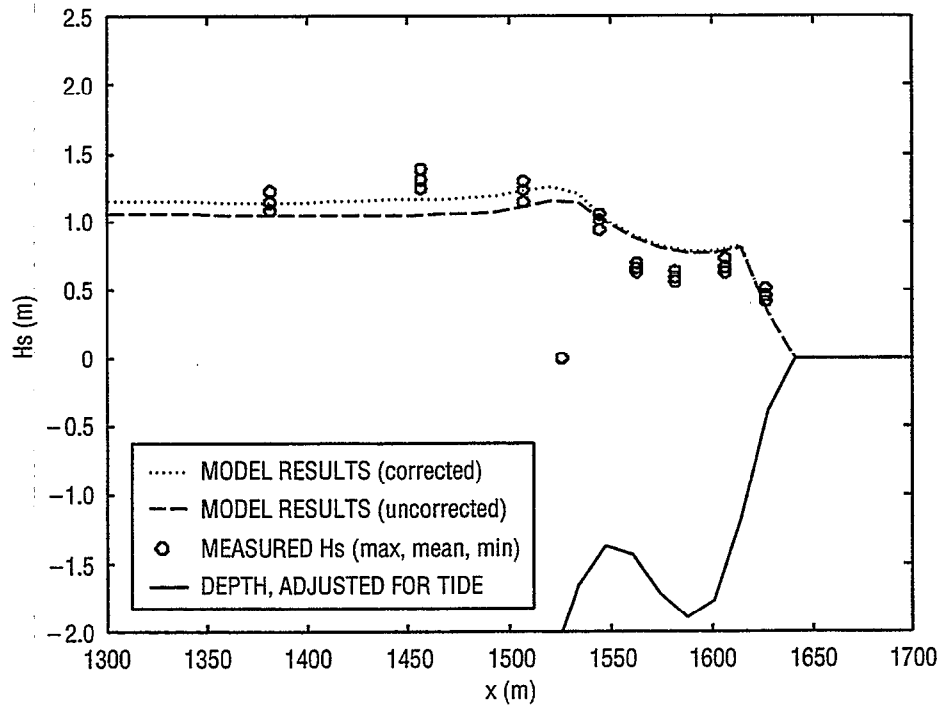


Fig. 8.6 — Comparison of wave heights from both corrected and uncorrected REF/DIF-S, the DELILAH experiment data for the time period beginning at 0700 EST, 10-12-90

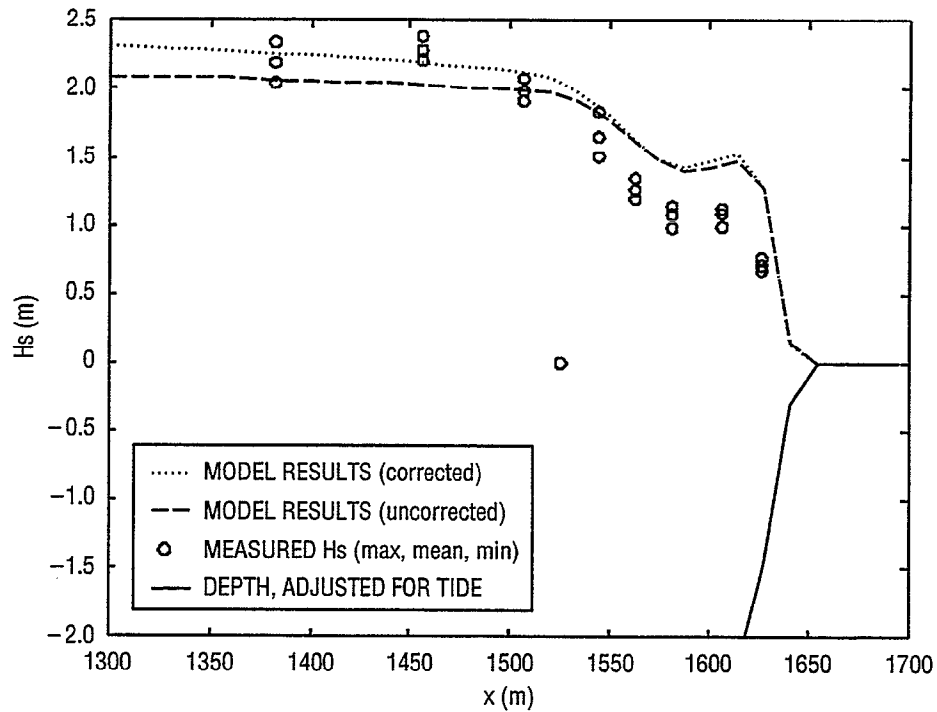


Fig. 8.7 — Comparison of wave heights from both corrected and uncorrected REF/DIF-S, the DELILAH experiment data for the time period beginning at 0100 EST, 10-13-90

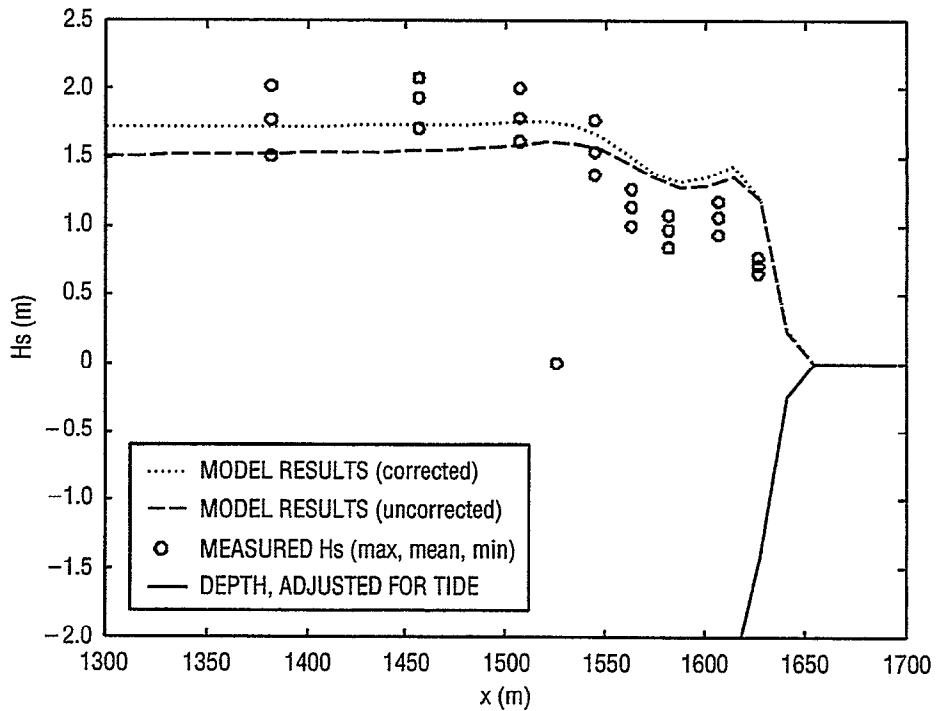


Fig. 8.8 — Comparison of wave heights from both corrected and uncorrected REF/DIF-S, the DELILAH experiment data for the time period beginning at 1600 EST, 10-13-90

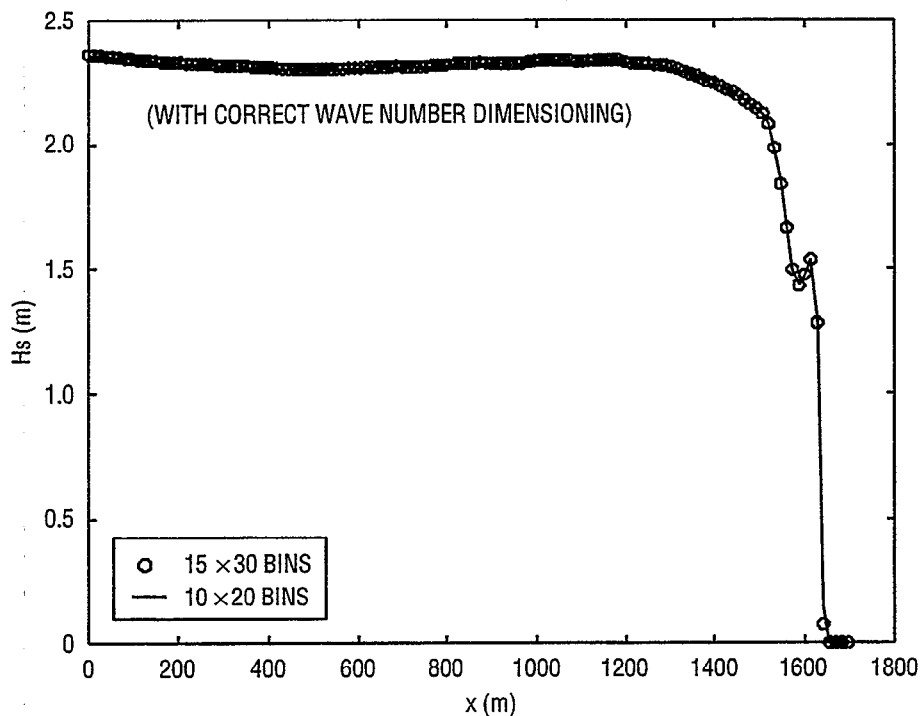


Fig. 8.9 — Comparison of corrected REF/DIF-S significant wave heights with different numbers of frequency and direction bins

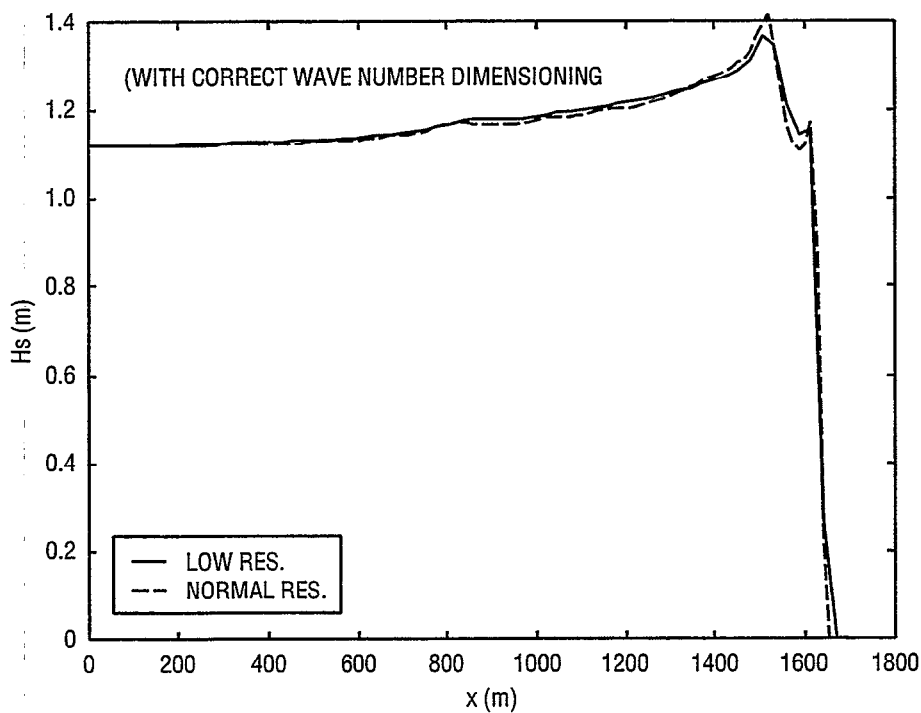


Fig. 8.10 — Comparison of corrected REF/DIF-S significant wave heights over low-resolution bathymetry and bathymetry at given resolution

8.2 Central Differencing for Wave Angle Calculation

The angle calculation routine in REF/DIF-S uses the gradient of phase function, as detailed in Part 1, Sec. 2.4. Version 1.2 of REF/DIF-S uses a centered difference in the y -direction to calculate the projection of the wave number along the y axis. The portion of the calculation concerned with accounting for phase wrapping over 2π rad had an improperly written set of finite difference equations for this calculation. This does not affect the wave height calculations, since wave angles are calculated apart from the primary solution procedure. This error is now corrected.

8.3 Nonphysical Numerical Damping

In subroutine FDCALC, a parameter $cdamp$ is specified with the value 0.0025. This parameter is a coefficient for a numerical smoothing scheme that artificially reduces the wave heights. The most likely reason for the presence of this smoothing routine is to damp high wave number numerical noise generated as a consequence of breaking; because the dissipation mechanism in REF/DIF-S (the irregular wave breaking model of Thornton and Guza 1983) is one-dimensional, local breaking events do not affect adjacent gridpoints in the longshore (y) direction, causing possibly steep y -gradients of wave height. Since REF/DIF-S does not have an option to explicitly turn off dissipation due to breaking, the effect of this numerical damping can go unnoticed unless the code were correspondingly altered. Commenting out the dissipation in the code and setting $cdamp = 0$ conserves the wave height for waves propagating over a flat bottom. However, the effect of the numerical damping scheme has not been evaluated on the results presented in previous sections. Additionally, it is not clear what the ideal value of $cdamp$ should be; more testing is required.

9.0 DIRECTIONAL SPECTRA

With the corrected model, directional spectra from REF/DIF-S model results can be calculated as stated previously. This ability was not an original option in the model; however, Chawla (1995) used the complex amplitudes from REF/DIF-S to calculate directional spectra of waves propagating over a submerged shoal.

Before discussing the method for calculating directional spectra, it is prudent to first discuss how directional spectra evolve in phase-resolving parabolic models, such as REF/DIF-S, compared to how they evolve in phase-averaged models such as SWAN (Simulating WAVes Nearshore) (Booij et al. 1996). As mentioned in Part 1, Sec. 2.1, phase-averaged models are expressed as an energy balance. These models are written in terms of directional spectral density $E(f, \theta)$ (e.g., Komen et al. 1994):

$$\frac{\partial E}{\partial t} + \nabla \cdot C_g E + \frac{\partial}{\partial \theta} (C_\theta E) + \frac{\partial}{\partial \omega} (C_\omega E) = S \quad (9.1)$$

where the right-hand side S consists of various energy source and sink terms, as well as energy exchange due to nonlinear wave-wave interaction. In the above equation, C_θ is the speed of propagation in direction space (i.e., the rate of the change in direction) and C_ω is the speed of propagation in frequency space (the rate of change in frequency). These derivatives are present when the wave propagates over varying bathymetry.

With this methodology, the frequency and direction bins used in the modeling scheme are constant. The energy in the spectrum, however, moves between the bins. This is not true with the

parabolic REF/DIF models; in these instances, the wave is followed and the direction bins change. This requires a different approach in modeling directional spectra. In this case, the complex amplitudes A_n and the resulting angles where directional spectra are desired are saved. A particular angle bin bandwidth (5° , for instance) is then chosen, and the wave angles are ranked accordingly. The expression for directional spectra is then:

$$S(f, \theta) = \frac{\sum_{n=1}^{NB} |A(f, \theta_n)|}{2\Delta f \Delta \theta}, \quad (9.2)$$

where NB is the number of wave components that fall in the angle bin under consideration. Frequency spectra can be calculated in a similar manner:

$$S(f) = \frac{\sum_{i=1}^{N\theta} |A(f, \theta_i)|^2}{2\Delta f}, \quad (9.3)$$

where $N\theta$ is the number of waves with frequency f .

Direct comparisons of directional spectra to DELILAH data, for example, are premature. This is because the nonlinear wave-wave interactions, responsible for the changes in the spectral shape, are not yet present in the model. However, the directional spectra can be calculated using the above formulas. Figures 9.1 and 9.2 show input and output directional spectra from REF/DIF-S using the

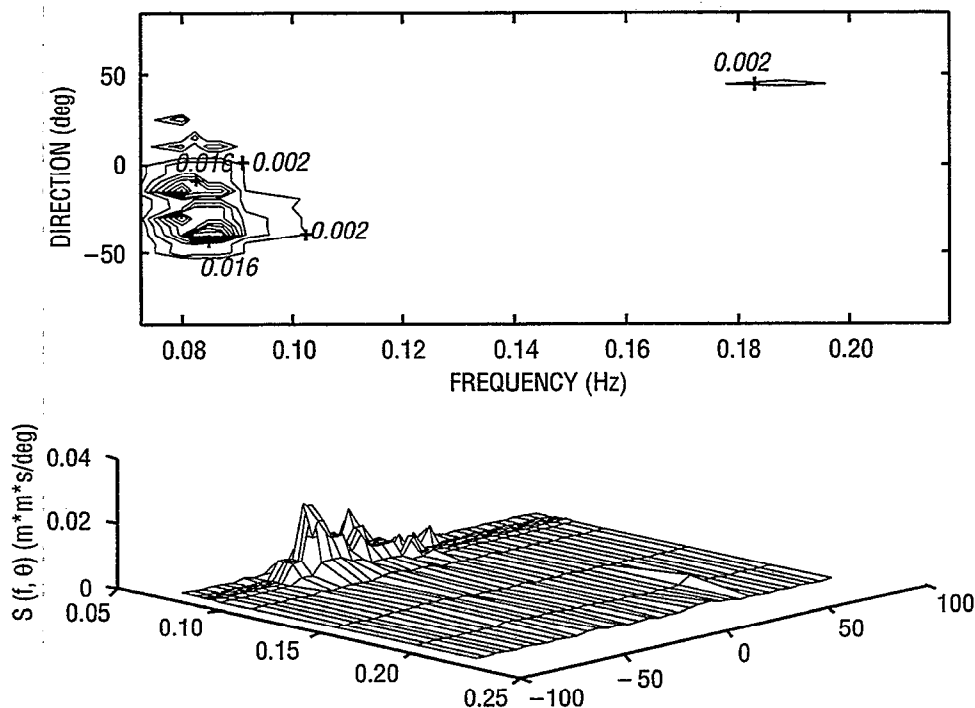


Fig. 9.1 — Directional spectra at offshore row of REF/DIF-S domain

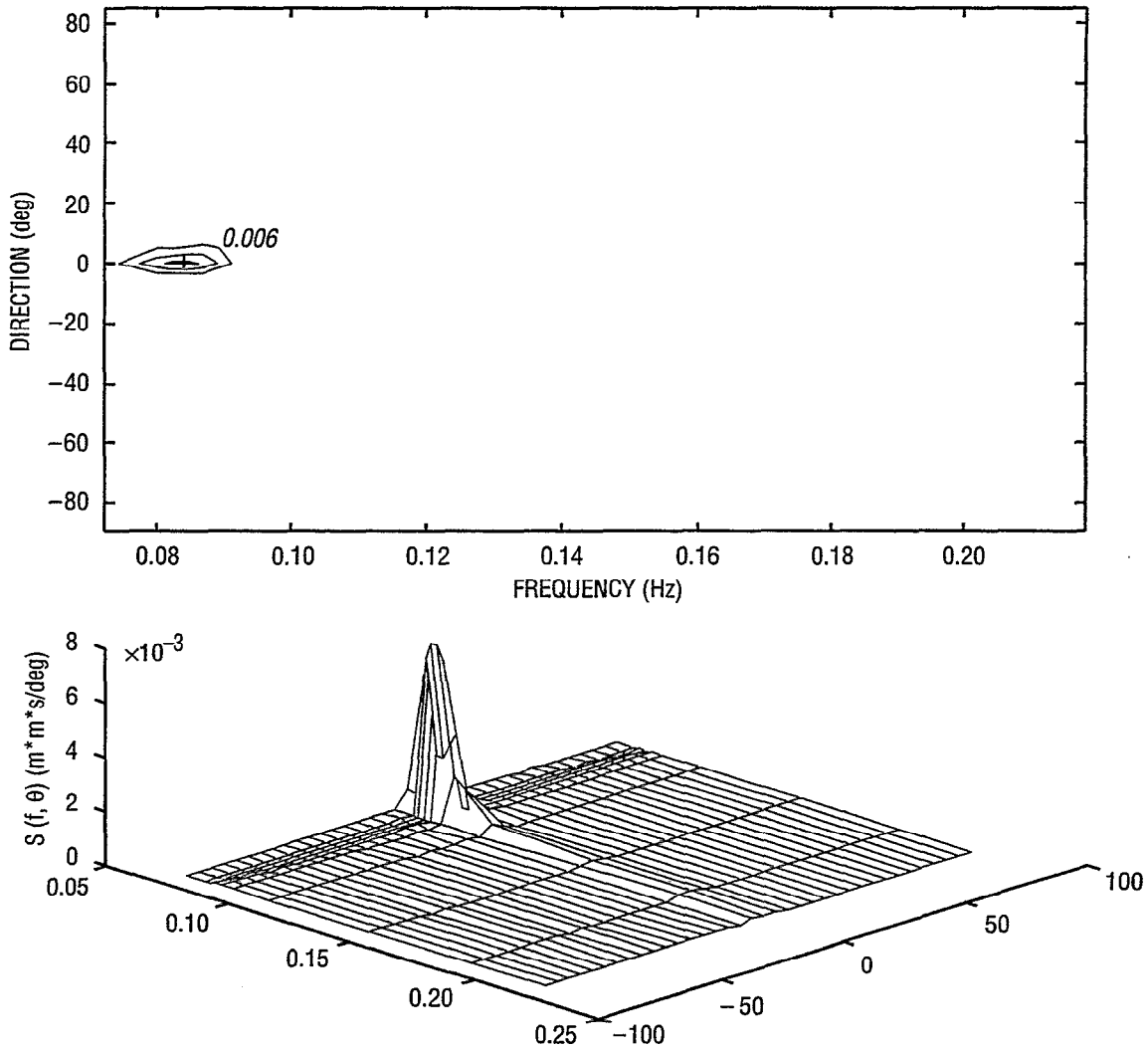


Fig. 9.2 — Directional spectra at nearshore location of REF/DIF-S domain

DELILAH spectra. The narrowing of the energy along the direction axis is clear; this corresponds to wave directions approaching shore normal (0°) as the waves refract.

10.0 CONCLUSIONS

It was intended to use REF/DIF1 to verify the model physics and REF/DIF-S to investigate the efficacy of using parabolic mild-slope models to simulate wave processes in field situations. The numerical experiments and comparisons were designed with this in mind. Within this framework, it appears that the models are reasonably accurate in general situations.

The battery of tests developed ranged from the fundamental (wave shoaling and refraction on a planar beach) to the operational (comparisons to the DELILAH experiments). It was found that the models simulate the relevant processes (refraction, diffraction, shoaling, dissipation) reliably.

These results, however, are still incomplete. The following phenomena are yet to be tested:

- (1) Wave-current interaction: A very idealized case of waves propagating both into and out of a spatially and temporally uniform current field was performed by Hsu et al. (1997). In that case, the model results were compared to analytical solutions (Peregrine 1976). The case of waves propagating into a spatially varying rip current (Arthur 1950) was addressed in the REF/DIF1 user's manual (Kirby and Dalrymple 1994). Several laboratory studies of wave/current interaction exist (e.g., Briggs et al. 1993); however, the measurements of flow were usually too sparse to be of practical value. It is intended to address this issue in conjunction with tidal flow models in future reports.
- (2) Rigorous generalized testing of wave angle output: In this study, testing of the wave angle output to the case of wave refraction was limited. Laboratory measurements of wave angle that are *not* derived from directional spectra are scarce. The only angle measurements from the DELILAH experiment in the nearshore are the "average angle" measurements derived from the nearshore directional arrays. Comparison of REF/DIF-S average angles to these measurements are misleading because nonlinear interactions can move energy between frequencies sufficiently to affect the estimates of mean direction from that of a linear model.
- (3) Rigorous testing of the transformation characteristics of the wave models to field data: As mentioned in Sec. 5.0, the wave models were verified with field data inside the surf zone only for the DELILAH experiment. The 8-m linear array at Duck was not utilized to verify the model since this would provide only *one* measure of significant wave height at a particular location. (This array can, however, be used to provide comparisons of the directional spectra to that of the model.)

In addition, several aspects of the models, both numerical and physical, require further investigation:

- (1) The proper value of the numerical damping coefficient $cdamp$.
- (2) The consequences of neglecting wind and its effects on wave growth and transformation: As mentioned in Part 1, both REF/DIF1 and REF/DIF-S do not account for wind. At present, there is no clear way of incorporating source terms like wind-induced wave growth into phase-resolved models. When comparing to the DELILAH data, conditions were explicitly chosen where the winds were low. It would be informative (though hardly definitive) to compare results from REF/DIF-S to those from a phase-averaged model with wind input as a source term (e.g., SWAN, STWAVE (Resio 1988)) for a variety of different wind speeds.
- (3) The relative importance of including wave diffraction in general modeling situations: While it is clear that wave diffraction is important in the near vicinity of coastal structures or local features in bathymetry, it is not apparent what the effect of neglecting diffraction is on a typical open coast with moderate bathymetric complexity. This has become a relevant question in recent years as more phase-averaged models (which presently can, at best, only approximate diffraction at the same scales as REF/DIF1 and REF/DIF-S) have appeared for use in near-coastal areas. Unlike RCPWAVE, diffraction is inherent in the formulation for REF/DIF1 and REF/DIF-S and cannot be turned off.
- (4) The consequences of the one-dimensionality of the breaking and energy dissipation mechanisms in both REF/DIF1 and REF/DIF-S: At present, there is no theory that dissipates spectral wave energy in both horizontal dimensions and that is consistent with the formulation of REF/DIF1 and REF/DIF-S. This can not only cause numerical difficulties due to severe local wave height gradients, but can also affect calculation of other nearshore flow phenomena (e.g., longshore currents) that utilize the wave height and angle information provided by these models.

11.0 ACKNOWLEDGMENTS

This report is a result of research conducted under the NRL Core 6.2 "Coastal Simulation" project, funded by the Office of Naval Research. Discussions with Dr. James T. Kirby and Mr. Arun Chawla (Center for Applied Coastal Research, University of Delaware) and Dr. Zeki Demirbilek (Coastal Engineering Research Center) have augmented the work; thanks is especially due Mr. Chawla for providing a copy of his master's thesis. Dr. Paul A. Work (Department of Civil Engineering, Clemson University) provided helpful input into the sources of error from bathymetric surveys; this was very useful in formulating the study on the effects of bathymetric uncertainty in the model. We also thank Mr. Lulin Guo and Dr. Robert A. Dalrymple (Center for Applied Coastal Research, University of Delaware) for providing a preprint of their conference paper prior to its publication. We gratefully acknowledge Dr. Charles Long and Mr. William Birkemeier (Field Research Facility, Coastal Engineering Research Center) for providing the DELILAH data.

12.0 REFERENCES

- Arthur, R. A., "Refraction of Shallow Water Waves: The Combined Effect of Currents and Underwater Topography," *Transactions, American Geophysical Union* **31**, 549-552 (1950).
- Berkhoff, J. C. W., N. Booij, and A. C. Radder, "Verification of Numerical Wave Propagation Models for Simple Harmonic Linear Waves," *Coastal Engineering* **6**, 255-279 (1982).
- Birkemeier, W. A., "DELILAH Investigators' Report (draft)," Technical Report, Coastal Engineering Research Center, U.S. Army Corps of Engineers Waterways Experiment Station, Vicksburg, MS, 1991.
- Booij, N., "Gravity Waves on Water with Non-Uniform Depth and Current," Ph.D. dissertation, Technical University of Delft, the Netherlands, 131 p., 1981.
- Booij, N., L. H. Holthuijsen, and R. C. Ris, "The 'SWAN' Wave Model for Shallow Water," Proceedings of the 25th International Conference on Coastal Engineering, ASCE, Orlando, FL, 1996, pp. 668-676.
- Borgman, L. E., "Directional Spectrum Estimation for the S_{xy} Gauges," Technical Report, Coastal Engineering Research Center, U.S. Army Corps of Engineers Waterways Experiment Station, Vicksburg, MS, 104 p., 1985.
- Briggs, M. J., E. F. Thompson, D. R. Green, and L. S. Lillycrop, "Laboratory Description of Harbor Idealized Tests. Volume 1: Main Text and Appendixes A through C," Technical Report CERC-93-1, Coastal Engineering Research Center, U.S. Army Corps of Engineers Waterways Experiment Station, Vicksburg, MS, 61 p., 1993.
- British Royal Navy, "The Assessment of the Precision of Soundings," Professional Paper No. 25, Hydrographic Department, Ministry of Defense, 24 p., 1990.
- Brown, M. G., F. D. Tappert, and S. E. R. B. Sundaram, "Chaos in Small-Amplitude Surface Gravity Waves Over Slowly Varying Bathymetry," *Journal of Fluid Mechanics* **227**, 35-46 (1991).

- Chawla, A., "Wave Transformation Over a Submerged Shoal," M.S. thesis, Center for Applied Coastal Research, University of Delaware, 240 p., 1995.
- Chen, H. S., "Combined Reflection and Diffraction from a Vertical Wedge," Technical Report CERC-87-16, Coastal Engineering Research Center, U.S. Army Corps of Engineers Waterways Experiment Station, Vicksburg, MS, 41 p., 1987.
- Ebersole, B. A., M. A. Cialone, and M. D. Prater, "Regional Coastal Processes Numerical Modeling System Report 1: RCPWAVE--A Linear Wave Propagation Model for Engineering Use," Technical Report CERC-86-4, Coastal Engineering Research Center, U.S. Army Corps of Engineers Waterways Experiment Station, Vicksburg, MS, 71 p., 1986.
- Guo, L. and R. A. Dalrymple, "Water Wave Fluctuations Induced by Irregular Bathymetry," Proceedings of the 25th International Conference on Coastal Engineering, ASCE, Orlando, FL, 1996, pp. 731-742.
- Hales, L. Z., "Erosion Control of Scour During Construction, Report 3: Experimental Measurements of Refraction, Diffraction, and Current Patterns Near Jetties," Technical Report HL-80-3, Hydraulics Laboratory, U.S. Army Corps of Engineers Waterways Experiment Station, Vicksburg, MS, 59 p., 1980.
- Holthuijsen, L. and N. Booij, "Bottom Induced Scintillation of Long and Short Crested Waves," Proceedings of the International Symposium: Waves--Physical and Numerical Modeling, Vancouver, B.C., 604-613, 1994.
- Hsu, Y.-H. L., J. M. Kaihatu, and A. MacNaughton, "Validation Test Report for Shallow Water Wave Refraction and Diffraction (REF/DIF1) Model," NRL/FR/7322--97-9669, Naval Research Laboratory, Stennis Space Center, MS, 1997.
- Hughes, S. A., "The TMA Shallow Water Spectrum: Description and Applications," Technical Report CERC-84-7, Coastal Engineering Research Center, U.S. Army Corps of Engineers Waterways Experiment Station, Vicksburg, MS, 39 p., 1984.
- Kaihatu, J. M. and H. S. Chen, "Combined Diffraction and Reflection of Waves from a Vertical Wedge: PCDFRAC User's Manual," Technical Report CERC 88-13, Coastal Engineering Research Center, U.S. Army Corps of Engineers Waterways Experiment Station, Vicksburg, MS, 42 p., 1988.
- Kirby, J. T., "Discussion of 'Refraction-Diffraction Model for Linear Water Waves,' by B. A. Ebersole," *Journal of Waterways, Port, Coastal, and Ocean Engineering* **114**, ASCE, Orlando, FL, 101-103 (1988).
- Kirby, J. T. and R. A. Dalrymple, "Combined Refraction/Diffraction Model REF/DIF1, Version 2.5: Documentation and User's Manual," CACR Report 94-22, Center for Applied Coastal Research, University of Delaware, Newark, DE, 171 p., 1994.
- Kirby, J. T. and H. T. Ozkan, "Combined Refraction/Diffraction Model for Spectral Wave Conditions REF/DIF-S, Version 1.1: Documentation and User's Manual," CACR Report 94-04, Center for Applied Coastal Research, University of Delaware, Newark, DE, 128 p., 1994.

- Komen, G. J., L. Cavaleri, M. Donelan, K. Hasselmann, S. Hasselmann, and P. A. E. M. Janssen, *Dynamics and Modeling of Ocean Waves* (Cambridge University Press, Cambridge, U.K., 1994), p. 532.
- Penney, W. G. and A. T. Price, "Part 1. The Diffraction Theory of Sea Waves and the Shelter Afforded by Breakwaters," *Philosophical Transactions of the Royal Society A244*, 236–253 (1952).
- Peregrine, D. H., "Interaction of Water Waves and Currents," *Advances in Applied Mechanics* **16**, 9–117 (1976).
- Radder, A. C., "On the Parabolic Equation Method for Water-Wave Propagation," *Journal of Fluid Mechanics* **95**, 159–176 (1979).
- Resio, D. T., "A Steady State Model for Coastal Applications," Proceedings of the 21st International Conference on Coastal Engineering, Malaga, Spain, 1988, pp. 929–940.
- Sobey, R. J. and T. L. Johnson, "Diffraction Patterns Near Narrow Breakwater Gaps," *Journal of Waterways, Port, Coastal, and Ocean Engineering* **112**, ASCE, Orlando, FL, 512–528 (1986).
- Sommerfeld, A., "Mathematische Theorie Der Diffraction," *Mathematische Annalen* **47**, 317–374 (1896).
- Stoker, J. J., *Water Waves* (John Wiley and Sons, New York, NY, 1957), 567 p.
- Thornton, E. B. and R. T. Guza, "Transformation of Wave Height Distribution," *Journal of Geophysical Research* **88**, 5925–5938 (1983).

Appendix A

DETAILS OF THE SPECTRAL INPUT PROGRAM SPECGEN

A1. BACKGROUND

In the model REF/DIF-S, two preprocessing functions (SPECDAT-CREATEV12 and SPECGEN) are provided to set up the offshore boundary condition for a two-dimensional (2-D) spectra input. In the program SPECDAT-CREATEV12, user specifies the significant wave height, peak frequency, and other wave parameters and selects among three options depending on the type of wave data available. Its output file SPECGEN.DAT is read by SPECGEN, which in turn generates an output file INDAT.DAT with corresponding frequencies, angles, and amplitude. Option 1 is used when no measured spectrum is available and input wave components are generated according to TMA frequency spectrum in conjunction with a wrapped normal direction distribution. Option 2 is used when only a measured frequency spectrum is available and SPECGEN provides the directional distribution as in option 1. In both options 1 and 2, SPECGEN divides the 2-D spectrum into bins of constant energy so that the spectrum is well resolved in the region of the peak frequency and mean angle of incidence. Option 3 is used when a measured 2-D spectrum is available. However, SPECGEN in this case only does the conversion of spectral densities to component amplitudes and does not provide equal energy bins. In this appendix, a brief description and documentation are given for a new option that produces output in equal energy bins for any measured 2-D spectrum.

A2. APPROACH

There are probably at least two ways to obtain equal energy bins for a given 2-D spectrum. One way is to find the mathematical functional form for a given 2-D spectrum using interpolation routines, then one can use the subroutines in the SPECGEN (using Simpson's rule of integration) to generate the equal energy bins. Many off-the-shelf interpolation routines can be found. But one needs to thoroughly test the routines using various wave conditions to make sure that no overshoot or other anomalies occur. Because of the fact that many different shapes of wave spectrum are possible, this task can be substantial. Our approach is to subdivide the input frequency and directional bins into many small bins, then sum them up to derive equal energy bins.

At first, each frequency spectrum band is subdivided into many small and equal bands, then energy is added until a specified energy level is reached. The energy level depends on the number of bins specified by the user. When the summation of energy satisfies the tolerance criteria, a new cycle is repeated. It is noted that the tolerance criteria is set to be a small ratio to the specified energy. In the original SPECGEN, an absolute energy level criteria is used. Our ratio criteria are more flexible in handling both low and high wave conditions. Similarly to the option 1, a weighted frequency (first moment divided by area) is then computed for each bin. The next step is to find the representing angles for these frequencies.